AD-A262 905

MASSACHUSETTS INSTITUTE OF TECHNOLOGY
LINCOLN LABORATORY

SWAT II OVERVIEW

R.R. PARENTI
P.N. EVERETT
R. KRAMER
D.A. PAGE
Group 54

PROJECT REPORT SWP-3
Revision 1

10 MARCH 1993

DTIC
S Apr 13 1993 D

Approved for public release; distribution is unlimited.

93-07582

LEXINGTON 98 4 12 0 16 MASSACHUSETTS

This report is based on studies performed at Lincoln Laboratory, a center for research operated by Massachusetts Institute of Technology. The work was sponsored by the Air Force Phillips Laboratory under Air Force Contract F19628-90-C-0002.

This report may be reproduced to satisfy needs of U.S. Government agencies.

The ESC Public Affairs Office has reviewed this report, and it is releasable to the National Technical Information Service, where it will be available to the general public, including foreign nationals.

This technical report has been reviewed and is approved for publication.

FOR THE COMMANDER

Gary Tutungian
Administrative Contracting Officer
Directorate of Contracted Support Management

Non-Lincoln Recipients

PLEASE DO NOT RETURN

Permission is given to destroy this document when it is no longer needed.

MASSACHUSETTS INSTITUTE OF TECHNOLOGY
LINCOLN LABORATORY

SWAT II OVERVIEW

R.R. PARENTI
P.N. EVERETT
R. KRAMER
D.A. PAGE
Group 54

PROJECT REPORT SWP-3
Revision 1

10 MARCH 1993

Approved for public release; distribution is unlimited.

LEXINGTON MASSACHUSETTS

ABSTRACT

All adaptive optics systems incorporate devices designed to measure and compensate phase distortions that accumulate over the propagation path of an optical beam. Measurement of the wavefront is accomplished with the aid of a bright source, or beacon, which must be accurately positioned along the beampath. In some scenarios of interest no physical beacon exists; for instance, the propagation of a laser beam to an exoatmospheric object moving at velocity v requires that the beacon lead the target by an angle $2v/c$. In the early 1980's it was proposed that laser backscatter in the atmosphere might provide a suitable alternative source in such cases. Although a synthetic beacon generated in this manner can be placed arbitrarily in angle, any range discrepancy between the target and the beacon can lead to a form of measurement error known as focal anisoplanatism.

Lincoln Laboratory's SWAT (Short-Wavelength Adaptive Techniques) program was initiated in 1983 to provide experimental verification of the most promising synthetic beacon concepts and to quantify the magnitude of the associated focal anisoplanatic errors. The test plan for this program includes passive imaging experiments using single and binary stars, as well as active experiments in which a scoring beam will be projected to rocket and satellite targets.

DTIC QUALITY

Accession For
NTIS
DTIC
Unannounced
Justification
By
Distribution/
Availability Codes
Dist
A-1

PREFACE

From 1982 to 1991 Lincoln Laboratory was supported by the Defense Department to develop the technology of uncooperative-target adaptive optics. A principal feature of this program was the development of synthetic beacons as the reference source for the adaptive-optics wavefront sensor. This technique overcame problems associated with point-ahead and target brightness.

In the late 1980's it became clear that synthetic-beacon technology could be of great value to the astronomical community, who routinely deal with dim objects. Moreover the basic concept had been reinvented by the astronomers with, apparently, no input from the US Defense community. The civilian community seemed on the verge of embarking on a major development program duplicating work the US Government had already paid for.

It seemed incumbent therefore on the DoD to provide to the astronomers the wealth of information that had been developed over the past decade. So, in May 1991 the US Air Force released virtually all of the development work and associated documentation. The immediate impact was that Defense workers began to present their material in open publication. We are now moving to republish a number of documents that seem of greatest import. To some extent these documents are dated as far as military work is concerned, but they are likely to be of great value to the astronomers. At a minimum they are of historical and archival significance.

The report that follows is one of many documents we are in the process of releasing. The original report numbered SWP-3 ("SWAT II Overview," dated 10 February 1988) is now updated. If you possess the original, it should be destroyed in accordance with current document-control procedures. We are providing a copy of this report to the Defense Technical Information Center (DTIC) so that users may request it. There are intended to be no distribution limitations on this document.

TABLE OF CONTENTS

Abstract		*iii*
Preface		*v*
List of Illustrations		*ix*
List of Tables		*xi*
1.	INTRODUCTION	*1*
2.	REVIEW OF CURRENT SYNTHETIC-BEACON CONCEPTS	*5*
2.1	Focused Beacon A-Method Concepts	*7*
2.2	Sheared Beacon S-Method Concepts	*11*
2.3	Critical Time Constant for Pulsed Correction	*16*
2.4	Beacon Laser-Energy Requirements	*17*
3.	SWAT II FIELD HARDWARE DESCRIPTION	*23*
3.1	External Beam Control and Tracking	*23*
3.2	Wavefront Control and Scoring	*25*
3.3	Synthetic Beacon Laser Sources	*33*
3.4	Experiment Control and Data Collection	*35*
3.5	AMOS Laboratory Layout	*43*
4.	LABORATORY EXPERIMENT TO VERIFY STITCHING CONCEPT	*47*
4.1	Principal Objectives	*47*
4.2	Scaling Theory	*47*
4.3	Optical Components	*49*
4.4	Experiment Control and Data Analysis	*54*

TABLE OF CONTENTS (Continued)

5.	EARLY SWAT II STAR-IMAGING EXPERIMENTS		*59*
	5.1	Passive Scoring Receiver Sensitivity Issues	*59*
	5.2	A-Method Figure Compensation Experiments	*71*
	5.3	Figure Compensation Performance Estimates	*83*
6.	SWAT II LASER PROPAGATION MEASUREMENTS		*87*
	6.1	LACE Satellite Experiments	*87*
	6.2	Sounding Rocket Tests	*88*
7.	FUTURE REPORTING		*91*

LIST OF ILLUSTRATIONS

2-1	Stitching terminology.	*6*
2-2	Collected photons as a function of scattering altitude.	*9*
2-3	"A" method beacon geometry.	*10*
2-4	Reconstruction error as a function of mirror diameter and stitching algorithm.	*12*
2-5	"S" method figure correction.	*13*
2-6	"S" method wavefront sensor.	*15*
2-7	Effect of source diameter on phase reconstruction error.	*21*
3-1	Acquisition and tracking systems.	*24*
3-2	SWAT II system block diagram.	*26*
3-3	Laser beam director schematic.	*29*
3-4	SWAT II wavefront sensor optics.	*30*
3-5	SWAT II deformable mirror.	*32*
3-6	Dye laser optical head.	*36*
3-7	Dye laser bench layout.	*37*
3-8	Dye laser heat exchanger.	*38*
3-9	Dye laser dye cleanup system.	*39*
3-10	Control and recording systems.	*41*
3-11	Analog recorder track assignments.	*42*
3-12	SWAT II laboratory layout.	*44*
4-1	Multiple-source test box for bench experiment.	*51*
4-2	Bench experiment optical configuration.	*53*
4-3	Experiment control and recording equipment.	*55*
4-4	Bench experiment timeline.	*56*
5-1	SWAT II system optical layout.	*60*
5-2	Bright star viewing dates.	*68*
5-3	Bright star elevation map for 1 March.	*69*
5-4	Single-beacon compensation experiment.	*72*
5-5	Single-beacon experiment timing diagram.	*73*
5-6	Multiple-beacon compensation experiment.	*77*

LIST OF ILLUSTRATIONS (Continued)

5-7 Multiple-beacon experiment timing diagram. *78*

5-8 Dual-altitude compensation experiment. *81*

5-9 Dual altitude experiment timing diagram. *82*

5-10 Predicted compensation system performance. *84*

6-1 LACE satellite detector configuration. *89*

6-2 Sounding rocket illumination and data recording. *90*

LIST OF TABLES

1-1	SWAT II Experiment Agenda	*2*
2-1	Rayleigh Scattering Definitions and Parametric Values	*18*
2-2	Sodium Resonance Scattering Definitions and Parametric Values	*19*
3-1	Wavefront Control Characteristics	*28*
3-2	System Component Time Constants	*33*
3-3	Synthetic Beacon Projection System Goals	*33*
3-4	Primary Data Recording Parameters	*43*
4-1	Laboratory Scaling Options	*49*
5-1	Optical Throughput Estimates	*62*
5-2	Aperture Irradiance Requirements	*64*
5-3	Bright Star List	*67*
5-4	Star Spectral Irradiance Data	*70*

1. INTRODUCTION

Adaptive-optics concepts for the propagation of near-diffraction-limited laser beams from ground installations to cooperative exoatmospheric targets have been successfully demonstrated in a series of laboratory and field experiments conducted in the last decade. All such systems require the target to carry some type of beacon to allow a phase-sensing instrument to sample the optical phase distortion along the propagation path; the conjugate phase is then imposed on a deformable mirror with a continuous, closed-loop servo system. This method of beam control is suitable for engagement scenarios in which cooperative relay mirrors are used to redirect the laser radiation above the atmosphere but would obviously be useless for direct target imaging or negation missions.

The first techniques for dealing with non-cooperative targets were developed by the adaptive-optics community in the early 1980's. Central to all proposed solutions is the replacement of a physical target-mounted beacon by a synthetic probe generated by atmospheric backscatter from one or more pulsed, ground-based lasers. Two major problems must be dealt with before this approach can be considered viable. The first is essentially an engineering task relating to the development of highly accurate, open-loop, adaptive-optics equipment. The second is more fundamental, and involves the anisoplanatic effects associated with the placement of synthetic beacons at altitudes well below the target's position. Research in both of these areas has been active in the last five years.

Lincoln Laboratory's SWAT (Short-Wavelength Adaptive Techniques) program was initiated in 1983 to provide experimental verification of the most promising synthetic beacon concepts. Phase I, which was completed in FY85, demonstrated a clear correlation between phase measurements obtained from star sources and laser returns from both low-altitude Rayleigh scattering and resonance backscatter from the sodium layer at 90 km. SWAT II represents a continuation of this work; it will field a fully operational system capable of conducting passive imaging experiments using single and binary stars, as well as active experiments in which a scoring beam will be projected to rocket and satellite targets. These tests are scheduled to begin in the third quarter of FY88, and encompass at least eight distinct compensation experiments over a three year period. A tentative list of the proposed experiments

is previewed below.

TABLE 1-1
SWAT II Experiment Agenda

Experiment	*Method*	*Demonstration*	*Scoring*
1. Single Beacon	"A"	Figure Compensation	Single Star Imaging
2. Multiple Beacons	"A"	Figure Compensation	Single Star Imaging
3. LACE Satellite	"A"	Figure Compensation	Scoring Laser
4. Open-Loop Figure	"S"	S-Method Viability	Interferogram Imaging
5. Rayleigh Bootstrap	"A"	Figure Compensation	Single Star Imaging
6. Rocket Experiments	"A"	Figure Compensation	Scoring Laser
7. Closed-Loop Figure	"S"	Figure Compensation	Single Star Imaging
8. Sodium Bootstrap	"A"	Figure/Tilt Compensation	Scoring Laser

While the first SWAT II report emphasized the use of instrumented rocket targets to characterize the degree of compensation applied to scoring lasers projected through the adaptive-optics system, the inclusion of so many additional tests has necessitated an expanded use of star imaging measurements as the primary diagnostic device. The use of passive scoring techniques is supported by the results of the third phase of the ACE (Atmospheric-Compensation Experiment) program, in which a high degree of correlation was found between laser beam profiles measured at exoatmospheric targets and the corresponding beacon images observed by high-resolution cameras on the optical bench. Figure compensation tests, in which overall tilt is ignored, can be performed by using a high-brightness star as the plane-wave reference, whereas binary stars with separation angles near 50 μrad are suitable for pointing experiments. Highly accurate beam-profile measurements are obtainable with low-noise CCD cameras developed by Lincoln Laboratory's Solid-State Division for the SWAT program.

The objective of the current SWAT effort is to follow a methodical (albeit somewhat accelerated) series of validation experiments, which will begin with the collection of star imagery using single-beacon figure-compensation techniques and smoothly evolve to propagation

measurements in which both the "A" and "S" atmospheric sampling methods will be explored. This report provides an executive summary of the proposed test sequence and serves as an introduction to future reports that will contain detailed plans for particular experiments. Although every effort has been made to identify all of the important aspects of the synthetic-beacon framework that are amenable to near-term verification and to allow a reasonable time interval for each test, significant changes to the present outline are to be expected as more information becomes available.

2. REVIEW OF CURRENT SYNTHETIC-BEACON CONCEPTS

A fairly extensive body of theoretical analysis covering a wide range of synthetic beacon architectures has been compiled at this writing, and a limited but growing base of experimental data lending support to the viability of the basic concepts has also been developed. Unfortunately, no systematic overview of current work has been assembled, and much of the information is confined to internal corporate documentation that is not easily accessible by the beam-control community. In lieu of a more comprehensive summary of the current state of the art, this section presents a brief review of the key elements as a means of motivating the scope of the SWAT II effort. It is convenient to begin with an introduction to some of the terminology that will be used frequently in subsequent discussions.

It has been recognized since the beginning of this program that the simpler beacon projection schemes provide no overall tilt information, since the absolute position of a beacon above the turbulence layer cannot be directly determined. "Pointing" measurements refer to experiments in which the pointing direction of a scoring beam is in some way inferred from beacon data and tracking information from the target body. Binary stars can also be used to test the performance of pointing schemes. The turbulence property that is probed in this type of measurement is the tilt component of point-ahead anisoplanatism.

The term "figure" is used to describe a phase measurement from which the average piston and tilt components have been removed. Measurements of figure can be made either by tracking a point source and obtaining its phase, or by transmitting a beam to an instrumented target equipped with a cooperative beacon in the point-ahead direction. The first set of SWAT experiments will be devoted to figure measurements of bright stars.

"Focal anisoplanatism" refers to the difference between the atmospheric disturbance encountered by a plane wave propagating through the atmosphere, and the turbulence encountered by rays emanating from a point source at a finite altitude. The use of multiple beacons has been proposed to reduce the effect of focal anisoplanatism, and the combination of phase data from several sources to produce a unified deformable-mirror figure has come to be known as "stitching." As indicated in Figure 2-1, stitching algorithms handle phase-sensor data

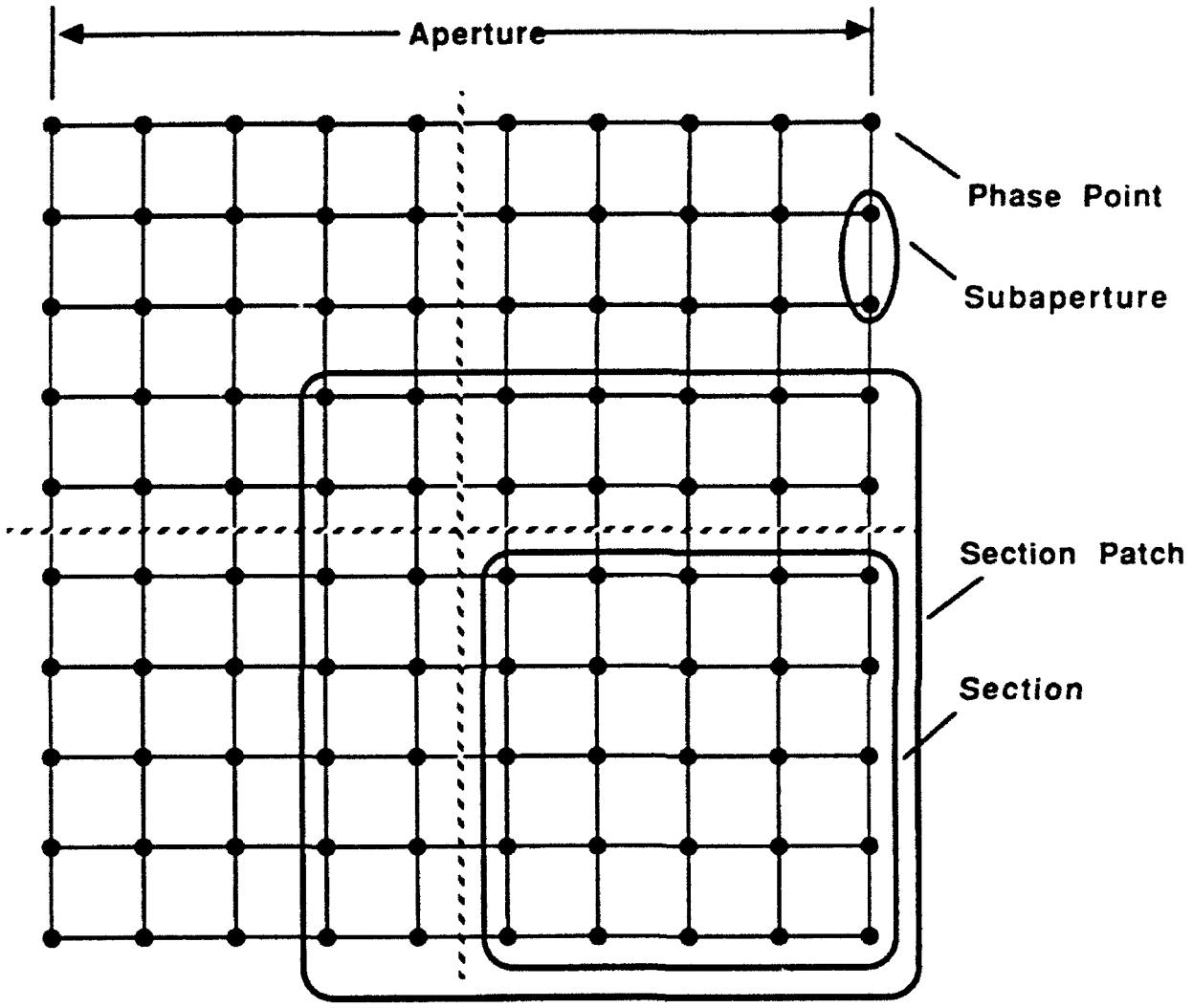

Fig. 2-1. Stitching terminology.

in an unconventional manner so that the mirror "sections" are primarily influenced by the beacon whose rays most closely resemble those from a collimated source. The individual sections are aligned by allowing some of the subapertures to simultaneously view two or more beacons, and the portion of the receiver that is sensitive to the radiation from a particular beacon is referred to as its "patch." A patch can be as small as a section surrounded by a single ring of subapertures, or it may encompass the entire receiver aperture. The process of deploying beacons at two or more altitudes either as a means of stitching aperture sections or performing an S-method measurement is often called "bootstrapping."

The synthetic-beacon methods encompass a fairly wide range of ideas for obtaining figure and pointing information from artificial beacons, but virtually all of the current approaches can be treated as variants of the two concepts described below.

2.1 FOCUSED BEACON A-METHOD CONCEPTS

The use of focused-beam atmospheric probes represents the first proposed remedy to the uncooperative target problem, and is probably the more easily understood of the two approaches. The concept has its origins in the LIDAR (LIght Detection And Ranging) studies initiated in the late 1960's, which to a large extent were aimed at the development of remote air sampling techniques exploiting resonant and non-resonant backscatter phenomena. Largely as a result of that work, highly accurate scattering cross-section and density parameters for a wide range of atmospheric constituents have been cataloged.

From the point of view of a system developer, the only quantity of real interest is the net backscattered energy available at a given laser output level, wavelength, and sample altitude. In the visible region, Rayleigh backscatter dominates out to 90 km, and the product of the scattering cross-section and the molecular abundance as measured by a sampling interval equal to 10% of the scattering range is roughly represented by[1]

$$n(R)\,\Delta R\,[d\sigma(\pi)/d\Omega] \approx 1.3\times10^{-28}\,\lambda^{-4}\,\exp(-R/9{,}000)\ \text{molecules/ster} \qquad (2\text{-}1)$$

where the range and the wavelength are both expressed in meters. Between 85 and 95 km, a

[1]Hinkley, E. D., Laser Monitoring of the Atmosphere, Springer-Verlag (1976).

stable layer of sodium molecules is encountered that has a cross-section-abundance product of $2x10^{-3}$ molecules/ster at 589 nm. When the R^2 receiver losses are factored into these values, the collection efficiency curve shown in Figure 2-2 is derived. It can be seen that any significant increase in probe altitude can only come at the expense of a dramatic improvement in the output power of the beacon laser.

In its simplest form, a focused-beam, figure-correction system would incorporate a single beacon positioned at the highest altitude permitted by the sensitivity of the equipment. As indicated in Figure 2-3, two types of sampling error arise from this arrangement. The first results from the conflicting needs to probe the entire transmission path through the atmosphere, while simultaneously achieving a strong beacon return signal by placing it in a region of high-molecular density. As a result, some fraction of the atmosphere will always be left unsampled.

Focal anisoplanatism represents the second principal source of error and, as alluded to earlier, refers to the fact that the rays from the beacon and a collimated source follow dissimilar paths, resulting in an incorrect turbulence measurement that becomes increasingly poor with altitude. This effect can also be reduced by either increasing the beacon altitude or deploying multiple beacons. Both of these approaches increase the power requirements on the probe laser system.

To first order, the focal anisoplanatic error is found to be related to the beacon range R, the receiver of diameter D, and the 5/3 turbulence moment $\mu_{5/3}$ in the following way

$$\sigma^2 \propto \mu_{5/3} (D/R)^{5/3} \tag{2-2}$$

which is the result expected from geometrical considerations. In principal at least, the use of n_b multiple sources effectively shrinks the receiver aperture so that Equation (2-2) can be rewritten

$$\sigma^2 \propto \mu_{5/3} (D^2/n_b^2)^{5/6} \quad . \tag{2-2'}$$

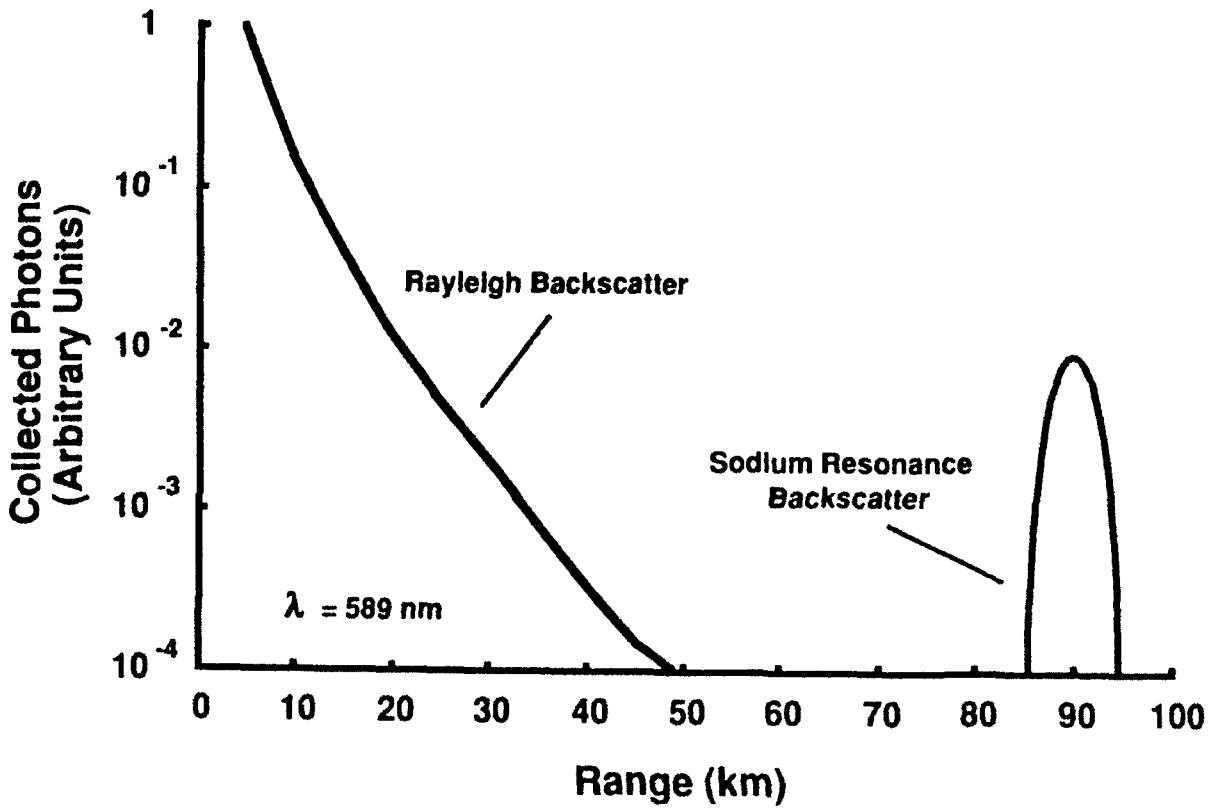

Fig. 2-2. Collected photons as a function of scattering altitude.

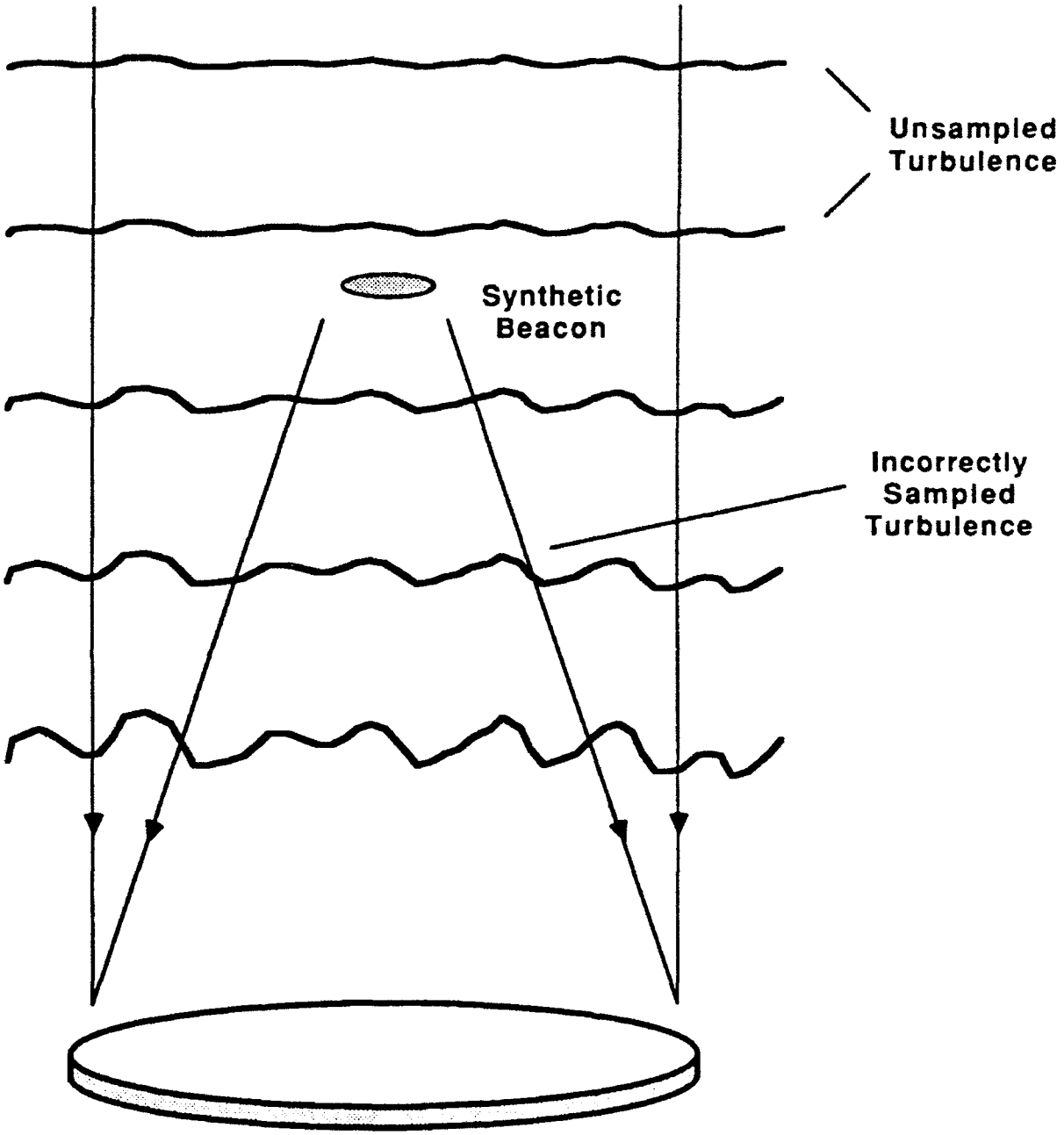

Fig. 2-3. "A" method beacon geometry.

Unfortunately, the performance improvement achievable with multiple beacons is not as great as Equation (2-2') would imply, because of errors associated with the reassembly, or "stitching," of the information from individual aperture sections. Section stitching is necessary because the beacons tend to wander randomly about their nominal positions due to differential turbulence effects along the transmission paths, so that the relative section tilt information is unusable. Failure to incorporate a tilt-invariant processing algorithm results in anomalous low-frequency figure modulations that almost completely negate the benefit of multiple sources. Section tilt invariance is typically achieved either by designing regions of overlap into the wavefront sensor so that some fraction of the gradient measurements derive from two or more adjacent beacons, or by deploying a high-altitude source to eliminate the low spatial-frequency errors. Preliminary estimates of the dependence of the stitching error with the number of sections employed have been obtained using Monte-Carlo numerical techniques, and a summary of this analysis appears in Figure 2-4. It can be seen from these data that the stitching error variance is strongly dependent on the beacon deployment geometry and can be an order of magnitude larger than that predicted by Equation (2–2') for large apertures. The use of a high-altitude source for section stitching will evidently be a requirement for any reasonably-sized system.

2.2 SHEARED BEACON S-METHOD CONCEPTS

Shortly after the introduction of the focused beacon strategies described above, an alternative approach involving the use of a single-sheared beam was proposed by Itek Corporation. According to Itek's calculations, an S-method atmospheric probe would require significantly less energy to achieve acceptable figure and tilt correction for large-aperture transmitters. Therefore, the SWAT program will incorporate a means to establish the existence of high-altitude fringe patterns produced by sheared beams and provide a quantitative measure of their correlation with phase measurements obtained from star sources.

The S-method concept contains several novel components that merit discussion. Its most distinct attribute, as indicated in Figure 2-5, is the use of a single-collimated beam to probe the atmosphere rather than a matrix of focused sources. The outgoing radiation is sheared by passage through a Wollaston prism to produce two coherent beams separated in angle by about 5 μrad and having orthogonal polarizations. (In an operational system this process would be repeated to provide gradient data in both the x and y directions.) In this way, an interference

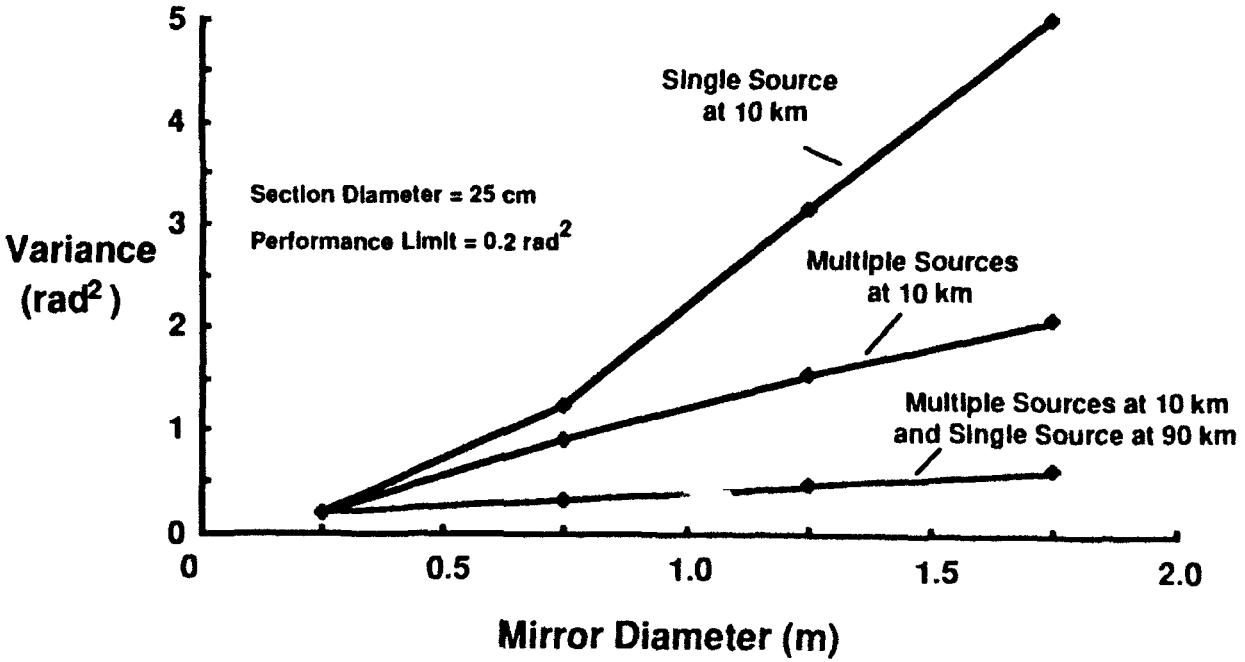

Fig. 2-4. Reconstruction error as a function of mirror diameter and stitching algorithm.

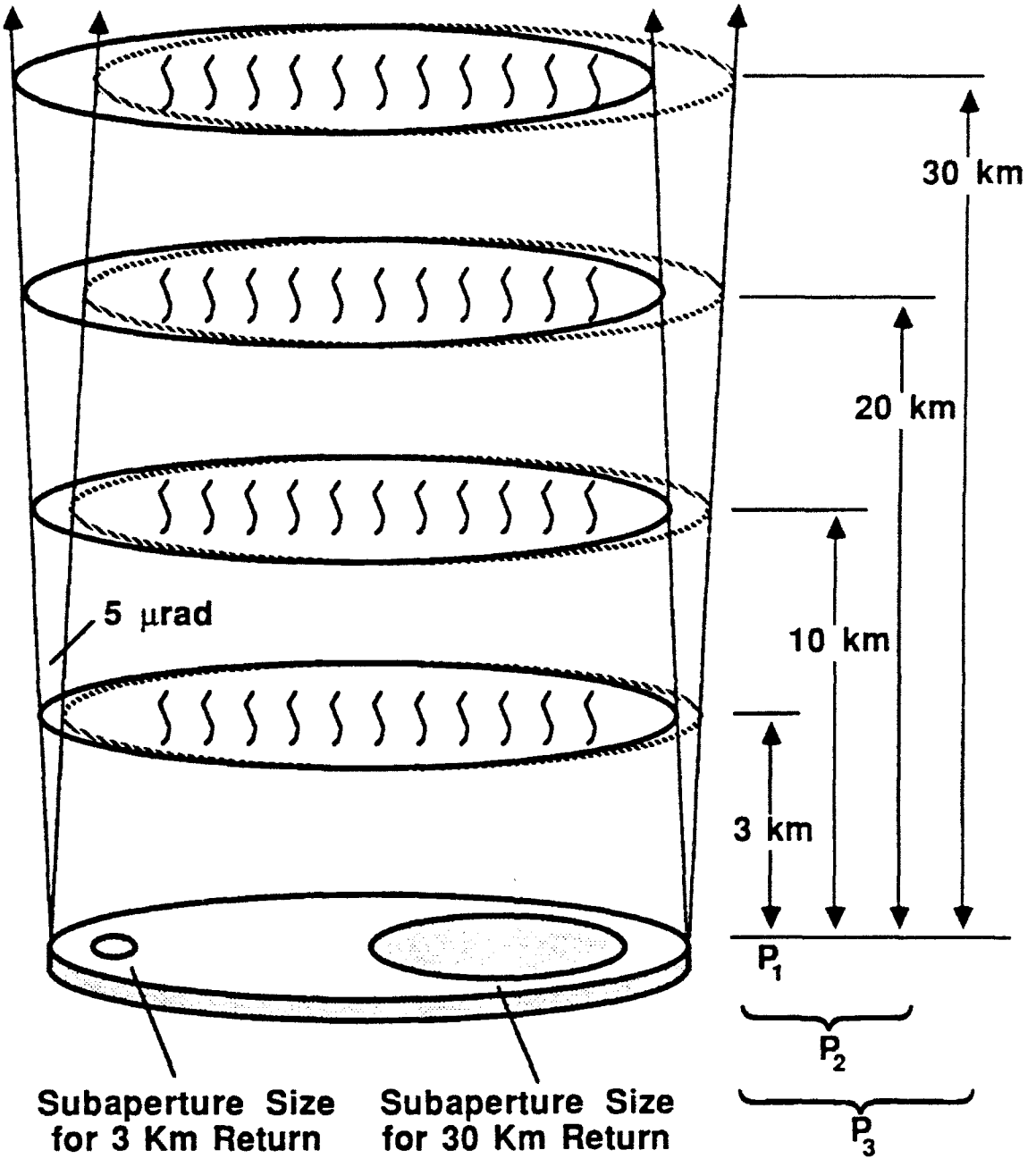

Fig. 2-5. "S" method figure correction.

pattern, which is characteristic of the integrated turbulence between the scattering layer and the transmitter, is generated in the upper atmosphere. Orthogonal polarizations are imposed on the two beams to allow them to be independently manipulated on the optical bench before recombination, thereby permitting the removal of diffraction-induced intensity fluctuations by sampling beams with several relative phase shifts. Four-bin processing, which provides reasonably good scintillation rejection, requires four separate optical paths and cameras to sample the recombined beams with 0°, 90°,180°, and 270° of relative phase difference. The structure of the requisite wavefront sensor is schematically illustrated in the lower right-hand corner of Figure 2-6. By placing a $\pi/4$ plate as indicated with its optic axes parallel to one of the shear polarizations, a 90° phase shift can be introduced into the two bottom-most beam paths on this drawing. The polarization beamsplitters would be oriented at a 45° angle to the polarization axes, thereby producing linearly polarized output beams with either a 0° or 180° phase shift between the input components. The algorithm for generating optical phase gradients from these four intensity images has the form

$$g(i, j) = \frac{(\pi/4)\left\{S_0(i, j) + 3S_{90}(i, j) - 3S_{180}(i, j) - S_{270}(i, j)\right\}}{S_0(i, j) + S_{90}(i, j) + S_{180}(i, j) + S_{270}(i, j)} - \pi/4 \qquad (2\text{-}3)$$

where $S_0(i, j)$ is the signal seen by the pixel at subaperture location (i, j) in the camera viewing the 0° phase-shifted beam. Scintillation suppression is achieved by the subaperture energy normalization of the first term in this equation.

There is at least one potentially serious problem with S-method sampling, relating to the need to obtain high-resolution imagery of high-altitude interference patterns through a partially-corrected atmosphere. If one thinks of these interference images as being produced and observed at the scattering layer, it is not difficult to imagine how this information could be used to characterize the atmosphere below. Unfortunately, in order to sample this information with a ground-based receiver, the interference pattern must pass through the same turbulence that the probe beam is attempting to measure. In principal, this apparent inconsistency can be overcome through a bootstrap procedure, in which sequential measurements are made at progressively longer ranges as a means of progressively clearing a greater fraction of the turbulence path.

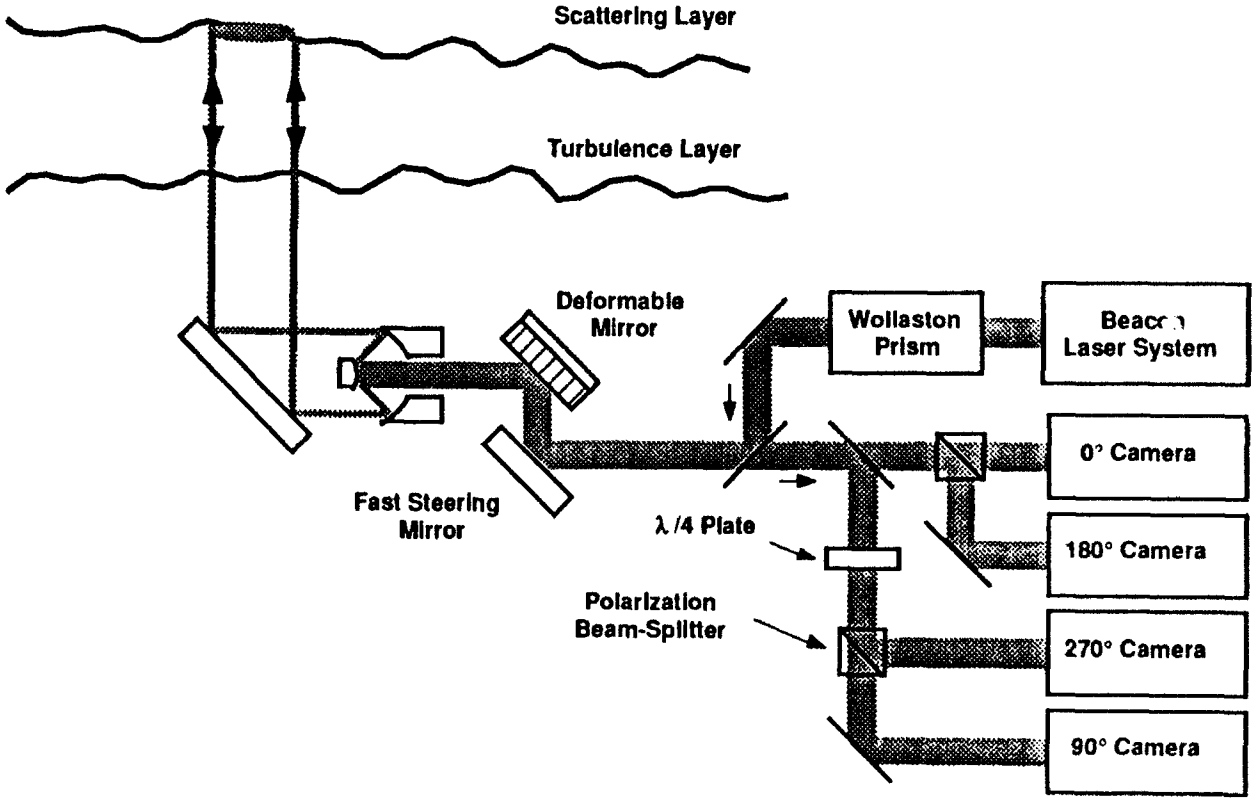

Fig. 2-6. "S" method wavefront sensor.

A second major difference between the "S" and "A" methods is associated with the use of progressively larger subapertures as the scattering layer altitude is increased. The obvious motivation for this adaptive procedure is the attendant improvement in the signal-to-noise ratio, and it is argued that the higher spatial frequencies are less important for scattering altitudes exceeding a few kilometers.

With regard to the question of scaling to larger systems, the beacon geometry and placement sequence are inherently independent of the aperture diameter for S-method sampling. As suggested in Figure 2-5, a total of six beacon pulses would be required to provide a measure of the x and y shear at four altitudes. Itek recommends that the first pair of pulses be used to probe and compensate to the first scattering layer at 3 km, returns from the second pair would be measured at 3, 10, and 20 km and used for subsequent compensation, while the third pulse pair would provide data at all four altitudes. By contrast, most of the analyses of focused beacon systems predict that the number of beacons must increase directly with aperture area to maintain constant performance.

2.3 CRITICAL TIME CONSTANT FOR PULSED CORRECTION

In at least one respect, phase-compensation hardware for synthetic-beacon systems can be regarded as unconventional and experimentally untested. All previous adaptive-compensation systems have incorporated closed-loop, null-seeking logic that is inherently insensitive to response non-linearities and calibration errors. For such systems, the requisite temporal response is specified by the Greenwood frequency,[2] which is of the order of 10-20 Hz for astronomical objects and 50-100 Hz for low earth-orbit satellites. The utilization of pulsed sources necessitates a somewhat different approach in which a completely uncorrected wavefront is first sampled, an open-loop correction is applied to the deformable mirror, and a short-exposure measurement is made of the quality of the correction. All three operations must be completed within an appropriate time interval, which becomes a primary design driver for much of the signal processing software and beam control hardware. The expression for Strehl degradation as a function of time from the point at which the turbulence sample is made is known to have the form

[2]Greenwood, Darryl P., "Bandwidth Specification for Adaptive Optics Systems," Journal of the Optical Society of America, 67, 390-393 (1977).

$$\text{Strehl} = \exp\left\{ -\left(t/\tau_c\right)^{5/3} \right\} \quad , \tag{2-4}$$

where the critical time constant is defined as

$$\tau_c^{-5/3} = 2.91 \ \sec(\zeta)\, k^2 \int C_n^2(h)\, v^{5/3}(h)\, dh \quad , \tag{2-5}$$

for a zenith angle of ζ. The standard wind velocity profile is specified by the Bufton model, in which the altitude and slew-rate parameters are represented by h and ω respectively

$$v(h) = v_g + 30 \exp\left\{ -\left[(h - 9{,}400)/4{,}800\right]^2 \right\} + \omega h \quad . \tag{2-6}$$

For a pulsed-compensation experiment, the angular slew rate ω would be 0 and the surface-level wind velocity v_g is usually assumed to be 5 m/sec. With these parameters, the critical time constant obtained for the SLC-day turbulence model is 2.4 ms. This corresponds to a 1-ms upper limit on the entire compensation and beam scoring sequence to maintain a Strehl of 0.5 or better. All of the pulsed experiment timelines for SWAT II have been developed in the context of this temporal constraint.

2.4 BEACON LASER-ENERGY REQUIREMENTS

Estimates of beacon-pulse energy requirements for A-method experiments have appeared in several analysis, and some preliminary work relating to beam quality requirements have recently been performed. A review of this work, along with a brief look at the requirements for S-method sources, is the subject of this section.

From the standard LIDAR scattering equation,[1] the following energy requirement expression is derived,

$$Q_o = \frac{(hc/\lambda)\, N_s\, (R^2/\Delta R)}{n(R)[d\sigma(\pi)/d\Omega]\, A_s \tau_a \tau_t \tau_r \eta} \quad , \tag{2-7}$$

where, for Rayleigh scattering, the following definitions and parametric values apply for SWAT II system-performance calculations. (See Section 5.0 for a more complete discussion of system throughput characteristics.)

TABLE 2-1

Rayleigh Scattering Definitions and Parametric Values

Parameter	*Definition*	*Value*
A_s	subaperture area	1×10^{-3} m^2
$d\sigma(\pi)/d\Omega$	scattering cross-section	$\approx 5 \times 10^{-57} \lambda^{-4}$ m^2/sr
N_s	photoelectrons for $\lambda/20$ phase error	400 (includes scintillation losses)
$n(R)$	molecular density	$\approx 2.6 \times 10^{29} R^{-1} \exp\{-R/9{,}000\}$ m^{-3}
R	nominal scattering altitude	10 km
ΔR	nominal scattering depth	R/10
λ	beacon wavelength	504 nm
η	detector quantum efficiency	0.1
τ_a	two-way atmospheric transmission	0.6
τ_r	phase sensor receiver efficiency	0.7
τ_t	transmitter efficiency	0.5

Applying Equation (2-7) to the numbers and parametric relationships presented in this table provides an approximate relationship between the pulse energy and the scattering altitude that is reasonably accurate for the altitudes of interest,

$$Q_o \text{ (J/pulse)} \approx 3.7 \times 10^{-9} R^2 \exp\{R/9{,}000\} \ . \qquad (2\text{-}8)$$

This corresponds to a minimum energy requirement of 1 J to achieve $\lambda/20$ compensation with a beacon placed at a mean altitude of 10 km.

Similar calculations can be made for sodium backscatter, but with the restrictions that the pulse energy is contained within the 2-GHz resonant bandwidth and the spot-energy density is held below the 3×10^4 W/m^2 sodium-saturation intensity. Two cases are of interest: the first employs the sodium beacon to perform full-aperture phase compensation in the conventional

way; the second uses the high-altitude beacon in conjunction with one or more low-altitude sources to remove residual low spatial-frequency turbulence components. In the latter case, the effective subaperture diameter is equal to the section diameter, thereby requiring a much more modest output from the beacon laser.

TABLE 2-2
Sodium Resonance Scattering Definitions and Parametric Values

Parameter	*Definition*	*Value*
A_s	subaperture area (single source)	1×10^{-3} m^2
A_s	section area (2-altitude stitching)	7×10^{-2} m^2
$d\sigma(\pi)/d\Omega$	scattering cross-section	7×10^{-17} m^2/sr
N_s	photoelectrons for $\lambda/20$ phase error	400 (includes scintillation losses)
n(R)	molecular density	3×10^{9} m^{-3}
R	scattering altitude	90 km
ΔR	scattering depth	10 km
λ	beacon wavelength	589 nm
η	detector quantum efficiency	0.1
τ_a	two-way atmospheric transmission	0.6
τ_r	phase sensor receiver efficiency	0.7
τ_t	transmitter efficiency	0.5

For this set of conditions, the requisite pulse energies for single-beacon correction and section stitching are as follows,

$$Q_o = \begin{cases} 25 \text{ J/pulse} & : \text{single - beacon correction} \\ 0.4 \text{ J/pulse} & : \text{high - altitude section stitching} \end{cases} . \qquad (2\text{-}9)$$

Work is currently in progress in the Lincoln's Solid-State Division to construct a 0.5-J/pulse laser that could be used to conduct a sodium stitching experiment within the first year of field

operation.

The construction of high-repetition rate lasers in the 1-10-J range is by no means a trivial exercise, and the associated technical risk is strongly tied to the perceived requirements on beam quality. At this point only limited analytical data exist linking beacon size and phase-sensing errors, but in two preliminary studies conducted at Lincoln it has been shown that anisoplanatic effects appear not to grow with beam diameter until the beacon exceeds the dimensions of the receiving aperture. The output from one of these studies is shown in Figure 2-7, which is an evaluation of SWAT II reconstruction errors for a single low-altitude beacon placed at 5 km. It can be seen that the system performance does not begin to depart significantly from the point-source baseline until the beacon diameter exceeds the 60-cm LBD (laser beam director) aperture diameter, which means that β values as large as 20 or 30 may be tolerable for A-method beacon lasers.

Beacon requirements for S-method compensation have thus far received only cursory analytical attention at Lincoln Laboratory, but the net energy demands for this approach appear to be very similar to those for A-method correction. The quantity of interest is $N_b Q_o$, which is the product of the requisite energy per pulse at a given compensation altitude and the number of beacons needed for acceptable compensation. As discussed earlier in this section, A-method sampling places one beacon over each d_o–sized aperture section, and all of the incident energy collected by an r_o-sized subaperture is used to make a gradient measurement. The effective depth of the allowable scattering region is usually assumed to be of the order of R/10. S-method sampling employs two collimated beams sheared in orthogonal directions to produce interference patterns that are imaged by receiver, and at least two sets of beams would be required to achieve compensation to 10 km. Therefore, the number of beacons deployed with this approach is at least 4. And although all of the energy reaching the detector array is collected by the entire aperture, each subaperture sees only an r_o–sized piece of the beam. The scattering depth in this case is restricted by the need to avoid crosstalk in the mapping of adjacent subapertures into the illuminated region. Given these assumptions, an estimate of the A-method/S-method net energy ratio can be developed;

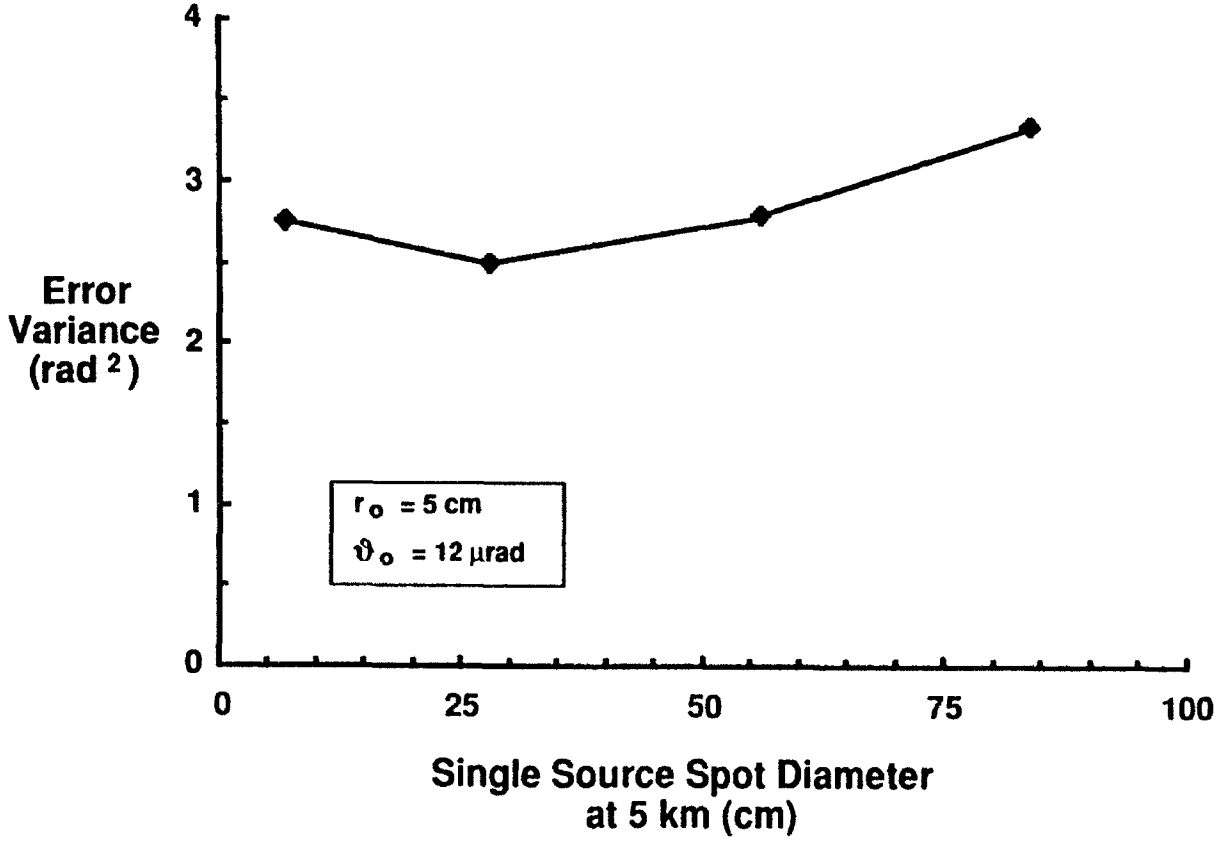

Fig. 2-7. Effect of source diameter on phase reconstruction error.

$$N_b Q_o \sim \frac{\{\text{number of beacons}\}}{\{\text{fraction of beacons viewed}\}\ \{\text{fractional receiver area}\}\ \{\text{fractional scattering depth}\}}$$

from which it can be seen that

$$N_b Q_o \sim \{(D/d_o)^2\} / \{1\}\ \{(r_o/D)^2\}\ \{1/10\} \qquad : \text{A-method}$$

$$N_b Q_o \sim \{4\}/\{(r_o/D)^2\}\ \{1\}\ \{r_o/D\} \qquad : \text{S-method} \ .$$

Notice that the photon collection factors $(r_o/D)^2$ are identical in these two expressions, so that any differences are driven by the beacon count and the scattering depth. The energy ratio would be

$$N_b Q_o (\text{A} - \text{Method}) / N_b Q_o (\text{S} - \text{Method}) \approx 2.5 D r_o / d_o^2 \qquad (2\text{-}10)$$

which is nearly unity for D = 1 m, r_o = 4 cm, and d_o = 30 cm. While it is likely that S-method beacon deployment will be the more attractive approach for very large apertures, neither technique appears to have a clear advantage for the demonstration systems planned for the near term.

3. SWAT II FIELD HARDWARE DESCRIPTION

In order to set the stage for the subsequent discussions of laboratory and field experiments, it will be useful to briefly review the baseline field configuration. Although a significant amount of rethinking has taken place during the past year in support of additional modes of operation, in many respects the present design is still optimized for an A-method stitching experiment. Considerably more work will be needed to prepare for the proposed S-method compensation measurements included in the present test plan.

The principal elements of the SWAT II system can be loosely organized into four semi-independent subsystems: External Beam Control and Tracking, Wavefront Control and Scoring, Dye-Laser Beacon Projection, and Experiment Control and Data Collection. The salient features of each of these subsystems are described in this section, along with a brief description of the laboratory layout at AMOS.

3.1 EXTERNAL BEAM CONTROL AND TRACKING

The acquisition and tracking procedures planned for the SWAT II experiments are essentially identical to those used previously during the third phase of the ACE program, in which compensated laser beams were projected from the 60-cm Laser-Beam Director (LBD) at AMOS to instrumented rockets launched from Kauai. A schematic of the ACE tracking system is shown in Figure 3-1. As indicated, final hand-off to the optical bench trackers is accomplished in three stages, with each tracking component having access to nominal flight parameters prior to launch. Initial acquisition, aided by a C-band transponder carried on board the rocket, is usually achieved immediately after lift-off by an FPQ-14 radar at Kaena Point, Oahu and an FPS-16 radar at Kokee Park, Kauai. Data from these instruments are fed into the trajectory computer at the AMOS facility, which then directs either the 1.2 or 1.6-meter optical telescopes to visually acquire the target vehicle using illumination provided by a pair of flashing lights situated at the rear of the payload. The accuracy of the subsequent hand-over to the Laser-Beam Director is generally better than 20 μrad. In the SWAT system, loop closure around the 20-μrad precision tracker will be achieved with the aid of a boresighted television camera covering a 1-mr field of view and a 300-μrad wide FOV tracking camera.

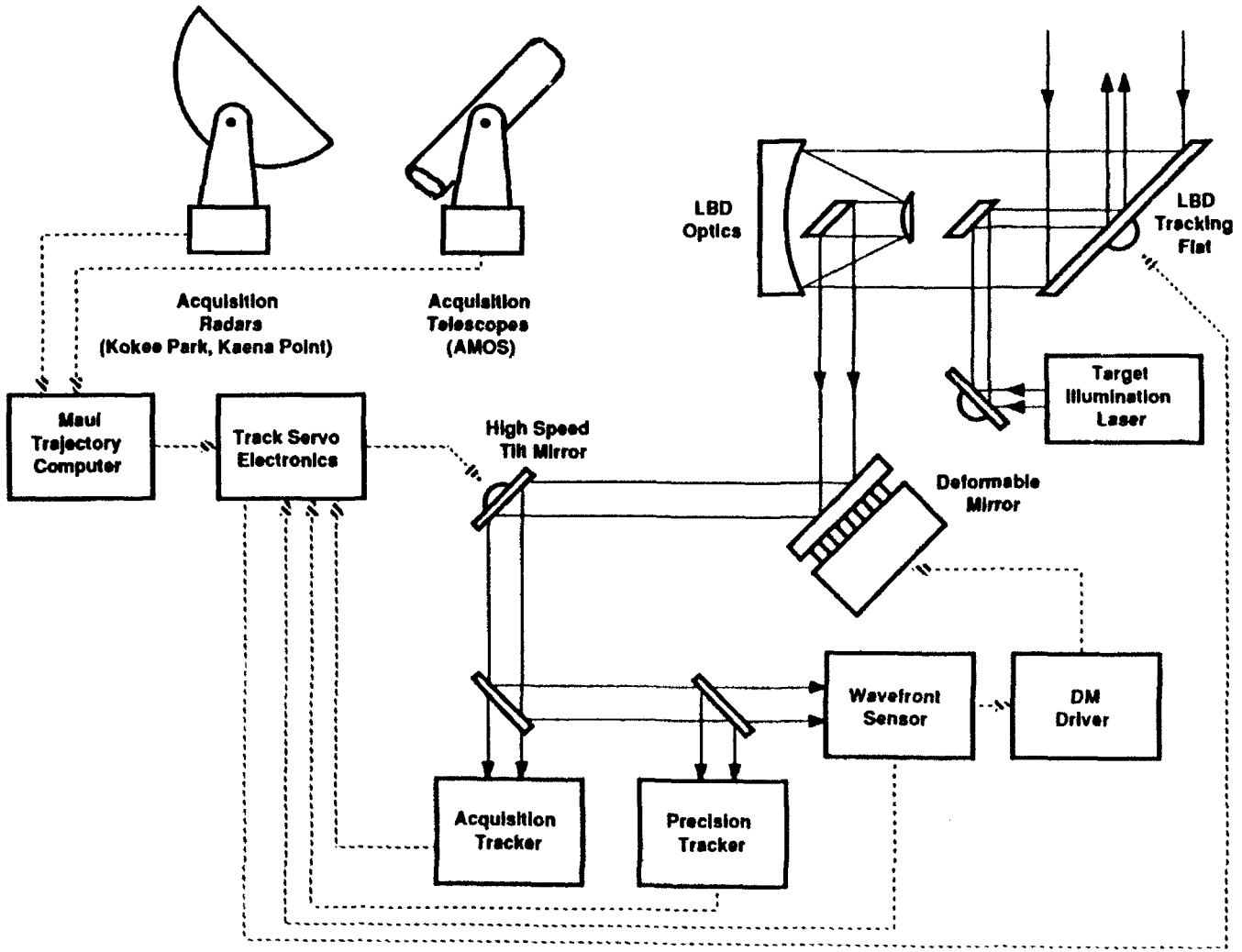

Fig. 3-1. Acquisition and tracking systems.

As discussed later in the Wavefront Control section of this report, high-precision tracking and pointing is achieved in a cooperative engagement through the placement of a bright beacon at an angle ϑ_{PA} = (2 x target velocity / speed of light) ahead of the target array. In the early SWAT II experiments, this source will be provided by a retroreflector mounted on the target and illuminated from the ground by a CW argon-ion laser operating at 488 nm. (This arrangement will also allow the high-spatial-frequency adaptive-optics system to operate in a fully-cooperative mode, thereby establishing a baseline against which the performance of the synthetic-beacon phase-compensation may be compared.) The retro-illumination laser is directed by a flat mirror that is mounted behind the secondary of the LBD and is conically scanned to provide an amplitude-modulated return signal that is used to center the beam. Once loop closure is achieved, error signals generated by the precision tracker are used to drive a 250-Hz fast-steering mirror on the optical bench. A signal proportional to the position of the fast-steering mirror is used to unload large-amplitude, low-frequency target motion to the Laser-Beam Director. Data from the LBD under precision-track control can be transmitted to the AMOS computer to continuously update the target trajectory, so that the acquisition sequence can be reentered in the event that the optical tracking loop is broken for any reason. It is standard practice to keep all acquisition and tracking aids on-line throughout an experiment.

3.2 WAVEFRONT CONTROL AND SCORING

The purpose of the Wavefront-Control Subsystem is to measure the atmospheric turbulence between the transmitter and the target, and subsequently impose the conjugate-phase error onto the deformable mirror. Under ideal conditions, an object viewed along the line of sight of the wavefront sensor can be imaged with diffraction-limited resolution, and a laser beam projected along the same path will exhibit diffraction-limited divergence characteristics above the atmosphere. Therefore, a quantitative evaluation of system performance can be achieved through an analysis of the beacon image at the wavefront sensor, or by a beam profile measurement of a laser projected to an instrumented exoatmospheric target. Figure 3-2 illustrates the the functional relationships between the major components of this subsystem.

The basic design parameters for the SWAT II system derive from the Laboratory's experience with the ACE test series, which established an upper limit of about 4 cm on actuator spacing and a 1-msec closed-loop response-time requirement for achieving high Strehl ratios at

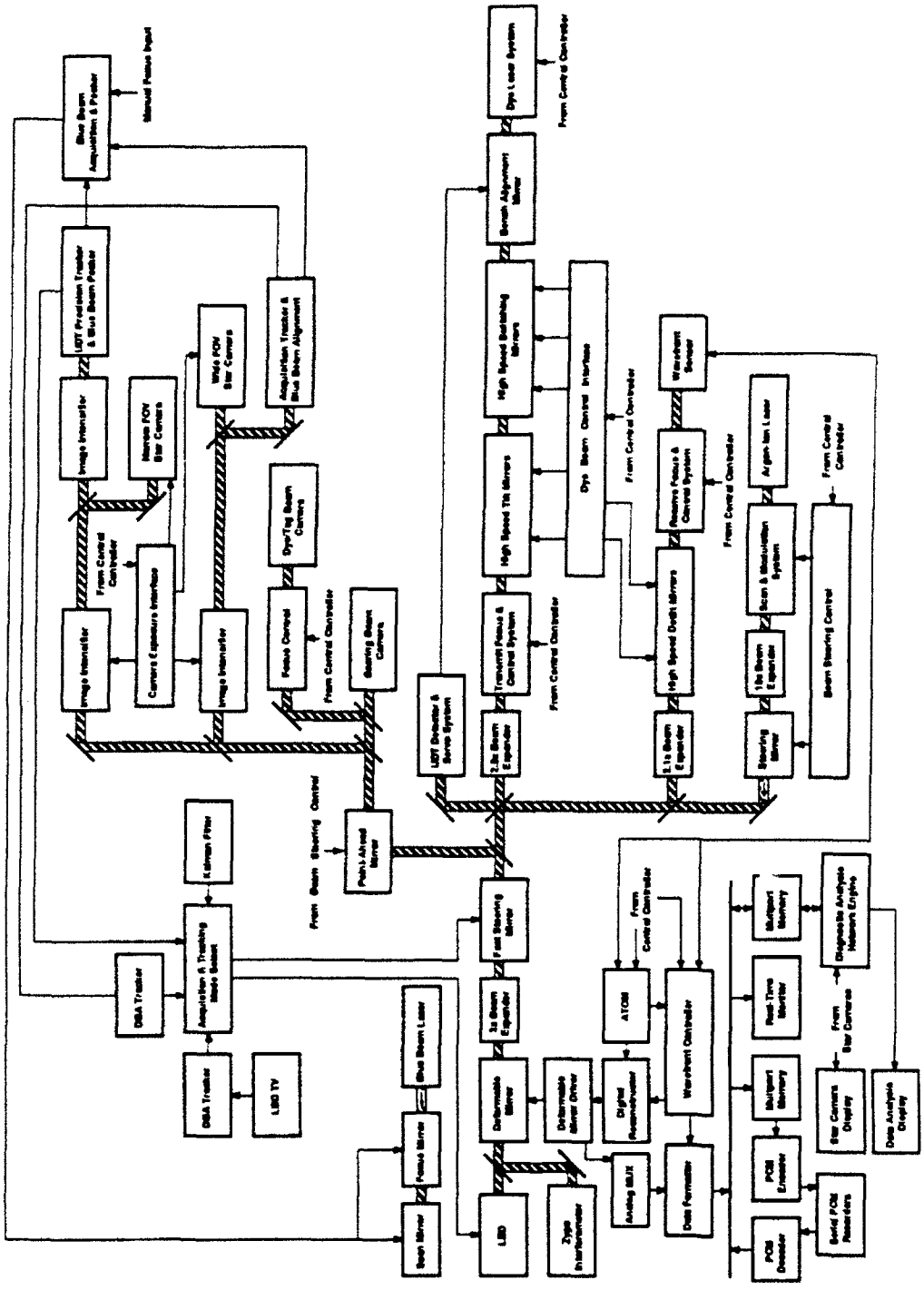

Fig. 3-2. SWAT II system block diagram.

visible wavelengths. Sufficient beacon radiation in the point-ahead direction must be provided to allow each subaperture to record at least 200 photoelectron events per dwell time. These restrictions led to the specification of a high-bandwidth, 241-actuator deformable mirror and mating wavefront sensor to be used with the 60-cm AMOS transmitter. A summary of the more interesting SWAT II component characteristics is provided in Table 3-1.

The Laser-Beam Director incorporates a series of fixed mirrors and beam expanders, which permit transmit and receive beams to be changed in size to use the full 60-cm Cassegrain telescope at the top of the dome tower. As shown in Figure 3-3, the output from the stationary Cassegrain is directed by a 1-m gimbaled tracking flat, which is capable of pointing the out-going beam through a 180° angle in azimuth and from -2° to 95° in elevation. The entire beam-director assembly is mounted on an azimuth turntable that is positioned and locked prior to a tracking operation. With the exception of the target-illumination laser, all transmit and receive beams follow a common path through the LBD. The retro-illumination beam (generally referred to as the blue beam) originates from an argon-ion laser situated inside the tracking dome and passes through a gimbaled, 5-cm mirror positioned in the shadow of the Cassegrain secondary. Radiation received by this mirror is used in a hill-climbing servo designed to maintain the center of the blue beam on the target's retroreflector.

The deformable-optics subsystem includes a modified Hartmann phase-gradient sensor, a digital phase-reconstruction unit, and a rapid-response deformable mirror (DM). The wavefront sensor has been built specifically for pulsed operation by the Adaptive Optics Associates Division of United Technologies and incorporates a number of novel and proprietary concepts. A block diagram of the main components of the Adaptive Optics Associates' sensor is presented in Figure 3-4. Two intensifier/detector assemblies record the centroids of an array of 224-subaperture fields generated by multiple lenslet modules (MLM) positioned in front of each unit. Each detector focal plane is made up of an array of 64 x 64 pixels that are electronically segmented into 4 x 4 pixel subapertures. The x and y-phase gradients are determined by the misposition of the spot centroids with respect to the center of each subarray.

TABLE 3-1

Wavefront Control Characteristics

Telescope
- 60-cm Cassegrain
- 18-cm central obscuration

Wavefront Sensor
- 16x16 modified Hartmann array
- 224 x and y toe-to-tail gradients operations /channel/sec
- 100-μsec reconstruction delay
- λ/20 performance with 4,000 input photons

Deformable Mirror
- 17x17 edge-clipped array
- 241 actuators
- 3.5-cm actuator spacing

Precision Tracking Laser
- 1-watt argon-ion
- $\lambda = 457.9$ nm

Digital Reconstructor
- 241 parallel channels
- 10^7 multiply & add

Scoring Laser
- 1-watt argon-ion
- $\lambda = 514.5$ nm

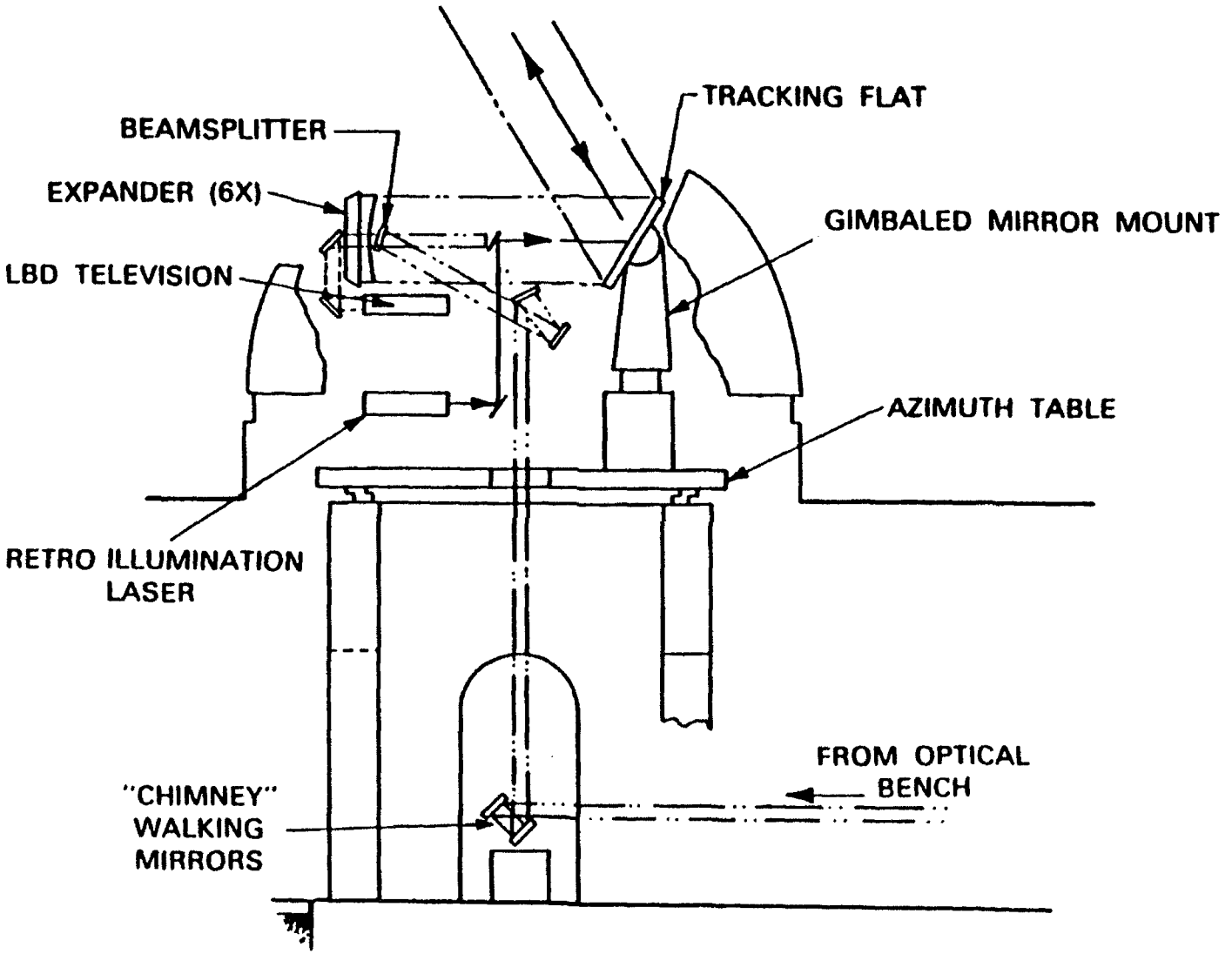

Fig. 3-3. Laser beam director schematic.

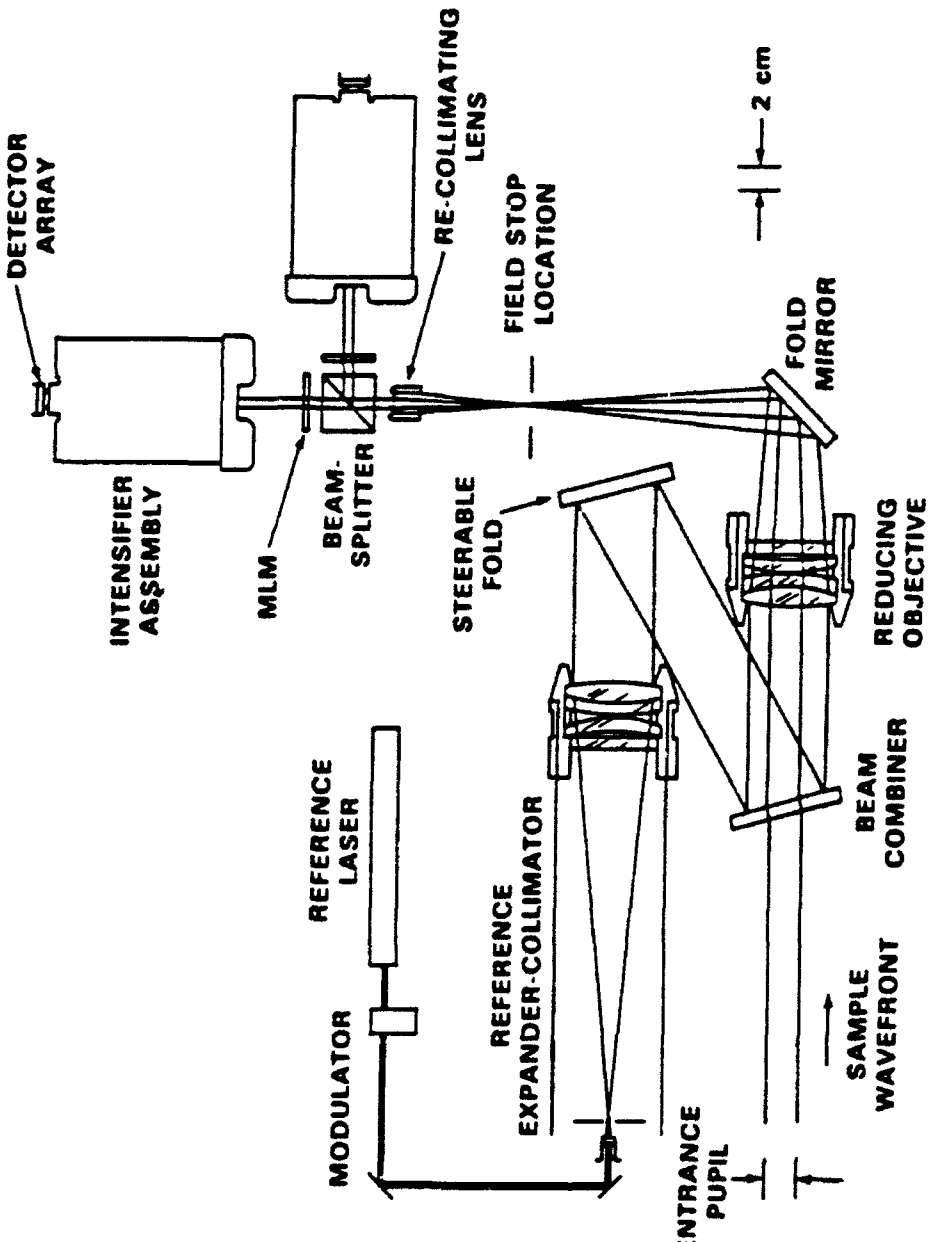

Fig. 3-4. SWAT II wavefront sensor optics.

These gradients are subsequently fed into a digital phase reconstructor designed and constructed at Lincoln Laboratory. The reconstruction of these data is performed by a matrix-multiplication operation requiring 500 separate add and multiply operations for each phase value using precalculated matrix coefficients. All phase points are computed simultaneously by using 241 identical parallel channels. Through the use of special purpose multiplier/accumulator chips the entire reconstruction process can be performed in less than 100 μsec, and a new set of matrix elements can be loaded into the reconstructor in less than 1 msec.

The 241-actuator deformable mirror purchased for this experiment was developed by the Itek Optical Systems Division of Litton Industries. The architecture illustrated schematically in Figure 3-5 incorporates a continuous faceplate common to all previously fielded systems, but the requirement for pulsed compensation necessitated some departure from prior designs. Specifically, the piston actuators used in this mirror are fabricated from lead magnesium niobate (PMN), which was selected on the basis of its low creep, high-voltage sensitivity, and hysteresis characteristics. Itek estimates that stable $\lambda/20$ performance can be achieved in less than 200 μsec.

Table 3-2 lists these key elements and the temporal delays associated with the specified functions. Each of these components have been developed specifically for the SWAT II program, and each represents state-of-the-art technology optimized for performance and speed. As a result, no major improvements to the numbers listed below are to be expected within the time frame of this field exercise. The impact of these component-induced delays depends on the number of beacons deployed and the number of mirror corrections made within the phase correction interval. Timing diagrams for the first of the SWAT II experiments are presented in Section 5.0.

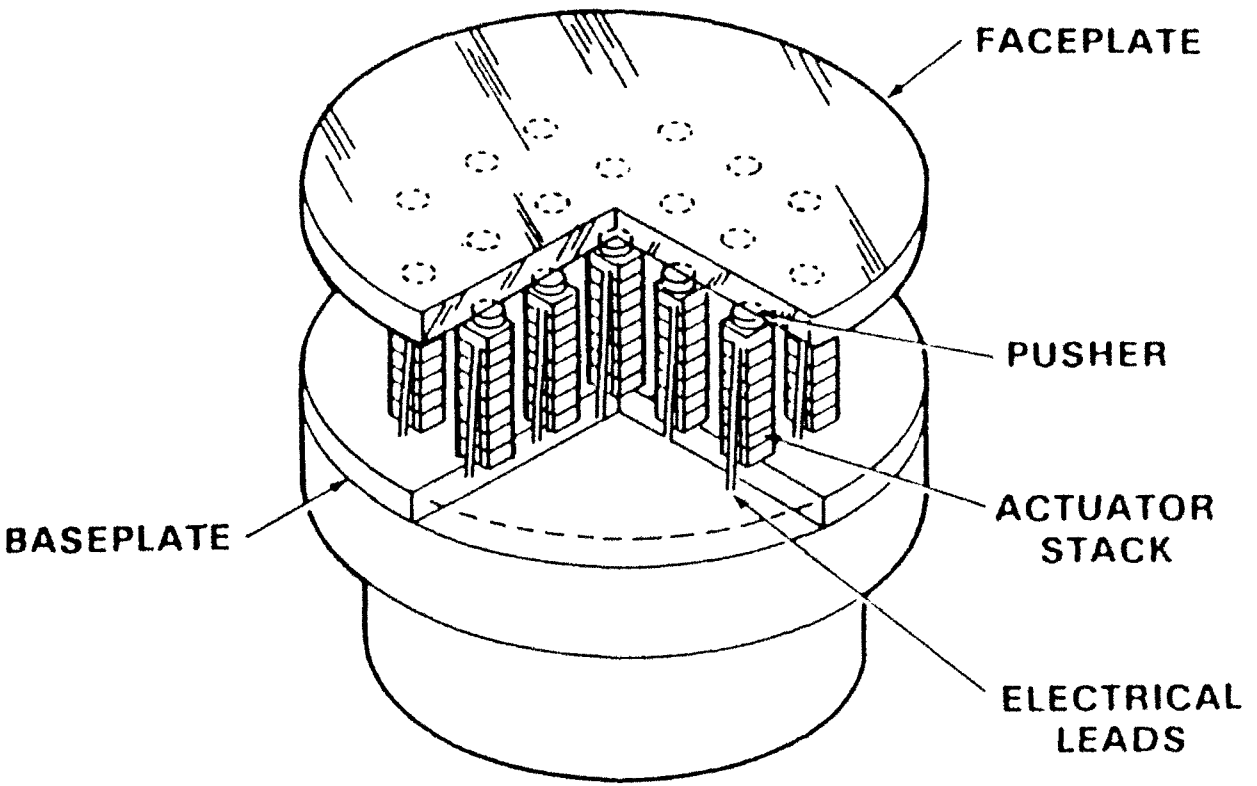

Fig. 3-5. SWAT II deformable mirror.

TABLE 3-2

System Component Time Constants

System Component	*Time Constant*
Phase Sensor	65 μsec data transfer
Reconstructor	55 μsec data processing interval
Deformable Mirror	200 μsec settling time
Switching & Tilt Mirrors	125 μsec settling time
CCD Camera System	20 μsec fast clear or buffer storage 500 μsec data transfer interval

3.3 SYNTHETIC BEACON LASER SOURCES

The beacon laser projection system is unquestionably one of the higher-risk elements of the SWAT II system, owing to the need to simultaneously achieve high-pulse energy, good beam quality, and high-pulse repetition rates. It became evident early in the design phase of this program that a multiple-beacon experiment would require multiple laser sources, which led to a decision to procure 6 laser units to allow for 4 primary sources, one precursor beacon, and one spare laser. A list of the source characteristics relevant to this discussion is given below.

TABLE 3-3

Synthetic Beacon Projection System Goals

Number of Beacons	6 (4 beacons, 1 precursor, 1 spare)
Pulse Energy	5 to 10 J/pulse
Beam Quality	75% of energy within 15 λ/D
Wavelength	450 to 550 nm
Spectral Bandwidth	< 1 nm
Pulse Length	< 2 μsec
Repetition Rate	5 to 10 pulses per second
Operating Time	> 30 minutes continuous operation

The repetition rate and continuous-operating-time requirements listed above are somewhat arbitrary and perhaps overly stressful, but would be highly desirable capabilities for the rocket scoring tests in which limited data collection intervals would be available. The energy requirements are also significantly larger than the first-order signal-to-noise calculations would require, but system throughput efficiencies are always somewhat less than anticipated.

Taken in total, the specifications listed in Table 3-3 were beyond the state-of-the-art for off-the-shelf hardware when the initial engineering designs were performed in 1984, but appeared to be most readily achievable with dye-laser technology. A prototype unit, obtained from Candela in 1985, is a modified version of their commercial flashlamp-pumped LFDL-20 dye-laser. It has since been extensively modified and improved as a result of a joint effort between Lincoln Laboratory and Candela, to increase the confidence that the design goals can be safely maintained in field operation.

The prototype laser initially comprised a pair of identical laser heads in a master-oscillator, power-amplifier (MOPA) configuration. An alternative configuration has since been developed in which both heads are placed in a single unstable resonator. This "double-dip" approach corrects many of the parasitic problems experienced with the first design.

Each of the laser heads contains a dye cell, roughly 24 inches long, through which a solution of Coumarin 504 dye flows longitudinally. To minimize the flammability risk at the 10,000-ft site altitude, a dye solvent mixture of 30% acetamide in water was selected following an extensive series of tests in which pulse energy, beam quality, and dye lifetime were measured. The dye cells are pumped by a pair of water-cooled, linear flashlamps in a close-coupled arrangement. The heads are individually supported by an associated modulator, which delivers 500 Joules to both lamps. The modulator uses spark gap switching and stores the pulse energy in 0.66-μF capacitors at 40 kV.

Each of the 6 laser sources required for the SWAT experiments will be generated by a separate dual-head confocal unstable resonator having a magnification of approximately 3; this geometry is indicated in Figure 3–6. For alignment purposes, a common argon-ion laser beam will be inserted into all of the resonator cavities through a series of 5% beamsplitters. This chain of beamsplitters also allows a portion of the dye-laser output to be directed into a series of

diagnostic devices that measure pulse energy, shape, timing, and far-field distribution. The entire assembly will be mounted on a custom-made 9'x16' vertical bench and completely enclosed by a screen room to provide electrical isolation from rest of the SWAT system. A drawing of the optical bench layout showing the laser heads, beam-steering mirrors, tag laser, and diagnostic equipment can be found in Figure 3-7.

Two external support systems are required to maintain long-term operation of the dye–laser system. The heat exchanger manifold for thermal stabilization is shown in Figure 3–8. When the lasers are running at full power, about 250 kW will be dissipated for periods of the order of 10 minutes. A 10,000 gallon tank of chilled water will be maintained as a temporary dump for these thermal bursts. The fluids leaving the lasers are restored to the desired temperature by means of actively-controlled heat exchangers connected to the chilled water reservoir.

Dye maintenance is a second concern, since the laser output degrades rapidly as a result of dye break-down produced by the intense flashlamp illumination. Present estimates point to a need for more than 30,000 gallons of fresh dye solution to sustain operation for a 30 minute period. Since a dye reservoir this large is not practical at the site, a real-time, dye-regeneration system with a capacity of about 360-gpm has been designed. The unit will consist of a bank of standard 30 inch activated carbon filters that are capable of absorbing 435-g of dye and degradation products. The rate at which the old dye is removed and fresh dye is added to the dye mixture is controlled by a pair of optical analyzers that measure the transmission, one near the 504-nm lasing wavelength, and the other in the absorption band of the dye at about 450 nm. The regeneration system is designed to maintain constant transmission loss under either continuous or intermittent laser operation. A schematic of this unit can be found in Figure 3-9.

3.4 EXPERIMENT CONTROL AND DATA COLLECTION

Due to the complexity of the SWAT II system and the short test duration of the planned rocket propagation experiments, a decision was reached early in the development of the SWAT hardware to incorporate a high degree of automated control and an on-line data-analysis capability. The overall organization of the more important components of the control and

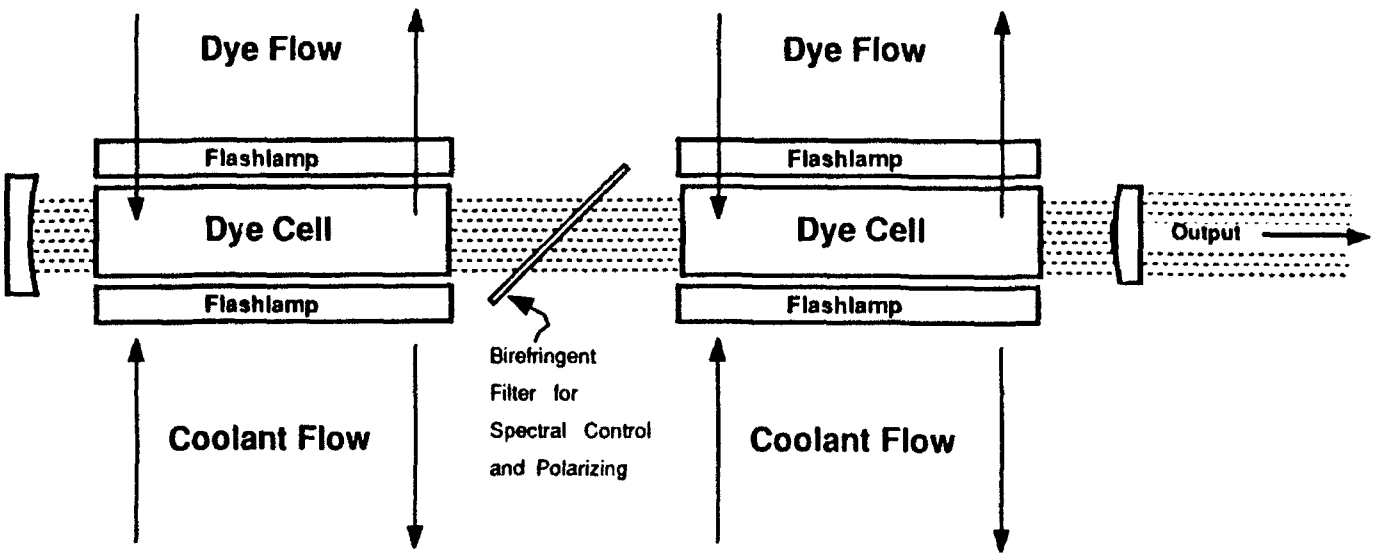

Fig. 3-6. Dye laser optical head.

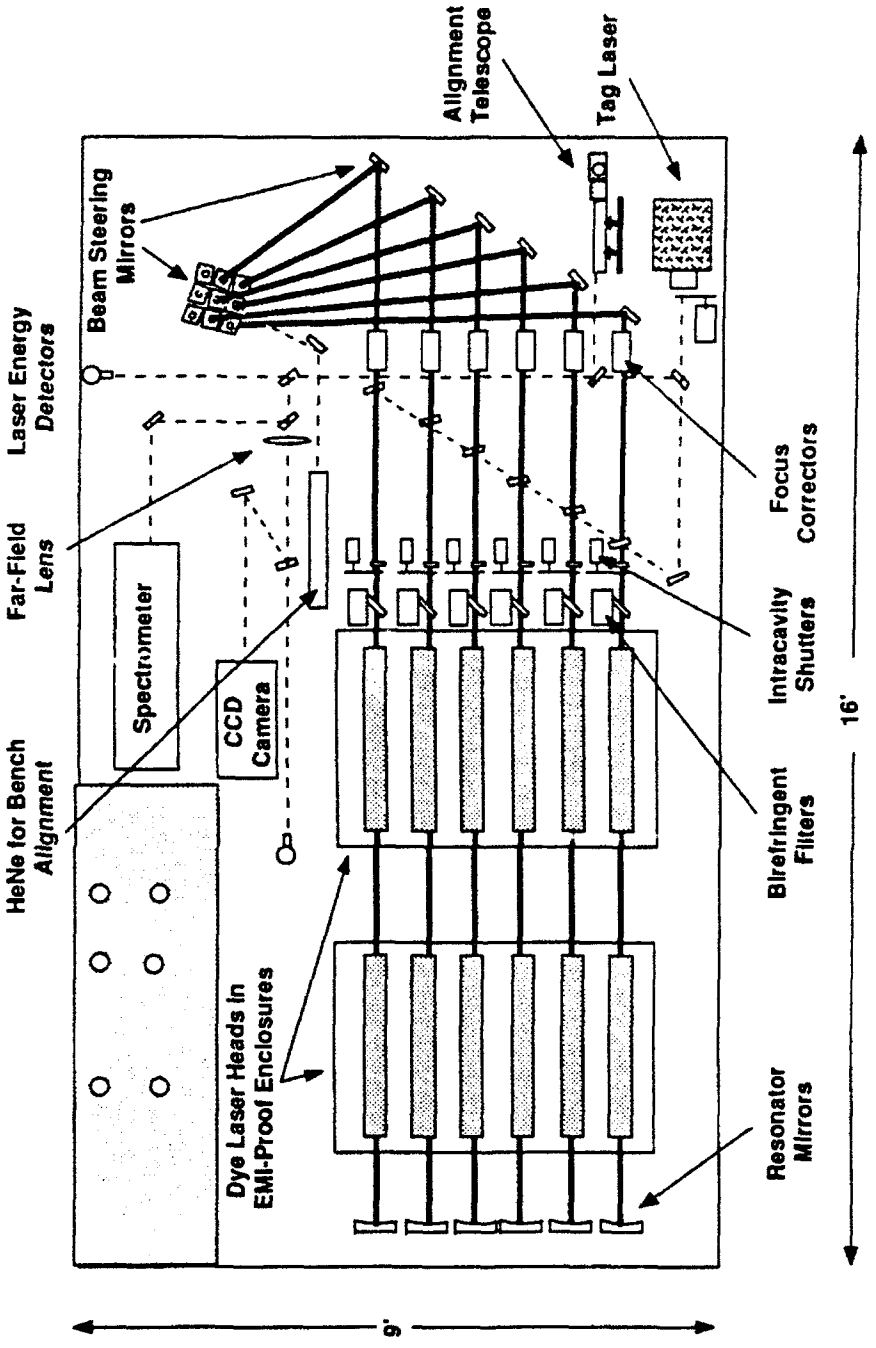

Fig. 3-7. Dye laser bench layout.

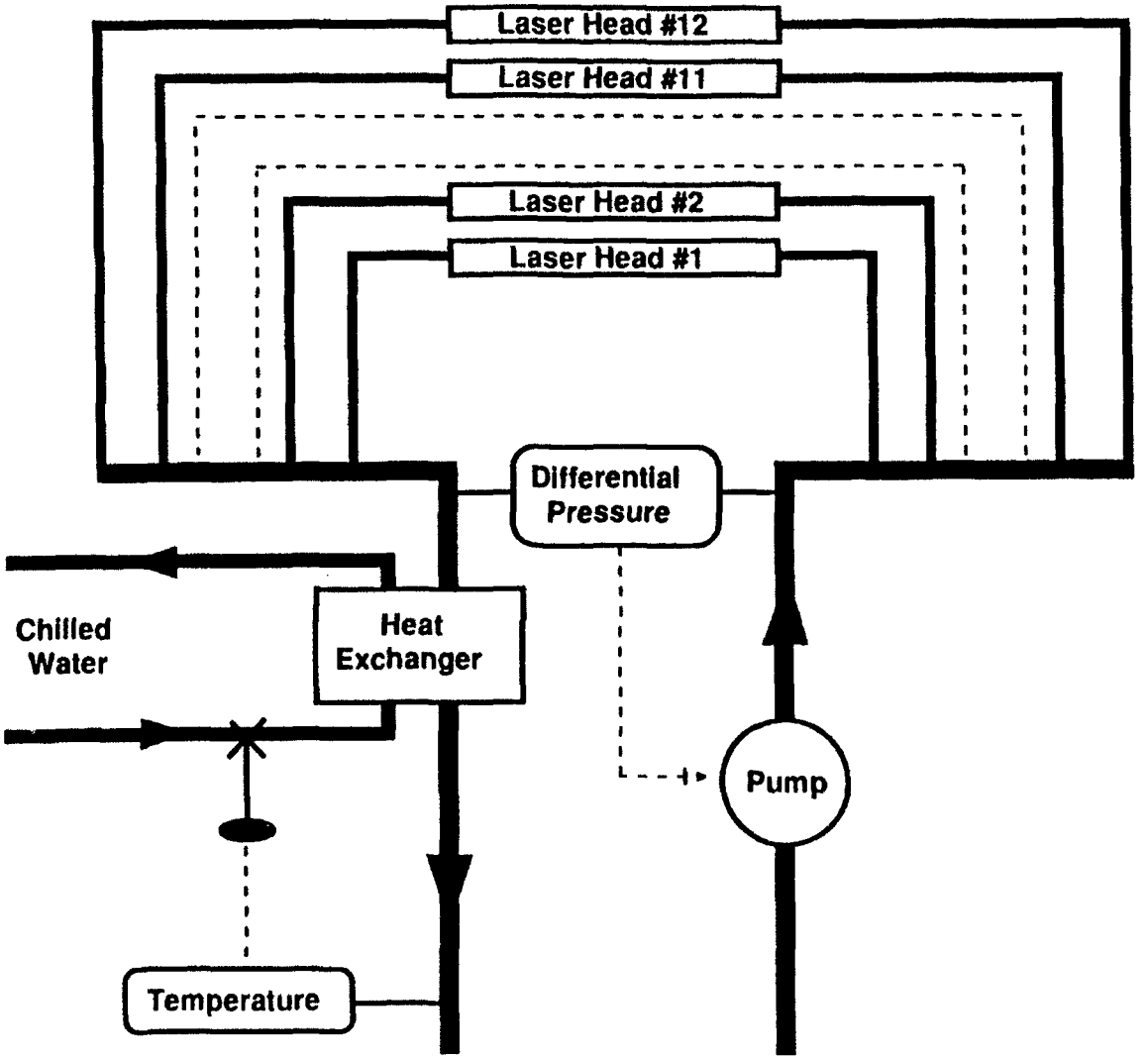

Fig. 3-8. Dye laser heat exchanger.

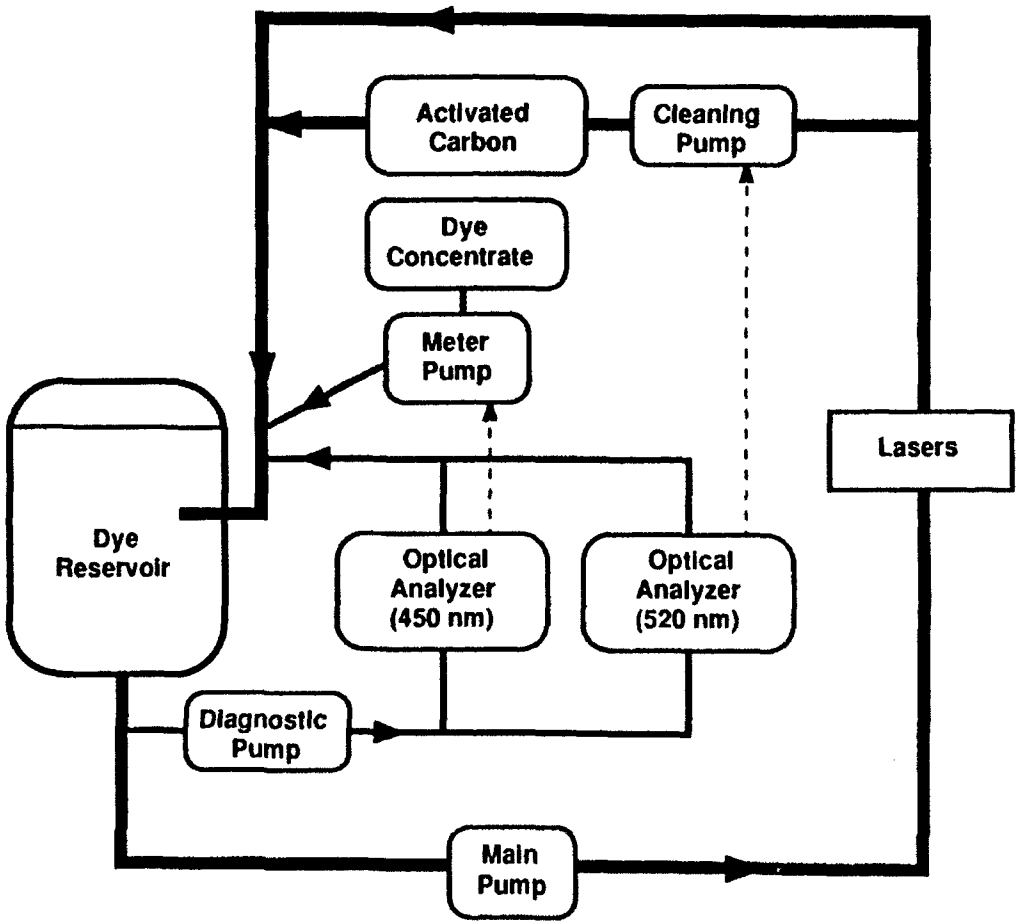

Fig. 3-9. Dye laser dye cleanup system.

recording subsystems is indicated in Figure 3-10. The heart of the control subsystem is a Laboratory-constructed programmable unit based on the Intel 286/310 processor chip, which is referred to in the system diagram as the Executive Controller. Human interface to the processor is provided by way of a menu-driven touch-screen and is linked to resident software capable of handling a wide range of scoring scenarios. The Executive controller interacts directly with all of the time-critical data collection sensors and indirectly with the phase-compensation system via the Wavefront Controller.

The recording subsystem comprises a pair of 14-track analog tape drives (for redundancy), which use a pulse-code-modulation data-collection format that provides an average data-rate capability of 10^6 12-bit words/second per track. The recorders are linked to the rest of the system through a set of formatted data buses, two of which are shown in the previous figure. The archived data include operational-mode and status parameters, a complete set of system-health indicators (such as the pulse energy from each of the dye lasers), and data from each of the primary system-performance sensors. Much of the low-bandwidth data is multiplexed onto single tracks through data formatters, such as the one shown for the phase compensation system. The high-bandwidth data generated by the CCD far-field imaging cameras is handled by a separate bus and uses a dedicated recording track.

A sample of some of the more important parameters and their associated recorder formats is tabulated in Table 3-4, and a complete set of track assignments is provided in Figure 3-11.

Direct interaction with approximately 10% of the data collected during CW operation of the compensation system is possible via a micro-VAX computer that is tied into both the compensation system and CCD camera data buses. This "quick-look" capability is expected to be particularly useful for obtaining immediate beam-quality information from either the far-field CCD cameras on the optical bench or target-mounted sensor arrays. A limited on-site analysis capability is available by operating the recorders in a play-back mode, thereby placing the data back onto the buses for post-experiment acquisition by the VAX computer.

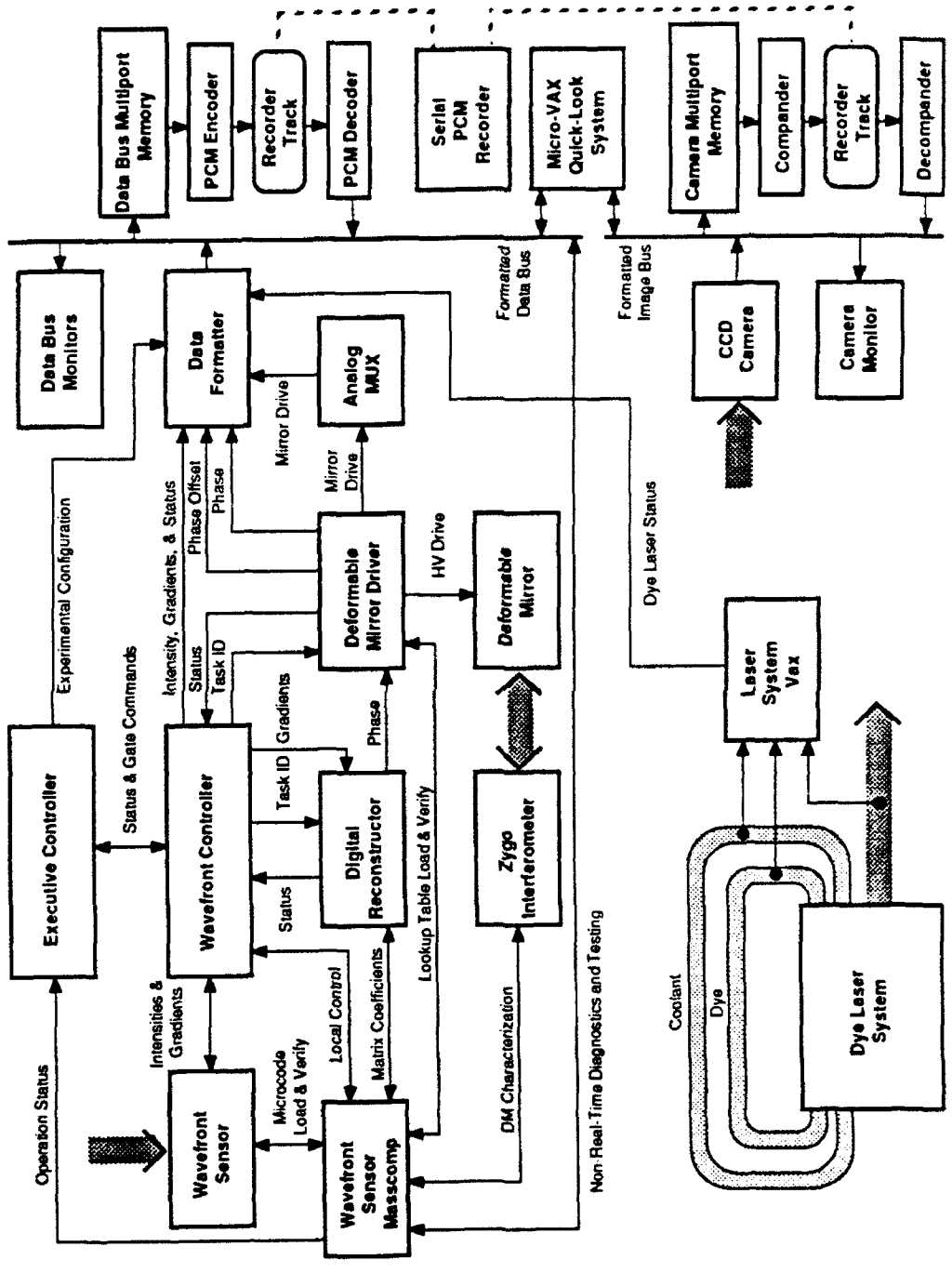

Fig. 3-10. Control and recording systems.

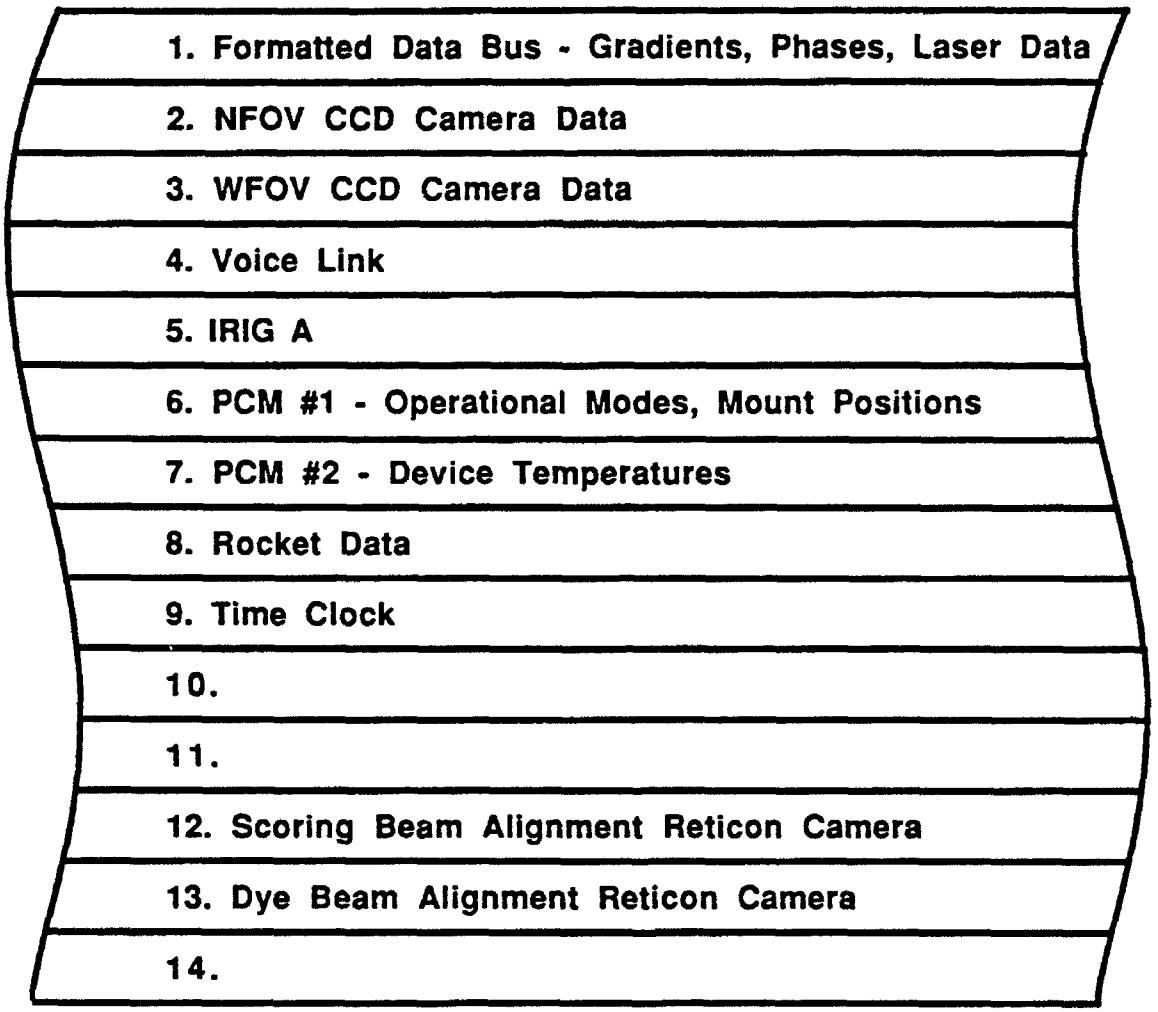

Fig. 3-11. Analog recorder track assignments.

TABLE 3-4

Primary Data Recording Parameters

Parameter	*Words/Sample*	*Bits/Word*
x & y Gradients	448	8
x & y Intensities	448	10
Reconstructed Phases	241	10
DM Drive Voltages	241	10
Wide & Narrow FOV CCD Cameras	8192	8 (companded)

3.5 AMOS LABORATORY LAYOUT

Following the completion of a series of laboratory integration tests at Lincoln, the SWAT system will be installed at the AMOS facility atop Mount Haleakala in Maui, Hawaii. This equipment will occupy the same laboratory space used by Lincoln during the Atmospheric Compensation Experiment program, as well as a 2,600 square foot addition constructed to house the dye laser-optics and support facilities. An exterior chiller farm and fluid-storage unit have also been constructed about 60 yards southwest of the main building to service the dye laser system.

A simplified floor plan of the new laboratory area in the AMOS building is shown in Figure 3–12. The space is divided into several large rooms that can be optically and thermally isolated from one another, thereby minimizing non-common-path turbulence effects while maintaining a reasonably comfortable work environment. Communication between these areas is aided by an intercom network and several television cameras.

The main optics bench supporting the all of the adaptive phase-correction elements is situated next to the Laser Beam Director tower, both of which are housed in the Optics Laboratory shown in the lower-right corner of Figure 3-12. The bench is a 9'x12' Newport table, which sits on a seismically isolated slab. The optical transmit/receive interface between the

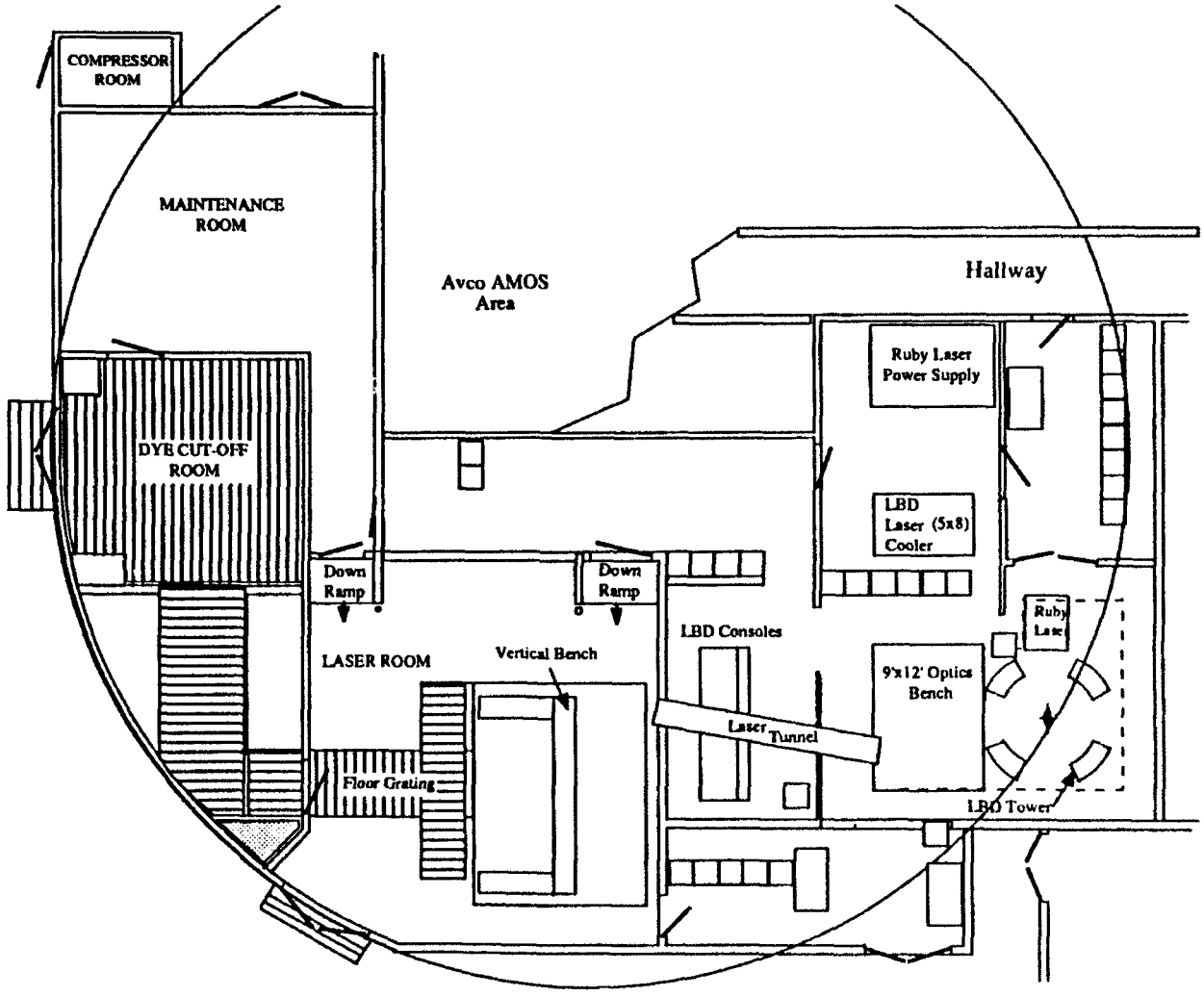

Fig. 3-12. SWAT II laboratory layout.

bench and the LBD occurs over a 15 cm diameter beam, which is redirected and expanded to 60 cm as shown earlier in Figure 3-3. The LBD tower also holds the "blue beam" laser that will be used to illuminate retroreflectors placed on the diagnostic targets to provide adequate tracking signals.

The Laser Laboratory occupies over half of the floor space in the new facility, and encompasses the six dye lasers, the dye circulating and control systems, the laser cooling system, the flashlamp power supply and firing system, and the safety system. The laser cavities and flashlamps are mounted on a vertical bench shown to the left of the Optics Laboratory in Figure 3-12, which is completely enclosed by a screen room for EMI suppression. Also mounted on the vertical bench are an extensive array of beam-diagnostic devices used to monitor the performance of each of the laser heads. The flashlamp power supplies, trigger circuits, and heat exchangers are located just to the left of the bench. The fluid storage and fluid handling equipment for the 6 lasers are located in the adjacent Dye Cut-Off Room.

The dye beams are transmitted to the main optics bench from the laser enclosure by a set of relay optics housed in an enclosed tunnel that passes over the Console Room. This enclosure is used both for safety reasons and to minimize path turbulence. Provision has also been made for the placement of a spatial filter at the focus of this relay system, if it is found to be necessary to maintain the requisite beam quality.

The Console Room is located between the Laser Laboratory and the Optics Laboratory, and serves as the nerve center for all system functions. It contains the control consoles for the LBD, which is usually operated by AVCO personnel, and the SWAT console containing the Executive Controller racks that will be the responsibility the Lincoln test director. Operation of the dye laser system is controlled from within the Laser Laboratory, under the supervision of the test director.

The analog recorders will be located in rack space adjacent to the main optics bench in the Optics Laboratory. These units will provide a time history of all wavefront conditions pertinent to the experiment, including gradients, phases, far-field beam images, and a host of tracking and house keeping items. Laser characteristics and laser fluid handling parameters will be recorded

by a separate device in the Laser Laboratory. All recording systems have access to a common IRIG time generator to facilitate off-line data analysis. Although the main analysis route will be through the transmission of analog tapes back to Lincoln, an extensive quick-look capability is available through the micro-VAX computer system, which will be placed in the maintenance area next to the Dye Cut-Off Room.

4. LABORATORY EXPERIMENT TO VERIFY STITCHING CONCEPT

The completed SWAT II system will contain several thousand discrete components, many of which are state-of-the-art elements that have been developed specifically for this program and never before tested in a laboratory environment. To ensure the successful integration and operation of the equipment at the AMOS facility, a complete set of laboratory tests will be conducted at Lincoln prior to the shipment of the SWAT hardware to Maui. The most important of these integration experiments is a laboratory verification of the A-method, multiple-beacon stitching concept.

4.1 PRINCIPAL OBJECTIVES

The first laboratory tests will have two major objectives. In addition to the obvious goal of demonstrating an ability to successfully operate a full-scale, 241-actuator, pulsed adaptive-optics system, this exercise will provide the first experimental data in support of the multiple-beacon phase-compensation concept. For this reason, the optical configuration has been chosen to duplicate, to the extent possible, the essential turbulence conditions attendant to the placement and sampling of multiple synthetic sources in the upper atmosphere.

The conceptual design of this experiment was originally proposed by Richard Sasiela and later refined by Ronald Humphreys. This document proposes a slight modification to the latter design in order to allow the simultaneous measurement of multiple low-altitude beacons by the phase sensor and a single collimated source by a high-resolution CCD camera. A set of two or more static phase screens will be used to introduce the requisite ground-level and upper-atmospheric turbulence effects.

4.2 SCALING THEORY

To a good approximation, all of the important turbulence parameters, including the coherence diameter (r_0), the anisoplanatic patch angle (ϑ_0), and the log-amplitude scintillation (σ_χ^2), can be approximated by an atmospheric model containing only two phase screens. The stronger of the two screens would be placed at ground level next to the collection aperture and scaled to produce the correct r_0 value, while the desired ϑ_0 and σ_χ^2 characteristics can be

achieved by adjusting the strength and placement of a second screen in the far field of the adaptive-optics system. The definitive expressions for the ground-level and upper-atmosphere screen strengths are given below.

Ground-level turbulence: $$C_n^2 L = (0.423\ k^2\ r_o^{5/3})^{-1} \quad (4\text{-}1)$$

Upper-atmosphere turbulence:
$$C_n^2 L = \begin{cases} (2.91\ k^2\ (h_o\ \vartheta_o)^{5/3})^{-1} & (4\text{-}2) \\ \sigma_\chi^2\ (0.564\ k^{7/6}\ h_o^{5/6})^{-1} \ . & (4\text{-}3) \end{cases}$$

where h_o represents the altitude of the high-altitude turbulence layer. According to the SLC-day model, $r_o = 4$ cm, $\vartheta_o = 12$ μrad, and $\sigma_\chi^2 = 0.05$ Nepers^2 for $\lambda = 500$ nm, which imposes the following set of constraints.

Ground-level phase screen: $$C_n^2 L = 3.2 \times 10^{-12}\ m^{1/3} \quad (4\text{-}4)$$

Upper-atmosphere phase screen: $$C_n^2 L = 6.2 \times 10^{-13}\ m^{1/3}\ ;\ h_o = 2.8\ km \ . \quad (4\text{-}5)$$

The practical restrictions on the placement and strength of the high-altitude phase screen are actually less severe than indicated in Equations (4-2) and (4-3), since the preservation of the correct log-amplitude scintillation is not of great concern for these experiments. As long as the integrity of Equation (4-2) is maintained, the important focal-anisoplanatic effects will be correctly simulated.

In order to shrink the collection aperture through the transformation $D \Rightarrow D/\gamma$, all of the altitude parameters must be reduced by γ^2 in order to preserve the Fresnel number, while phase screen strengths must be increased by $\gamma^{5/3}$. The Table 4-1 summarizes the optimal geometries (including log amplitude scintillation scaling) as a function of the collection aperture diameter. All of the listed displacements are referenced to the front surface of the collection aperture.

TABLE 4-1
LABORATORY SCALING OPTIONS

Collection Aperture (cm)	γ	*Upper-Altitude Phase Screen (m)*	*Beacon Displacement*
60	1	2,800	10,000
0.5	120	0.19	0.7
1.0	60	0.78	2.8
1.5	40	1.75	6.3
2.0	30	3.11	11.1

The selection of one of these configurations involves a trade-off between constraints established by space limitations on the optical bench and C_n^2L strengths achievable with the existing phase plates. The $\gamma = 40$ option appears to represent a fairly reasonable compromise, since the requisite 6.3-m path length can be obtained with a single fold along the long dimension of the bench. The ground-level C_n^2L value for this case is $(40)^{5/3} \cdot 3.2 \times 10^{-12} = 1.5 \times 10^{-9}$ $m^{1/3}$, while the corresponding number for the upper-level screen is 2.9×10^{-10} $m^{1/3}$. A set of 11 ion-milled plates is currently available, each of which has an unscaled integrated strength of 2.6×10^{-10} $m^{1/3}$, as well as a number of usable photoresist screens of somewhat lower strengths. Therefore, it should be possible to assemble a reasonably accurate $\gamma = 40$ simulation with a set of 6 ion-milled plates for the ground-level turbulence and 1 or 2 ion-milled plates for the upper-level turbulence.

4.3 OPTICAL COMPONENTS

The baseline SWAT II experiment will incorporate a set of 5 dye lasers that will be sequentially fired so that each of the returns can be viewed by the full aperture without ambiguity. A realistic simulation of this arrangement will require a means to generate and independently control 5 closely-spaced sources. A conceptual design for the multiple source box was presented by Ronald Humphreys, in which he pointed out that LEDs would not provide

sufficient light for this application and that a small argon laser would be much more appropriate. His layout achieves 5 separate beam paths through an arrangement of beamsplitters and pyramid prisms; see Figure 4-1. Each of the paths includes a remotely-controlled shutter, and a pinhole that is sized to be unresolved by the full aperture. The pinholes will be mounted on translation stages so that the sensitivity of the stitching algorithms to small positional source offsets can be conveniently investigated.

For the $\gamma = 40$ design discussed above, the speed of the adaptive-optics collection system will be f/420, which corresponds to a diffraction-limited pinhole diameter of 0.5 mm. The use of a 100-μm pinhole has been suggested in order to ensure a uniform illumination of the deformable mirror. An aperture of this size is also well matched to the 700-μm output beam diameter of the laser. The net efficiency of the multiple-source box per output beam at the entrance aperture of the wavefront compensation system is

$$\tau_{source} = \frac{1}{5}\left(\frac{100\mu m}{700\mu m}\right)^2 \left\{1 - J_0^2\left(k\left(\frac{d}{2}\right)\left(\frac{D}{2L}\right)\right) - J_1^2\left(k\left(\frac{d}{2}\right)\left(\frac{D}{2L}\right)\right)\right\} \quad , \qquad (4\text{-}6)$$

where the third term is the expression for the pinhole radiation collected by an aperture of diameter D at a distance L from a pinhole of diameter d. For $\gamma = 40$, an evaluation of Equation (4-6) yields $\tau_{source} \approx 5 \times 10^{-4}$.

The CW laser power requirement for a wavefront sensor having an actuator count $N_{actuator}$, a system throughput τ_{system}, a quantum efficiency η, an effective gain G_e, a noise floor n_{noise}, a photon count requirement n_{photon}, and a dwell time τ_d can be shown to be

$$P_{laser} = (hc/\lambda)\, n_{photon}\, N_{actuator}\, n_{noise} / G_e\, \eta\, \tau_{source}\, \tau_{system}\, \tau_d \quad . \qquad (4\text{-}7)$$

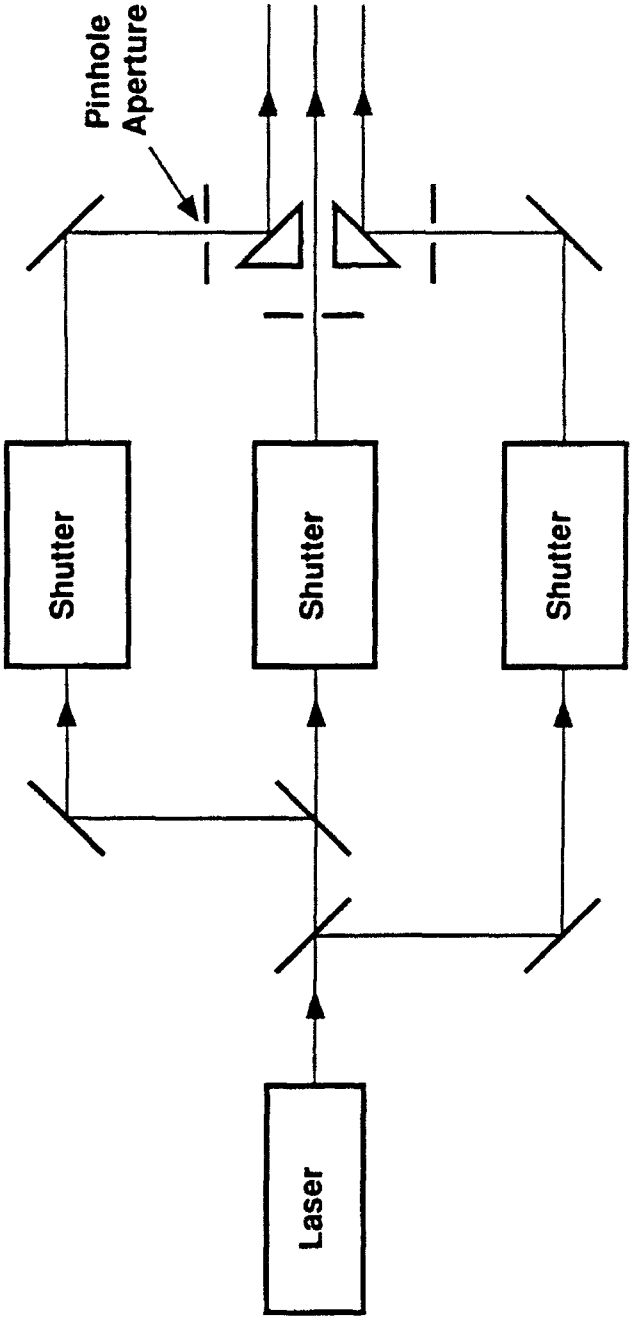

Fig. 4-1. Multiple-source test box for bench experiment.

The appropriate numerical values for the SWAT wavefront sensor configuration are given below. The included dwell time of 100 μsec represents a very conservative lower limit on the temporal stability of the non-common-path bench turbulence, and the effective intensifier gain of 200 encompasses losses related to the optical fiber and the Reticon camera quantum efficiency.

n_{photon}	= 200	η	= 0.14
$N_{actuator}$	= 241	τ_{source}	= 5×10^{-4}
n_{noise}	= 10,000	τ_{system}	= 0.5
G_e	= 200	τ_d	= 100 μsec

With these numbers, it can be seen that $P_{laser} \approx 0.3$ mW, which is a little lower than the result derived by Humphreys.[23] Argon lasers at this power level are readily available and, if needed, a better signal-to-noise ratio should be obtainable by increasing the sensor dwell time.

A similar power-requirement calculation can be made for the input to the CCD camera. In this case we are interested in collecting a few hundred photoelectrons per dwell time in each pixel of the detector array. The Laboratory's Solid State Division has constructed a pair of 64 x 64 pixel cameras for the SWAT II program with a 20-electron noise floor and a quantum efficiency at 500 nm of 0.2. From these numbers, the following list obtains

n_{photon}	= 200	η	= 0.2
N_{pixel}	= 4096	τ_{source}	= 2.5×10^{-3}
n_{noise}	= 20	τ_{system}	= 0.5
G_e	= 1	τ_d	= 100 μsec

which also results in a power requirement of about 0.3 mW. Therefore, it appears that a pair of argon lasers in the 5-mW range will be more than adequate to perform this experiment.

A simplified sketch of the laboratory configuration is presented in Figure 4-2. The multiple-beacon and the collimated point-source simulators are shown in the upper-left corner of this drawing. Light produced by these two components is combined by a beamsplitter, and is subsequently passed through two sets of phase screens before being collected by a 75-mm

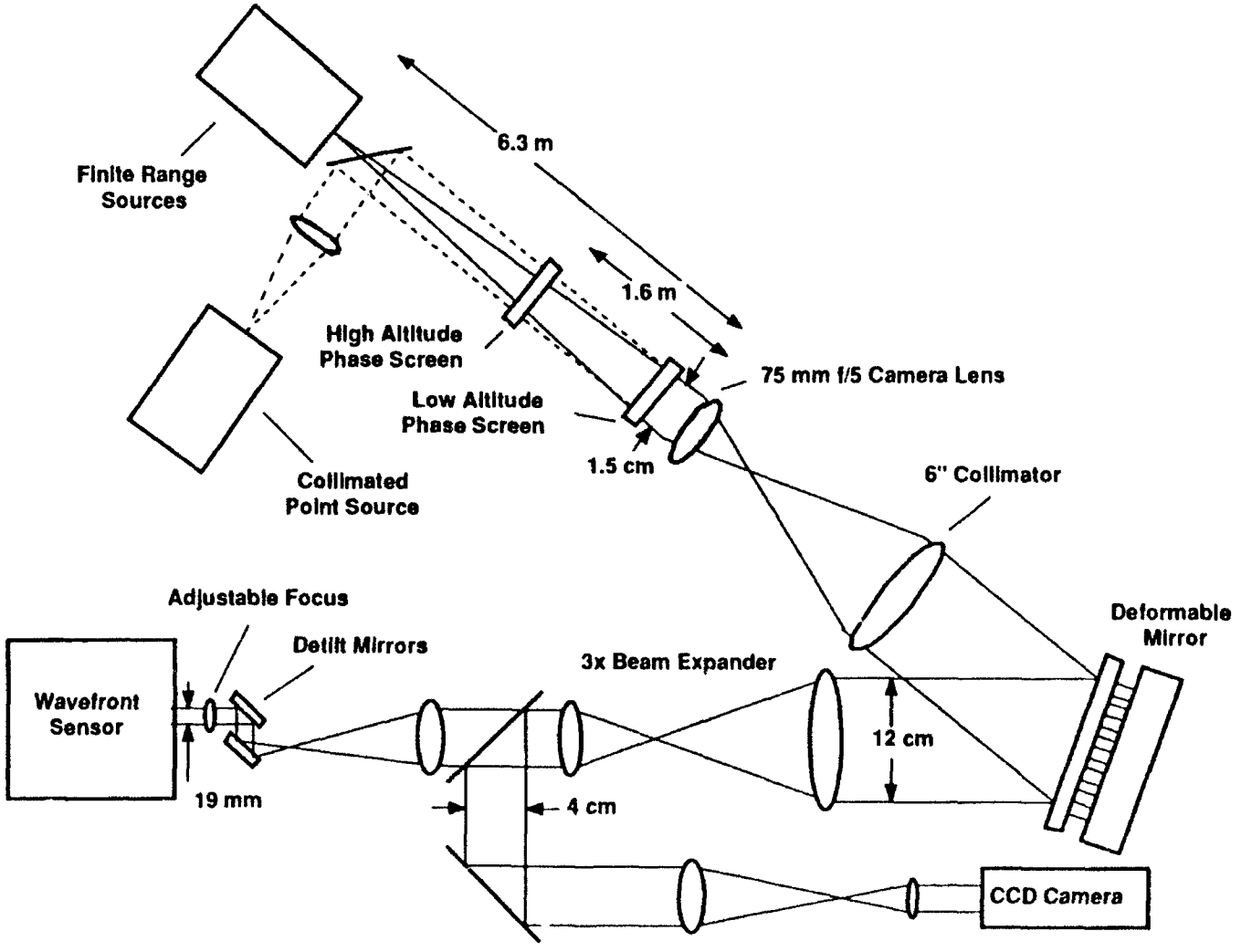

Fig. 4-2. Bench equipment optical configuration.

camera lens. This element, in conjunction with a 25" focal-length mirror from Space Optics, forms a 8x beam expander that interfaces directly with the deformable mirror. From this point, the reflected radiation is transmitted to the wavefront sensor and a high-resolution imaging camera by way of a 3x beam expander and ancillary relay optics. The adjustable detilt and focus components shown directly in front of the phase sensor serve to remove the low-order static aberrations associated with beacon misposition errors.

The deformable-mirror drive voltages generated by the phase sensor are tailored to provide the appropriate correction for a planewave input. A quantitative measure of system performance can be obtained by viewing the collimated source in the image plane of the wavefront sensor. The CCD camera shown in the lower-right corner of Figure 4-2 is intended to perform this function; it will provide near real-time output via a dedicated Micro-VAX computer.

4.4 EXPERIMENT CONTROL AND DATA ANALYSIS

Figure 4-3 presents an interconnect drawing that incorporates all of the major non-optical components essential to the successful completion of a beacon stitching experiment. With the exception of the source boxes and associated control logic, all of the elements shown are part of the present SWAT II configuration. The recording system has been simplified by the complete elimination of the analog recorders and interface hardware, since the Micro-VAX (referred to here as the Diagnostic Analysis Network Engine) will be able to handle all of the recording and analysis functions. The requirements on the Central Controller will be similarly eased owing to the limited amount of automatic interaction needed to collect a complete set of beacon data.

A nominal timing diagram for the source boxes, Wavefront Controller, and Camera Exposure Interface is given in Figure 4-4. The indicated shutter control sequence is intended to mimic the baseline A-method stitching experiment, which incorporates an initial correction to the deformable mirror using a single (precursor) Rayleigh beacon that is immediately followed by a second correction derived from the stitching of 4 subsequent laser returns. The detilt mirror is moved in conjunction with the action of the source shutters to minimize the overall tilt component seen by the adaptive-optics system. A measure of the quality of applied compensation is obtained by viewing the simulated star source each time the deformable mirror is driven.

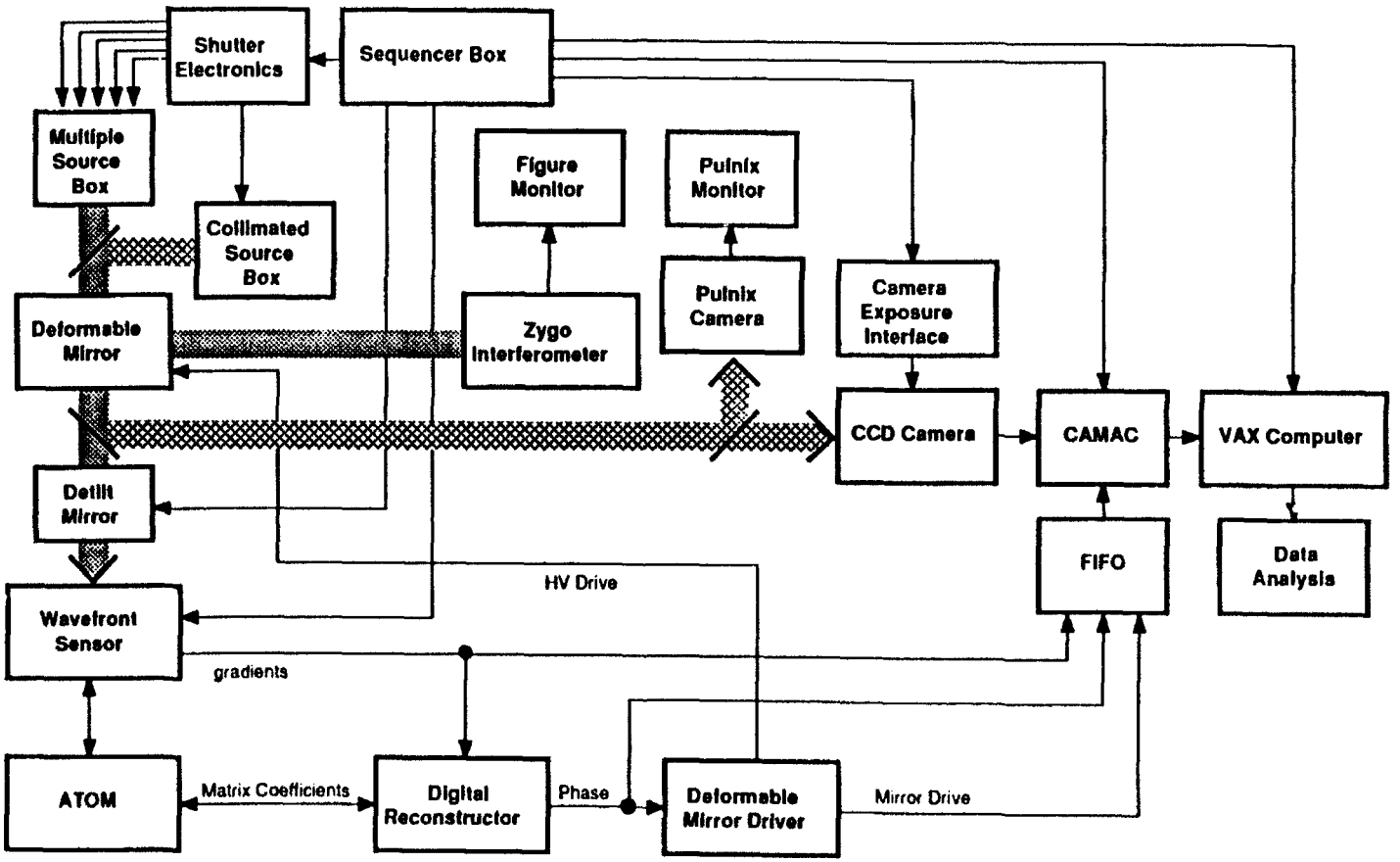

Fig. 4-3. Experiment control and recording equipment.

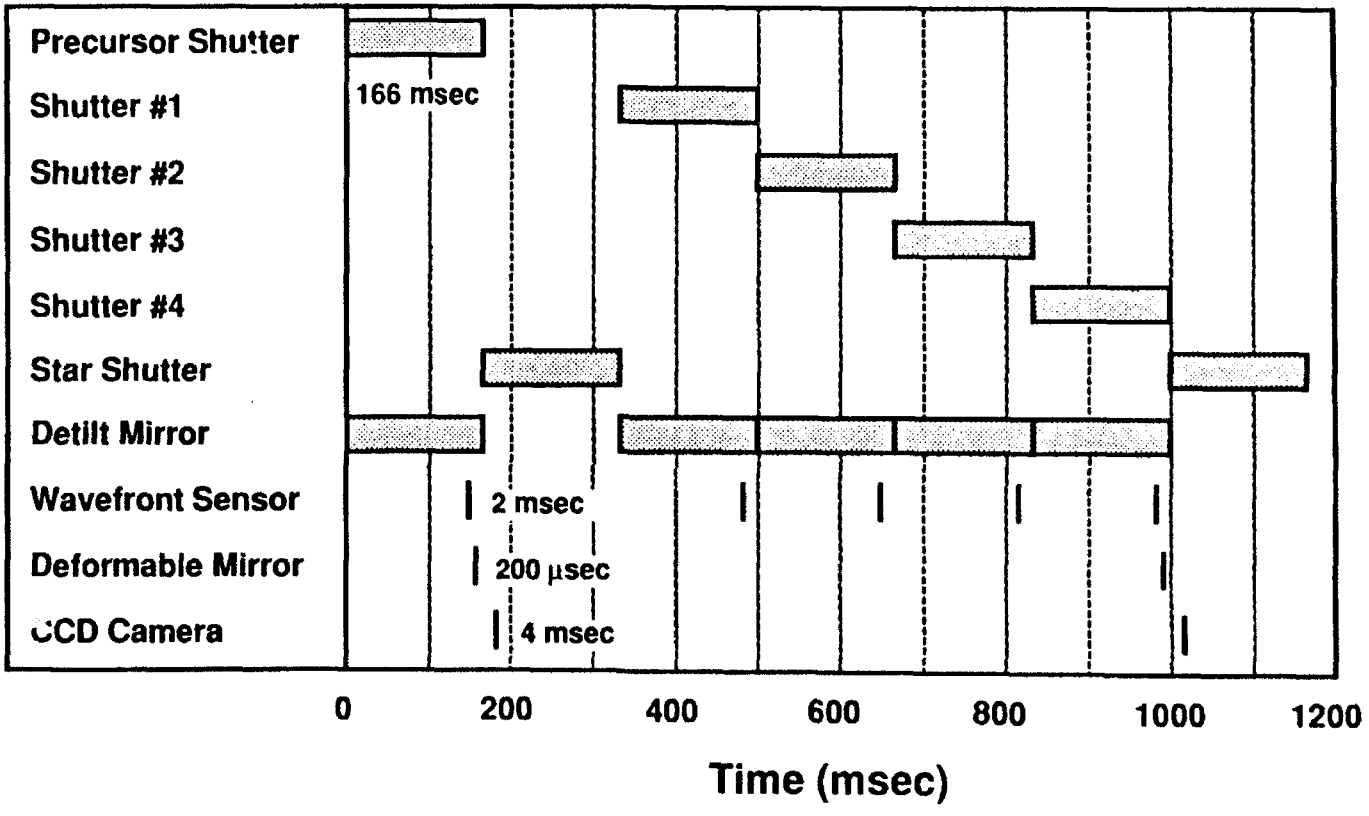

Fig. 4-4. Bench experiment timeline.

In this way, all of the essential aspects of the first set of tests planned for Maui can be readily simulated, albeit at time scales of the order of 1,000 longer than those required for field conditions. Potential parametric studies include the investigation of beam altitude, misposition, and size effects, as well as the performance of alternative reconstruction algorithms. The successful completion of these laboratory tests will represent the first hardware verification of the synthetic beacon technique for uncooperative target illumination.

5. EARLY SWAT II STAR-IMAGING EXPERIMENTS

Phase conjugation is based on the concept of reciprocity, which states that the phase retardation experienced along a given optical path is independent of the direction of the probe beam. A corollary to this statement is that the Strehl ratio of a beam projected from a ground-based station can be accurately determined by measuring either the phasefront or the focused-beam profile of a distant object viewed along the compensation path. The first series of SWAT A–method experiments will be evaluated through profile measurements of bright stars by intensified CCD imaging devices.

5.1 PASSIVE SCORING SENSITIVITY ISSUES

It was demonstrated in Section 2.0 that the attainment of high Strehl ratios requires the atmospheric sampling, mirror drive, and scoring sequence to be completed within a time interval of about 1 msec. Given this restriction on the camera integration period, great care must be taken in the design of the optical system to ensure high-optical throughput and in the selection of suitable candidate scoring stars. This section discusses the projected transmission efficiency of the SWAT optical system, and the radiation characteristics of the brightest stars visible from Maui. Aperture irradiance requirements for each of the optical sensors in the beam-control and scoring subsystems will also be derived.

5.1.1 Aperture Irradiance Requirements

System throughput is a major consideration in determining the suitability of a particular star for passive Strehl measurements. Figure 5-1 is a greatly simplified schematic of the optical layout that will be employed for the first set of experiments, but it includes all of the major adaptive beam-control components and high-loss beamsplitting elements. The system is drawn roughly to scale. As discussed in Section 3.0, the synthetic beacons are generated by a set of 6 dye lasers housed in a separate, electrically shielded room, and coupled to the optical bench through a closed-loop tilt and offset stabilization system.

Following the outgoing beacon path, the first elements encountered are the tilt and focus fixtures that control the placement of the beacons over the transmitter and the focus altitude respectively. Insertion into the common beam path is accomplished through the use of a

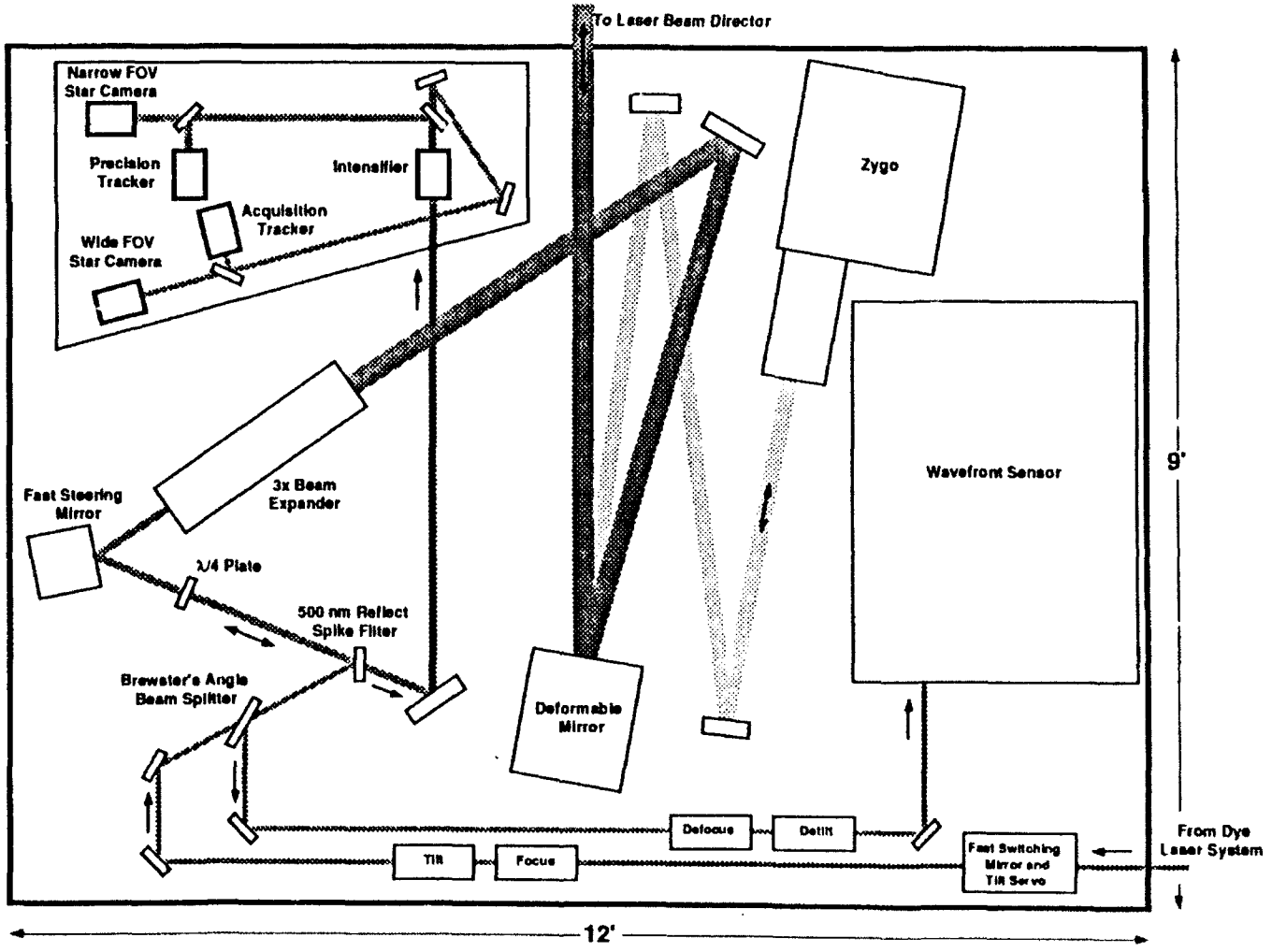

Fig. 5-1. SWAT II system optical layout.

narrow-band transmission filter, which provides the requisite discrimination between the 504-nm beacon radiation and the broadband return from celestial sources. (The average reflectivity of this element over the 460 to 560-nm spectral region is approximately 50%.) The outgoing and backscattered dye-laser beams are separated by a rotation of the optic axis achieved by Brewster's angle beamsplitter and 1/4-wave plate combination. Low spatial-frequency phase components associated with the placement of the synthetic beacons are removed by the detilt and defocus elements located near the entrance of the wavefront sensor.

The active components in the common beam path consist of the deformable mirror and the fast-steering mirror, both of which are controlled by the wavefront sensor. To enhance the efficiency of the deformable mirror at the beacon wavelength, a multi-layer dielectric coating has been applied that is optimized for 504-nm and also has a high reflectivity at the scoring laser wavelength of 514.5-nm. The broadband characteristics of the mirror are less well suited for passive scoring measurements using bright stars, but the reflectivity of the surface has been found to be no worse than 75% between 420 and 540-nm.

Starlight received by the LBD is reflected from the adaptive-optics elements, passes through the spike filter, and is eventually fed into an enclosure containing several trackers and imaging cameras. The camera unit functions both as a precision tracking system and the main-beam diagnostic device for all of the compensated imaging tests. Two optical paths are provided within the enclosure with a magnification difference of about 10. The wide-field-of-view camera, designed to measure uncompensated sources, will cover a 100-μrad angular region; whereas, the narrow-field-of-view camera will view a 10-μrad region. Photon noise-limited operation will be achieved by all of the camera and tracker units through the use of a series of image intensifiers, as indicated in Figure 5-1.

With the components in place for propagating and sensing synthetic beacons, the SWAT system becomes a 60-cm diffraction-limited telescope with a compensated field-of-view of about 10 μrad and a 1-msec integration period. Any exoatmospheric object with an angular extent less than 1 μrad and with sufficient brightness to be imaged in 1 msec can be used as a compensation reference. However, with the present DM coating, only about 20% of the available visible light from blue stars passes through the 420-460-nm spectral filter formed by the dye-laser dichroic

and the deformable mirror. Plans are being made to either purchase a second deformable mirror or recoat for broadband radiation, which can be expected to improve the collection efficiency of the star camera beam path by a factor of 2 to 3.

Two slightly different optical configurations are likely to be used in the first few months at Maui. The operational configuration for the star imaging tests has been described, but for the initial sensor setup tests the 500-nm dichroic would be replaced with a 50/50 beamsplitter to allow the wavefront sensor to also view the star reference. The transmission efficiencies for these two layouts are given in the following table.

TABLE 5-1
Optical Throughput Estimates

Transmission Path	Setup Tests		Star Imaging	
	Transmission	*Bandpass*	*Transmission*	*Bandpass*
Beacon Output	--	--	50%	504 nm
Phase Sensor Input	35%	420-540 nm	70%	504 nm
Camera System Input	18%	420-540 nm	36%	420-460 nm

These numbers include all of the optical elements from the LBD to the indicated device. Atmospheric losses and device throughput losses are accounted for separately.

The input signal requirements for the phase sensor and camera systems differ by several orders of magnitude, owing to differences in the number of independent output parameters generated by these sensors. The accepted rule-of-thumb for the phase sensor is that the photon-noise-limited rms phase error is approximately $\lambda/(2N_s)^{1/2}$, where N_s is the average number of photoelectrons collected by each subaperture. For $\lambda/20$ operation, this leads to a prerequisite for 200 photoelectrons per subaperture, or approximately 50,000 photoelectrons for the SWAT II compensation system. The requirements for target tracking and passive Strehl measurements made with imaging sensors are significantly less severe.

Compensated image displacement: $\sigma_{centroid} \approx (\lambda/D)\, N_a^{-1/2}$ (5-1)

Compensated beamwidth measurement: $\sigma_{width} \approx 3\,(\lambda/D)\, N_a^{-1/2}$, (5-2)

where N_a is the number of photoelectrons collected by the full aperture. Assuming a need to estimate both of these quantities to an accuracy of $\lambda/10D$, Equations (5-1) and (5-2) lead to a specification for 100 and 1,000 photoelectrons for beam centroid and beamwidth measurements respectively.

These numbers can be translated into a set of aperture irradiance requirements for a detection device having a collection aperture diameter D and quantum efficiency η through the expression

$$N = H(\lambda/hc)\,(4/\pi)\,D^2\,\tau_a\,\tau_o\,\tau_d\,\eta \tag{5-3}$$

where τ_a, τ_o, and τ_d represent the atmospheric transmission, optical transmission, and detector dwell time respectively. For most calculations, a one-way atmospheric transmission of 80% is assumed, along with a detector quantum efficiency of 10%, and an effective sensor dwell time of 1 msec. For wavefront sensing, an additional factor of $1/(1 - \sigma_{I/I_o})$ should be included in Equation (5-3) to allow for signal loss due to scintillation effects. The probability density function for intensity fluctuations due to scintillation is log-normal, and is characterized by the parameter σ_χ^2

$$p(I/I_o) = \left\{(8\pi)^{1/2}\sigma_\chi (I/I_o)\right\}^{-1} \exp\left\{-\left[\ln(I/I_o) + 2\sigma_\chi^2\right]^2 / 8\sigma_\chi^2\right\} \tag{5-4}$$

For $\sigma_\chi^2 < 0.1$, the normalized intensity distribution is approximately Gaussian, with unity mean and a standard deviation

$$\sigma_{I/I_o} \approx 2\left(\sigma_\chi^2\right)^{1/2} , \tag{5-5}$$

resulting in an irradiance fluctuation of approximately 50% for $\sigma_\chi^2 = 0.05$ Nepers^2. Combining this information with the data presented in Table 5-1 yields an estimate of the minimum aperture irradiance needed to drive each of the primary measurement sensors for a 1-msec dwell time.

TABLE 5-2
Aperture Irradiance Requirements

Detection Device	Measurement Requirement (photoelectrons)	Aperture Irradiance for 1 msec Dwell Time (W/m^2)	
		Setup Tests	*Star Imaging*
Phase Sensor	50,000	3.2×10^{-9}	--
Camera System	1,000	6.2×10^{-11}	3.4×10^{-11}

5.1.2 Candidate Stars

The first set of experiments in the test schedule exploit the plane-wave radiation produced by celestial sources to quantitatively gauge the quality of the turbulence compensation afforded by the SWAT II adaptive-optics system. In planning experiments using such sources, two parameters are of principal interest -- the stellar brightness and location on the celestial sphere. Brightness is generally given in units of visual magnitude, which is a logarithmic irradiance scale based on the the response of the human eye. The visible irradiance, as observed at the top of the atmosphere, produced by a star having a visual magnitude m_v is given by[3]

$$H(W/m^2) = 3.8 \times 10^{-9} \cdot 10^{-0.4\, m_v} \quad . \tag{5-6}$$

To a good approximation this represents an integrated blackbody irradiance within the 505-605-nm waveband.

[3]Lang, K. R., Astrophysical Formulae, Springer-Verlag (1980).

The position of stars in the night sky can be determined from tables listing right ascension and declination. Right ascension is a 24-hour time associated with the astronomer's sidereal clock and specifies the date on which the star will reach its highest point at midnight. A right ascension of 0 hours and 00 minutes corresponds to 21 September, the date of the autumnal equinox. Declination is the angular distance north or south of the celestial equator; numbers to the north of the equator are assigned positive values. Only those stars whose declination angle matches the local latitude will appear to cross zenith at some point during each day.

The star zenith angle ψ for a given date and hour can be estimated from the following expression

$$\psi = \tan^{-1} \left| \frac{\left[(\cos\beta \sin\gamma)^2 + (\sin\alpha \cos\beta \cos\gamma - \cos\alpha \sin\beta)^2 \right]^{1/2}}{\cos\alpha \cos\beta \cos\gamma + \sin\alpha \sin\beta} \right| , \qquad (5\text{-}7)$$

where α is the latitude of the observation site, β is the star's declination, and γ is the rotation angle about the celestial axis between the present position of the star and its local apex position. The relationship between the angle γ and right ascension RA is

$$\gamma = \left| \{360°/24 \text{ hours}\} \left\{ \left[a(D_o - 264) - RA \right] + T_o \right\} \right| , \qquad (5\text{-}8)$$

where D_0 is the observation day (number of days since 1 January), T_0 is the observation hour (number of hours since midnight), and a = 0.0656 hours/day is the difference between the sidereal day ($23^h\ 56^m\ 4^s$) and the solar day.

Having previously established a set of lower limits on aperture irradiance for phase sensing and passive scoring measurements, it is now possible to identify the stars that are most likely to be suitable for these tasks. The first step is to modify Equation (5-6) to obtain an irradiance expression for the correct spectral wavebands,

$$H = C(\lambda_c,\ \Delta\lambda, T) \cdot 3.8 \times 10^{-(0.4\ m_v + 9)} \quad . \qquad (5\text{-}9)$$

The correction factor $C(\lambda_c, \Delta\lambda, T)$ relates the measured star irradiance within a bandwidth $\Delta\lambda$ and at a center wavelength λ_c to the human eye response, which for rough calculations can be assumed to be unity over the 505 to 605-nm region and zero elsewhere. A reasonably accurate estimate of C is obtained from the following Planck blackbody function ratio

$$C\left(\lambda_c, \Delta\lambda, T\right) \approx 5.27 \times 10^{-25}\, \Delta\lambda \left(\lambda_c\right)^{-5} \exp\left\{\left[2.59 \times 10^{4} - 1.44 \times 10^{-2}\left(\lambda_c\right)^{-1}\right] T^{-1}\right\} \quad . (5\text{-}10)$$

From the AMOS site at Maui (21° latitude), about a dozen stars are sufficiently bright and close to zenith to be useful for compensated imaging measurements. These 12 sources[4] are listed in order of decreasing brightness in Table 5-3, and their midnight apex dates appear in Figure 5-2. Assuming a 6-hour nighttime viewing window, each of the stars listed above can be observed for a minimum of 3 months at apex, making it possible to find at least one suitable reference star on any given observation date. As an example, Figure 5-3 provides a map of the star positions as a function of time for 1 March. Note that it will be possible to observe 6 stars of magnitude 1.2 or brighter during the nighttime hours on this date.

By applying the data listed in Table 5-3 to Equation (5-10), aperture irradiance numbers for the two wavebands of interest are derived, which are compiled in Table 5-4. It can be seen that all of the stars listed are predicted to be suitable for passive Strehl measurements, and about 5 of the stars (shown in bold type) should be bright enough to drive the wavefront sensor. It is clear, however, that the margin for error is very small with regard to wavefront sensing, and it is not inconceivable that Sirius will be the only star bright enough to be used for passive compensated-imaging experiments.

[4]Ramsay, R. C., "Spectral Irradiance from Stars and Planets, Above the Atmosphere, from 0.1 to 1000.0 Microns," Appl. Opt. Vol. 1, No. 4, p. 465 (July 1962).

TABLE 5-3

Bright Star List

Star Name	Intensity Information		Position Information	
	Visual Brightness	Surface Temperature	RA (hours)	Declination (degrees)
Sirius	-1.60	11,200°	6.72	-16.65
Vega	0.14	11,200°	18.59	+38.73
Capella	0.21	4,700°	5.22	+45.95
Arcturus	0.24	3,750°	14.22	+19.27
Rigel	0.34	13,000°	5.20	-8.25
Procyon	0.48	5,450°	7.61	+5.35
Altair	0.89	7,500°	19.81	+8.73
Betelgeuse	0.92	2,810°	5.88	+7.40
Spica	0.96	28,000°	13.38	-10.90
Aldebaran	1.06	3,130°	4.55	+16.42
Pullux	1.21	3,750°	7.71	+28.15
Antares	1.22	2,900°	16.44	-26.32

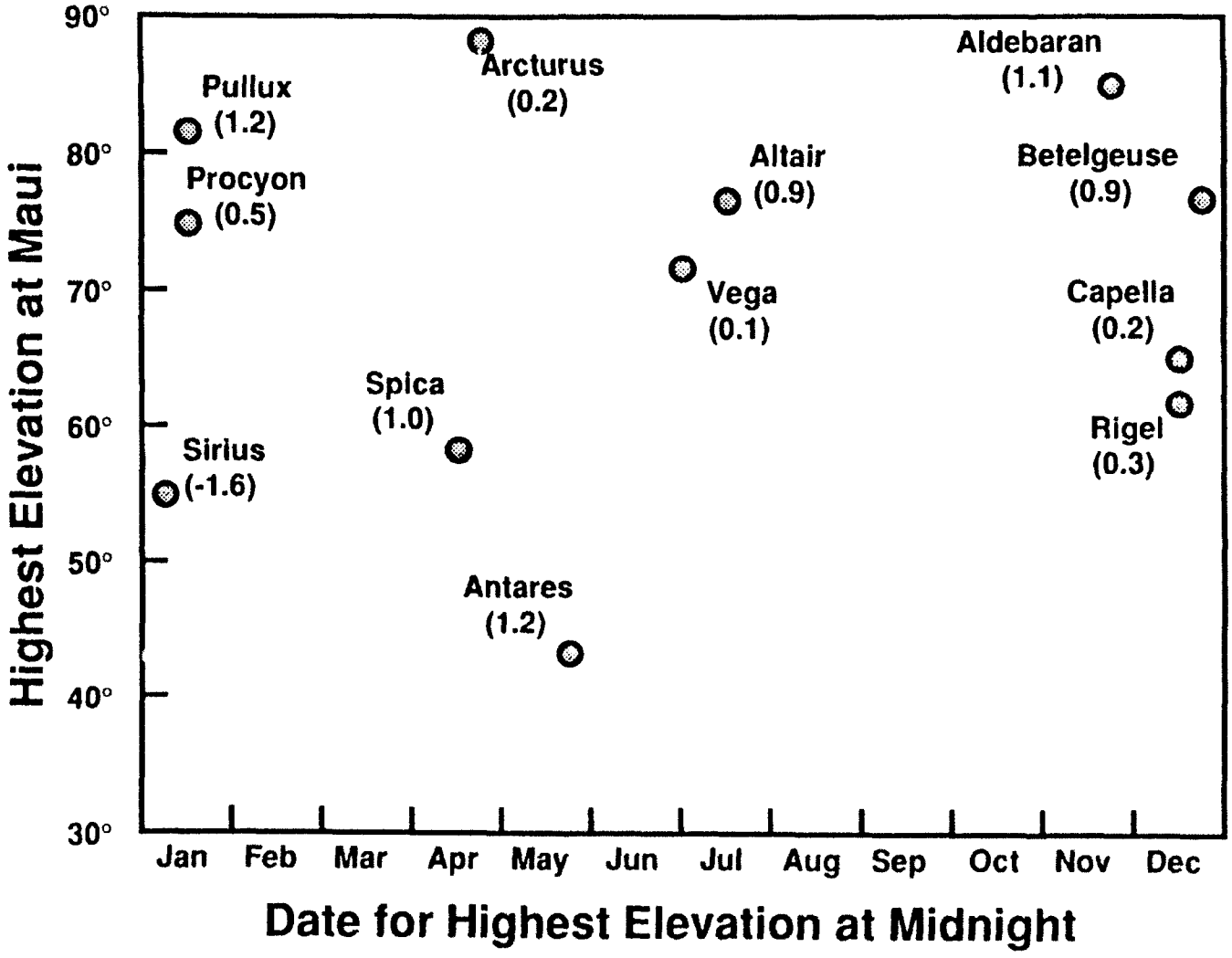

Fig. 5-2. Bright star viewing dates.

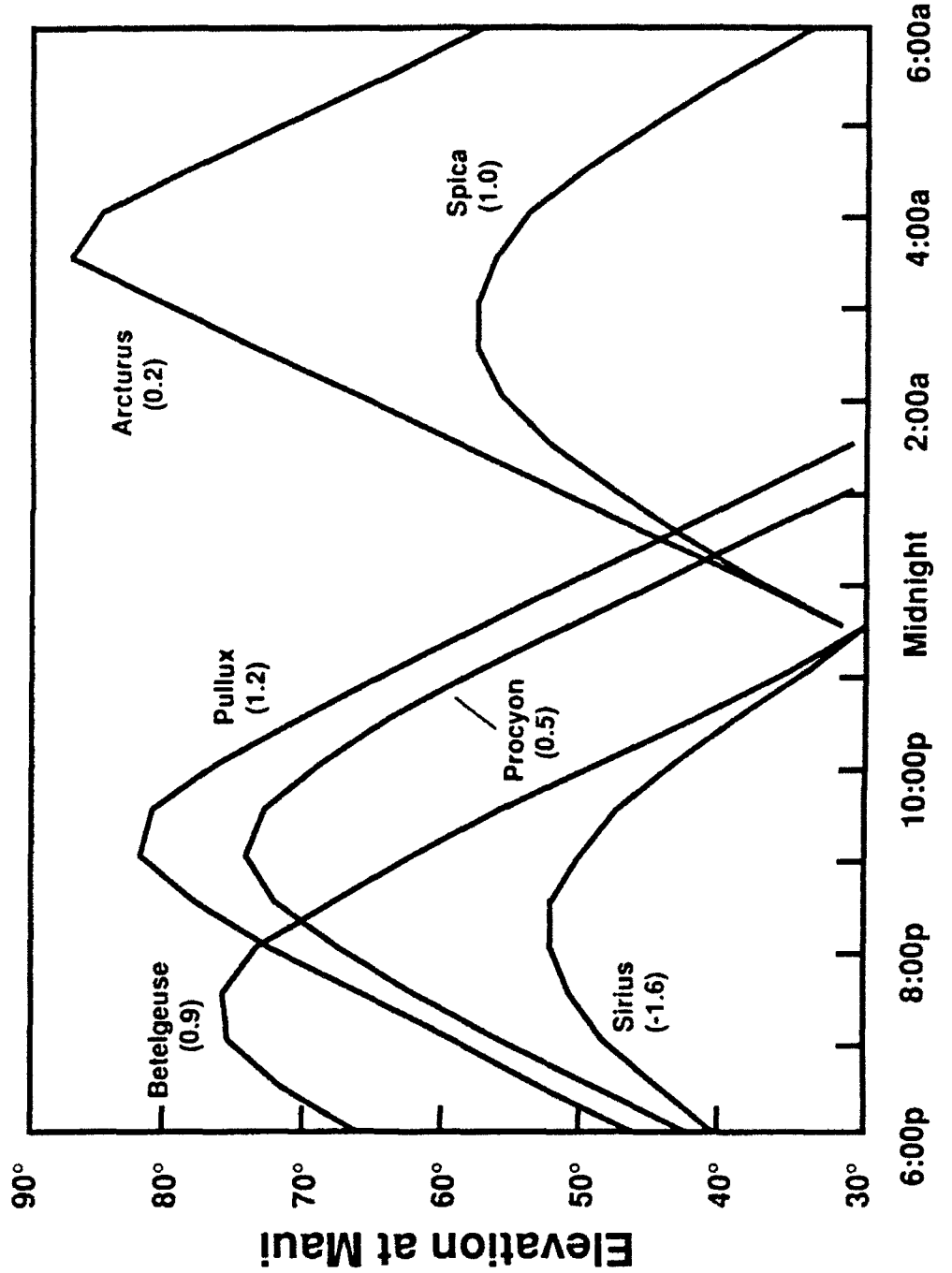

Fig. 5-3. Bright star elevation map for 1 March.

TABLE 5-4

Star Spectral Irradiance Data

Star Name	Position Data		Irradiance Data (W/m^2)	
	Midnight Apex Date	Elevation at Apex	420-460 nm	420-540 nm
Sirius	2 January	51.4°	1.1×10^{-8}	2.8×10^{-8}
Procyon	16 January	73.4°	9.0×10^{-10}	2.8×10^{-9}
Pullux	17 January	82.9°	2.6×10^{-10}	1.1×10^{-9}
Spica	13 April	58.1°	1.4×10^{-9}	3.2×10^{-9}
Arcturus	25 April	87.5°	6.4×10^{-10}	2.6×10^{-9}
Antares	29 May	42.7°	1.5×10^{-10}	7.8×10^{-10}
Vega	1 July	73.3°	2.2×10^{-9}	5.6×10^{-9}
Altair	19 July	76.7°	8.5×10^{-10}	2.4×10^{-9}
Aldebaran	29 November	85.4°	2.1×10^{-10}	9.9×10^{-10}
Rigel	9 December	59.1°	2.0×10^{-9}	4.9×10^{-9}
Capella	10 December	61.1°	9.5×10^{-10}	3.3×10^{-9}
Betelgeuse	20 December	76.6°	1.9×10^{-10}	9.9×10^{-10}

5.2 A-METHOD FIGURE COMPENSATION EXPERIMENTS

The laser beam-control community has generated a wealth of analytical output over the last 5 years in support of various figure-compensation schemes ranging from the simple to the exotic, while experimental verification of the synthetic-beacon concept is, at this, point essentially non-existent. The SWAT II program is expected to provide the first physical evidence of the potential utility of synthetic beacons and ascertain the degree to which focal-anisoplanatic effects can be overcome. The significance and level of risk associated with the earliest of these measurements should not be underestimated.

A set of three A-method, passive scoring tests are scheduled for completion in FY88. The following sections specify the optical layouts, timing sequence, and principal experimental parameters for each exercise.

5.2.1 Single-Beacon A-Method Figure Compensation

Focused-beacon figure correction using low-altitude Rayleigh backscatter from a single synthetic source represents the simplest implementation of the synthetic-beacon concept. In an experiment of this type, focal-anisoplanatic effects are the main quantity of interest and, in a properly designed system, the chief source of Strehl degradation. This means that all other potential sources of wavefront distortion (e.g., poor signal-to-noise ratio, fitting error, mispointing error, and inadequate temporal response) must be held to a minimum. The magnitude of these effects is reasonably well understood as a result of extensive experience gained during the ACE program, and it is within this framework that the basic design parameters of the SWAT II system have been established. The design goal in the absence of focal anisoplanatism is $\lambda/15$ rms phase error, corresponding to a Strehl of 0.8.

The optical layout for the single-beacon experiment is shown in a highly-simplified schematic format in Figure 5-4, and its associated timing diagram appears in Figure 5-5. The experiment begins with the projection of a 2-μsec dye-laser pulse through the uncorrected adaptive-optics system; the return energy is gated at the wavefront sensor to accept a range sample having a depth of approximately 10% of the source altitude. The phase-compensation 'clock' starts near the end of the beacon return when the low-altitude turbulence is sampled, and stops at the end of the CCD camera integration period. The minimum duration of the

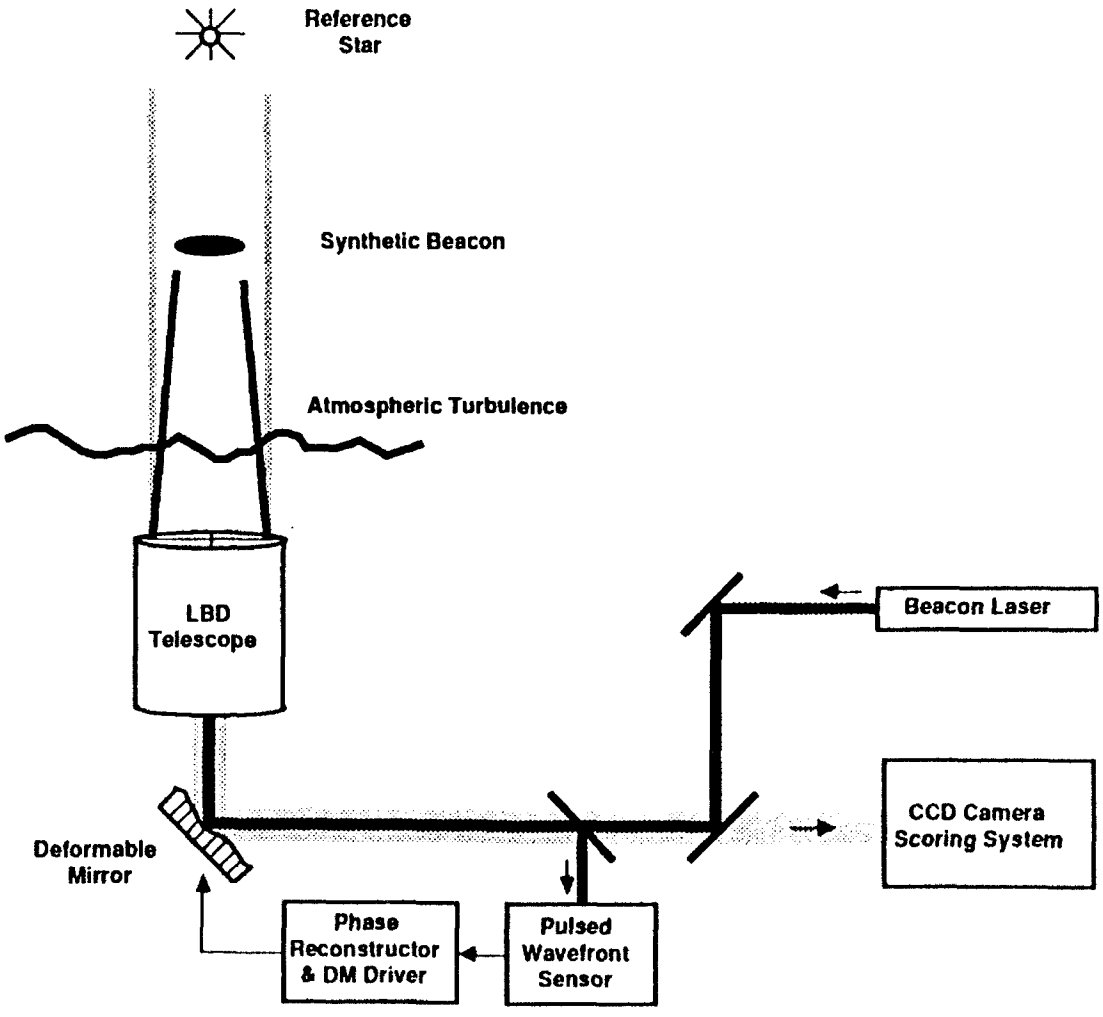

Fig. 5-4. Single-beacon compensation experiment.

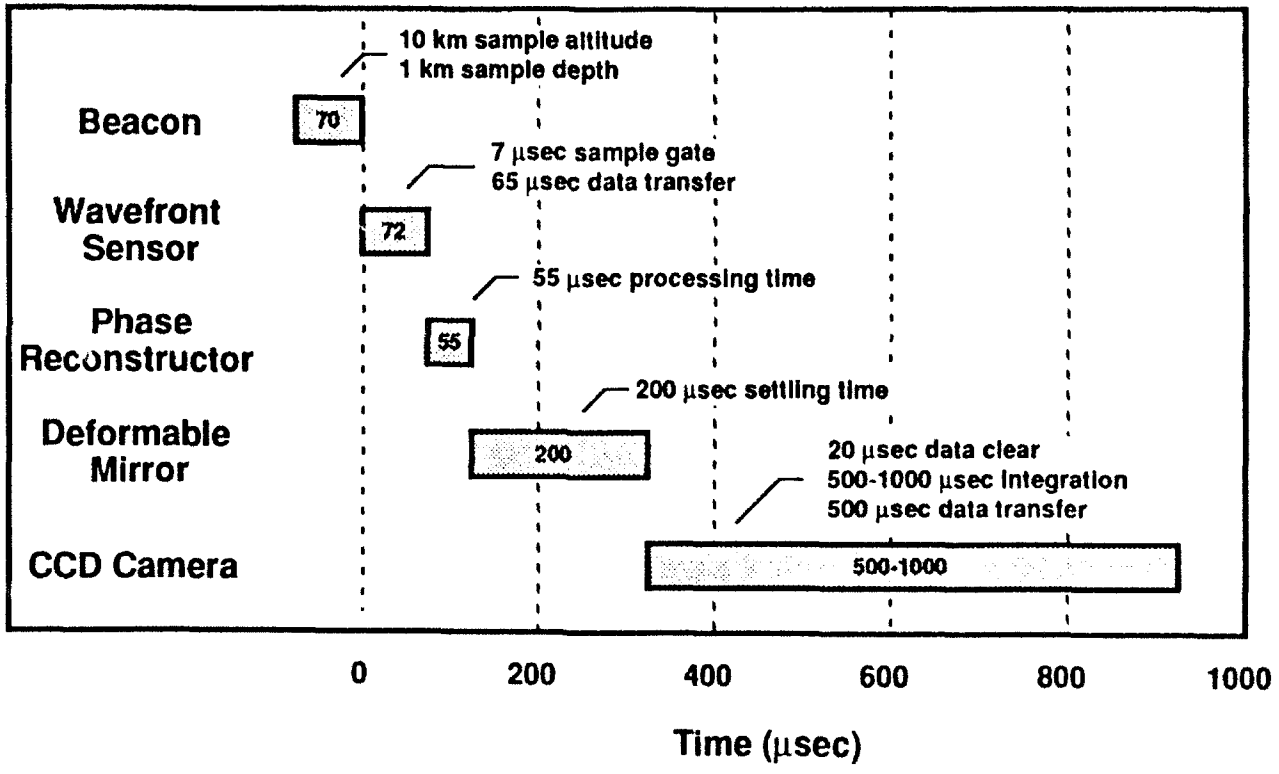

Fig. 5-5. Single-beacon experiment timing diagram.

compensation and scoring interval is established by the data-transfer time of the phase sensor, the reconstructor processing time, the deformable-mirror settling time, and the camera integration interval. As can be seen from Figure 5-5, the camera integration period is the largest single source of delay; it is expected to range between 500 and 1,000 μsec depending on the optical efficiency of the camera system and the intensity of the reference star. The nominal timeline shows the entire process as being completed in just under 1 msec.

Despite the apparent simplicity of the single-beacon construct, it readily lends itself to a fairly wide range of parametric investigations. These measurements will provide the first hard data on a number of interesting atmospheric effects and offer guidance in selecting the best operational configurations for the experiments that follow. The following is a partial list of high-priority single-beacon tests.

(1) Sampling Delay. As discussed in the Section 2.0, the ability to perform all of the necessary compensation tasks within an atmospheric time constant is crucial to the design of a pulsed system. The sampling delay and sampling interval are commanded by the Executive Controller, which can be programmed to automatically vary these parameters on a pulse-to-pulse basis during an experimental sequence. There is essentially no limitation on the sampling delay that can be imposed on the camera system.
Parametric Range : 0 - 5,000 μsec

(2) Beacon Altitude. Signal-to-noise requirements and focal-anisoplanatic effects compete in the selection of the most appropriate beacon altitude in both single and multiple-beacon systems. The SWAT system has been designed with sufficient sensitivity and processing speed to allow the deployment of beacons at altitudes between 5 and 15 km. Therefore, it should be possible to vary the strength of the focal-anisoplanatic effect by at least a factor of 2.
Parametric Range : 5 - 15 km

(3) Sampling Depth. At this point in time, analytical data concerning the potentially detrimental effects of finite probe size is sketchy at best, but once again it is likely that signal to noise and anisoplanatic effects compete unfavorably. The sample depth can be varied by adjusting the integration interval of the wavefront sensor cameras.
Parametric Range : 10 - 100% of beacon altitude

(4) Beam Diameter. Theoretical work in this area has consistently shown that the beacon diameter can expand to the size of the collection aperture without degradation in performance. Since this result has important implications regarding the requisite beam quality of the beacon projection system, a variation of beacon diameter through adjustments to the transmit beam focus is likely to be one of the earlier tests to be performed in this sequence.

Parametric Range : λ/r_0 - $10\lambda/r_0$

(5) Beacon Displacement. The effect of beacon displacement should be completely predictable given an accurate measure of ϑ_0. Fixed offsets of any magnitude from the scoring star position can be easily imposed on the transmitted beacon laser through an adjustment of the point-ahead mirror.

Parametric Range : 0 - 20 μrad

(6) Phase Reconstruction Methods. One of the principal benefits of the digital phase-reconstruction hardware used in the SWAT system is its ability to quickly change its reconstruction matrix. Although the conventional Gauss reconstructor is likely to be the default matrix for the majority of the single-beacon experiments, a number of alternative algorithms have been proposed with the hope of improving system performance by making use of a priori information about local turbulence conditions. The SWAT reconstructor has been designed to store 7 sets of matrix coefficients, which can be loaded in any order between beacon returns. In this way, competing schemes can be efficiently tested under nearly-identical atmospheric conditions.

These single-beacon parametric measurements are likely to establish the baseline operational procedures and performance standards for all subsequent measurements. For this reason, it is expected that a minimum of 3 months will alloted to this segment of the SWAT II field effort.

5.2.2 4-Beacon A-Method Figure Compensation

The deployment of multiple beacons introduces several non-trivial complications to the dye-laser deployment and data-manipulation processes. Beacon multiplexing through temporal discrimination was selected for this program as the approach of lowest risk, but its success depends upon the ability to rapidly modify the beam path to allow the insertion of up to six beams in sequence. Specifically, a set of 3 fast-switching mirrors have been added to the optical bench layout to insert the active laser into the bench-optics beam train, and a 2-axis tilt/detilt

mirror pair have been introduced to correctly position the outgoing beams above their respective sections while removing section tilt from the return beam.

The new arrangement is shown in Figure 5-6, and the corresponding timing diagram appears in Figure 5-7. The intent in this case is to perform two sets of phase compensation within one atmospheric time constant, one directly after a precursor beam centered over the aperture and a second with a 4-beacon arrangement. The timeline for this experiment is considerably more difficult to interpret, and arrows have been added to indicate the process initiation points. For the precursor pulse, the switching and tilt mirrors in the output path can be moved as soon as the beam leaves the transmitter so that the 125-μsec settling process can begin; similarly, the detilt mirror can be actuated as soon as the backscatter signal is received. From this point, the timeline is similar to that shown in Figure 5-5, in which the process flows sequentially from the phase sensor, the reconstructor, deformable mirror, and the star-imaging cameras. The CCD camera integration period is shown as extending into the deployment of subsequent pulses, but is gated off each time a beacon pulse is launched to minimize the possibility of collecting near-field backscatter.

The multiple-beacon pulses follow one another as indicated, and it can be seen that the mirror switching delays are the most important determinant in establishing the minimum pulse spacing. The gradient data from each pulse are fed into the reconstructor, but the mirror drive for the 4-beam correction occurs only at the end of the fourth return. The complete 5-beacon phase-compensation process should take no more than 1.5 msec.

The experiments anticipated for this configuration will be directed principally to probe the process of deploying multiple beacons and processing the return signals. The degree of section overlap used in the stitching algorithm will be an important parameter in this investigation.

(1) Single/Multiple Beacon Comparison. This experiment embodies the original thrust of the SWAT II effort and is the highest priority task following the successful completion of the single-beacon test sequence. The incorporation of precursor correction permits a direct comparison to be made of single and multiple-beacon compensation within the same atmospheric time constant. As described later in this section, it is predicted that a

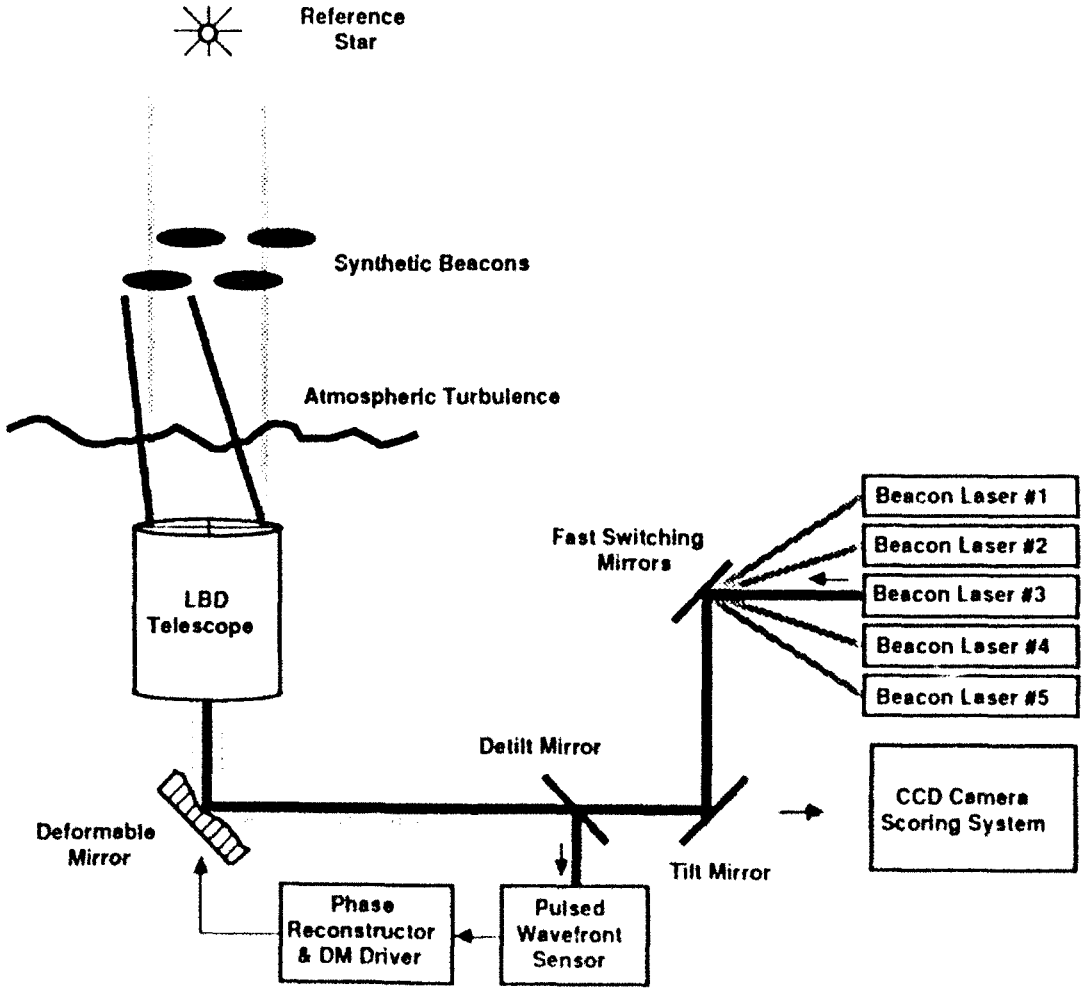

Fig. 5-6. Multiple-beacon compensation experiment.

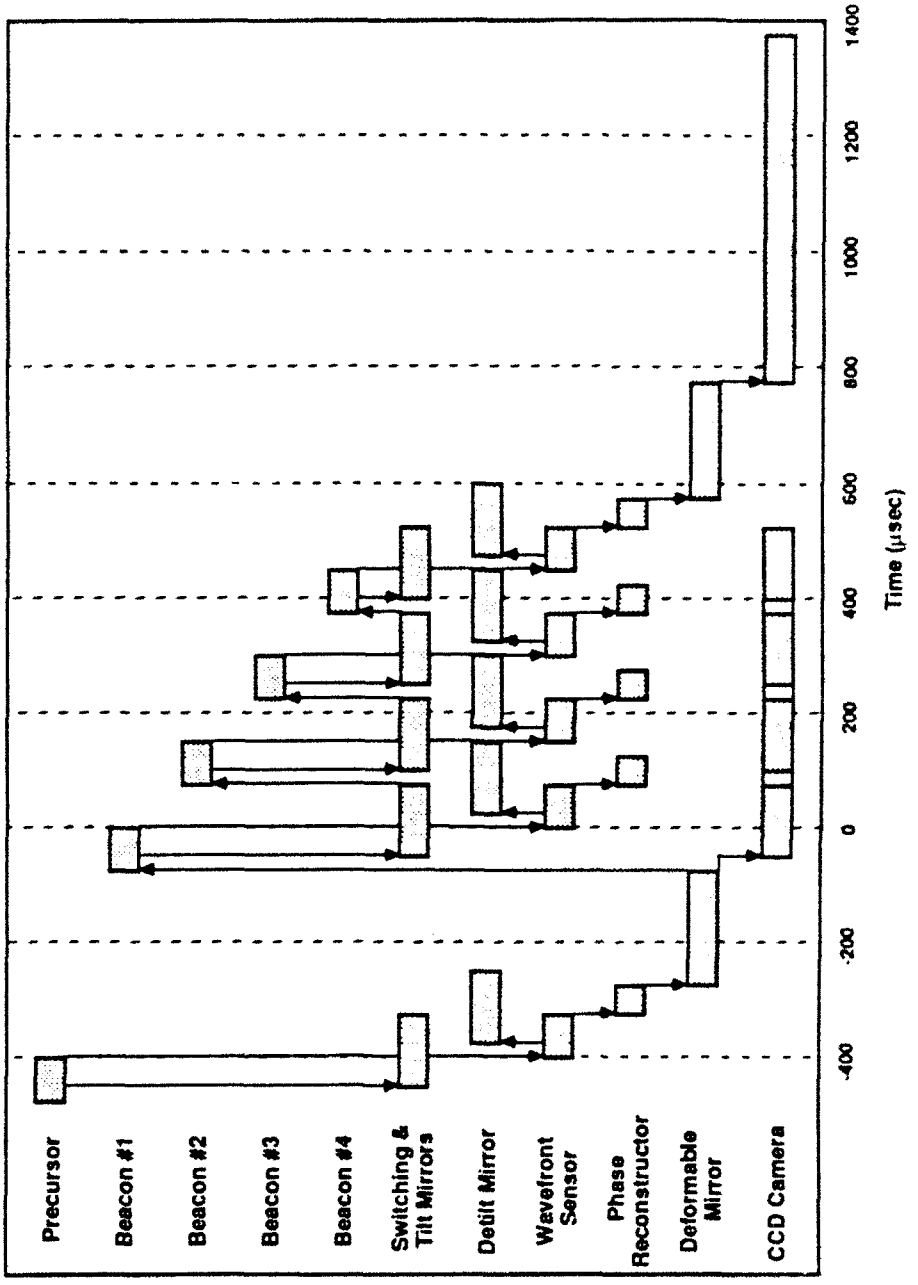

Fig. 5-7. Multiple-beacon experiment timing diagram.

factor of 2 difference in Strehl will be found between the two phase reconstruction approaches.

Parametric Range : 1 or 4 beacons

(2) Beacon Position. A-method stitching procedures require the individual beacons to be positioned over the center of their respective aperture sections for best performance, but a properly designed stitching algorithm should be insensitive to minor displacement errors. The ability of the system to perform as expected with small beacon displacements can be probed by adjusting the offset applied to the tilt/detilt mirrors under command from the Central Controller.

Parametric Range : 0 - 10 μrad displacement

(3) Stitching Algorithm. The optimization of stitching algorithms has spawned considerable debate over the years, and it was with this question in mind that the phase reconstructor was designed with the capability to store 7 different linear operators. By cycling through the different procedures for an extended period, it should be possible to uncover any statistically significant differences between the various processing techniques.

Parametric Range : single-subaperture overlap to full-aperture overlap

These multiple-beacon tests are likely to be considerably more difficult to perform successfully than the single-beacon experiments described in the last section, and will probably require 6 to 12 months of dedicated effort to complete. Much depends on the reliability of the dye-laser system and the performance of the fast-switching mirrors to insert and accurately position the individual beacons.

5.2.3 Two-Altitude A-Method Figure Compensation

Multiple-altitude beacon geometries have been considered as an adjunct to, as well as a replacement for, an array of low-altitude sources. In principal at least, high-altitude data can be obtained from the same laser pulses used to generate the low-altitude sources, and high signal-to-noise ratios can be preserved (at the expense of spatial resolution) by summing the outputs of several adjacent subapertures. When used in conjunction with several low-altitude sources, a high-altitude beacon might be incorporated into the stitching algorithm to remove residual section tilts. But in a broader context, the high-altitude source can be thought of as a means of removing

any residual low spatial-frequency phase distortion left over from an earlier high-spatial frequency, low-altitude correction attempt. A wide range of stitching procedures have potential utility in the processing of returns from dual-altitude sources, and, as discussed earlier, the reconstruction hardware will permit the concurrent testing of multiple approaches.

The optical layout and beacon timing diagrams for the proposed two-altitude beacon experiments appear in Figures 5-8 and 5-9 respectively. (Note that the laser deployment sequence is essentially the reverse of the one presented in the previous section.) The experimental goals for these tests are summarized as follows.

(1) High-Altitude Beacon Placement. The placement and processing of the high-altitude beacon is expected to play a key role in the performance characteristics of the phase reconstruction process, but at this point the engineering trade-offs between beacon altitude, subaperture diameter, and reconstruction algorithm have not been thoroughly studied. It is anticipated that Rayleigh beacon altitudes in excess of 15 km will be attained with the dye-laser system, and that experiments using sodium sources at 90 km will also be possible using a prototype sum-frequency Nd:YAG laser currently under development at Lincoln Laboratory.[5]

Parametric Range : 10 - 15 km and 90 km (with a single low-altitude beacon fixed at 5 or 10 km)

(2) High-Altitude Beacon-Subaperture Geometry. This test would be performed in conjunction with the previous experiment to probe the trade-offs involved in adjusting the dimensions of the subapertures exposed to the high-altitude source. (A reduction in the subaperture diameter would extend the phase compensation to higher spatial frequencies, but would also lower the phase sensor's signal-to-noise ratio.) In principal, it is possible to vary the effective subaperture size through a modification of the reconstruction matrix, but a higher signal-to-noise ratio can be achieved by incorporating a separate low spatial-frequency wavefront sensor for the high-altitude beacon.

Parametric Range : 4 - 25 high-altitude beacon subapertures

---

[5]Jeys, T. H., Killinger, D. K., Harrison, J., and Moorandian, A., "Nd:YAG Sum-Frequency Generation of Sodium-Resonance Radiation," CLEO '87 Conference on Lasers and Electro-Optics (27 April 1987).

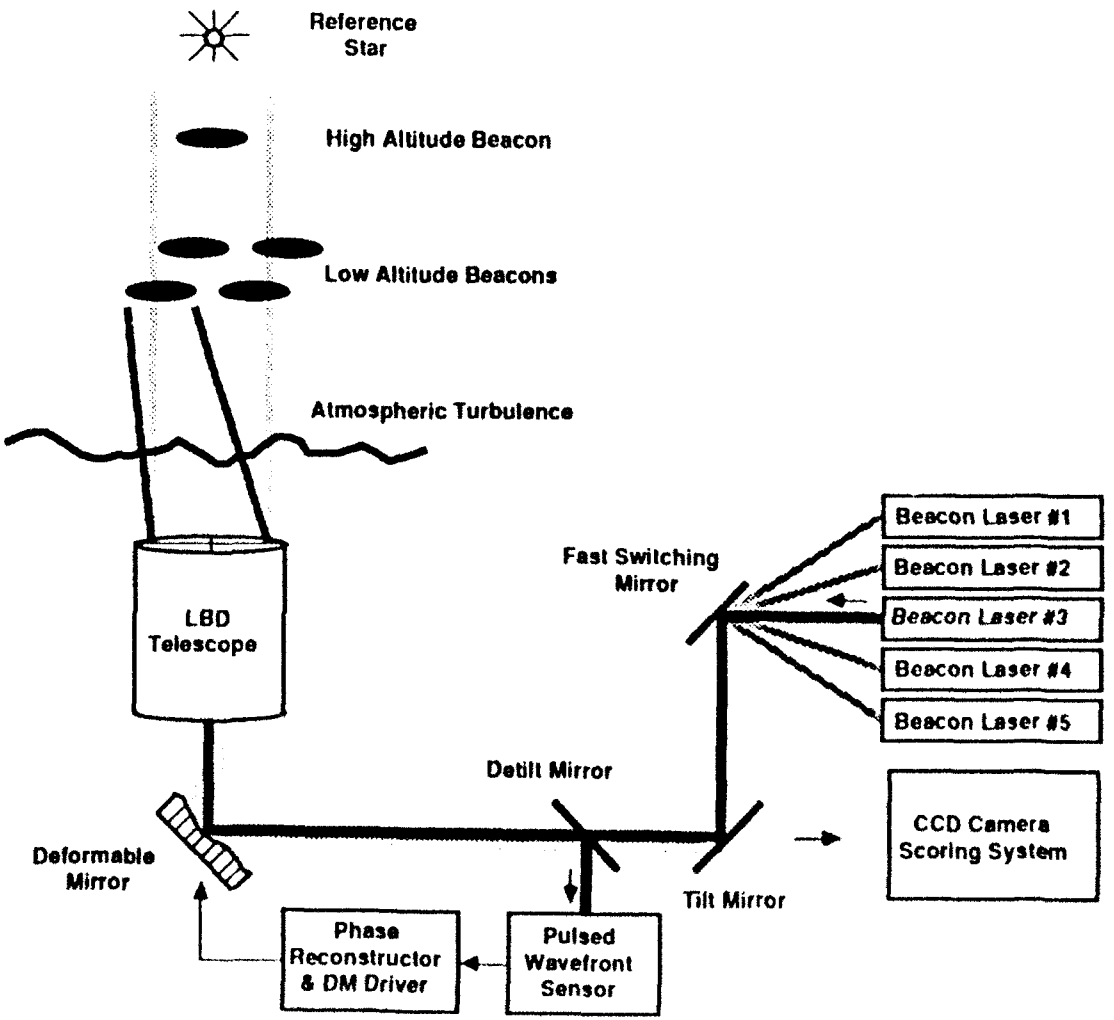

Fig. 5-8. Dual-altitude compensation experiment.

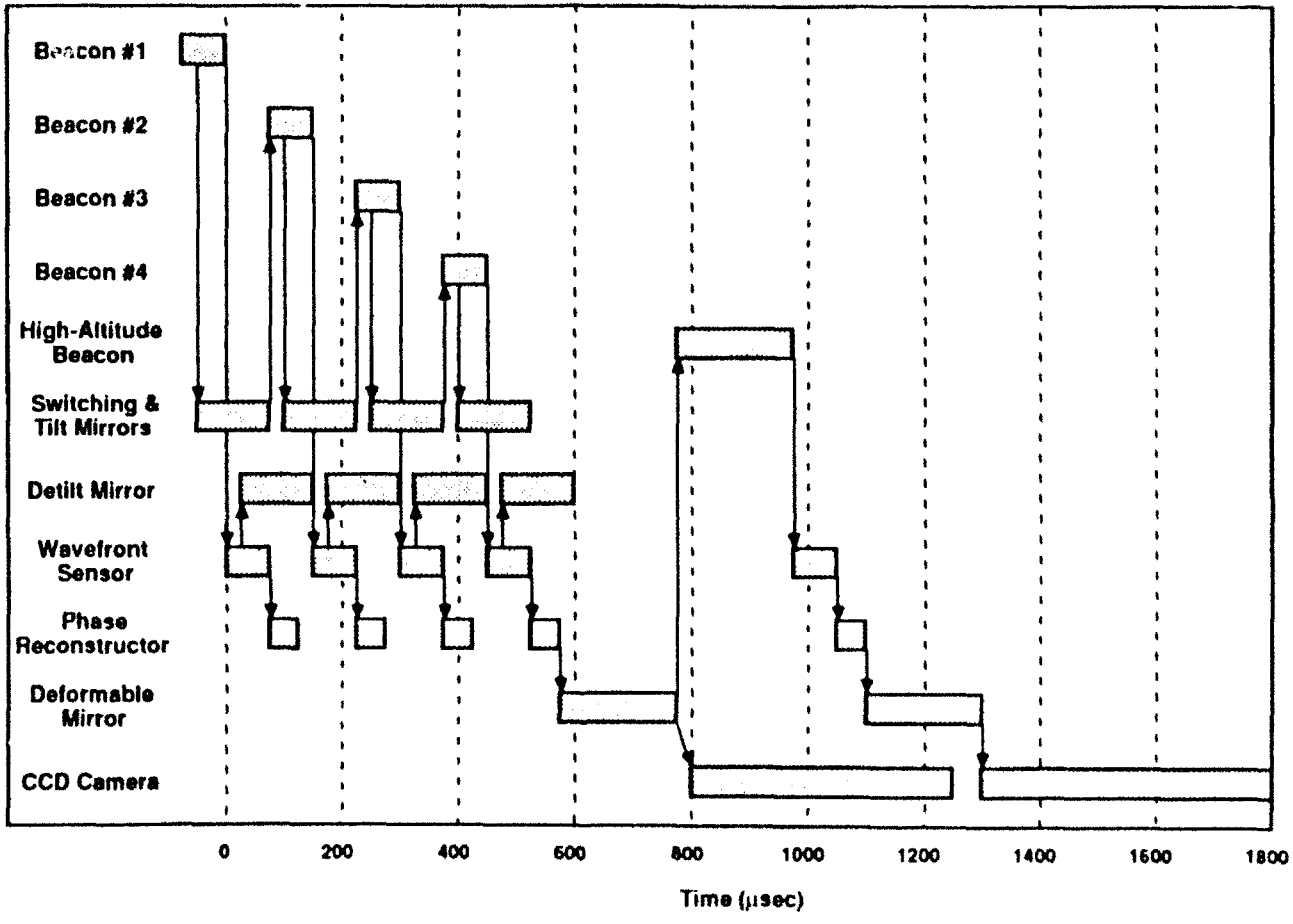

Fig. 5-9. Dual-altitude experiment timing diagram.

(3) Single/Multiple Low-Altitude Beacon Comparison. Preliminary analytical studies have shown only small performance differences between single and multiple low-altitude beacon arrangements used in conjunction with a high-altitude source. This result is readily tested through a minor adjustment to the laser firing sequence.
Parametric Range : 1 or 4 low-altitude beacons

This concludes the overview of the SWAT II compensated-imaging series scheduled for FY88 and early FY89. In the next section, a recent analytical treatment pertaining to these early measurements will be reviewed.

5.3 FIGURE COMPENSATION PERFORMANCE ESTIMATES

A brief discussion of reconstruction errors as a function of aperture diameter was presented earlier in Section 2.0 of this report. A set of calculations specific to the SWAT II mirror configuration has also been performed to address the expected Strehl difference between single-beacon and multiple-beacon reconstruction schemes for the 60-cm LBD aperture, as well as the potential benefits of deploying a single high-altitude source. For these Monte-Carlo runs, the receiver aperture was subdivided into 4 sections, each under the control of a separate synthetic beacon. Source displacement errors were explicitly removed through the use of a two-step, section-tilt removal process using section overlap or the high-altitude beacon source to sense relative section tilts. The analysis incorporated a set of 5 turbulence realizations, which were used in pairs to provide r_o and ϑ_o values of 5 cm and 12 μrad respectively, and which covered an 18 x 18 phase point grid having a subaperture spacing of 3.5 cm.

Residual figure errors for the 3 most interesting beacon placement scenarios are summarized in Figure 5-10. The uppermost curve shows the predicted error variance for a single point-source beacon as a function of beacon altitude. (The error bar attached to this plot indicates the rms variation between realizations for the 5-screen data ensemble.) The second solid curve represents a performance summary for 4-beacon stitching with full-aperture overlap section tilt removal. Note that the difference between these two curves is of the order of 1 rad^2 for the 5-km scattering altitude, but that the absolute difference falls below the simulation uncertainty (and possibly the wavefront sensor noise floor) at altitudes greater than 10 km. Clearly, any measurements directed at showing an unambiguous distinction between the two reconstruction

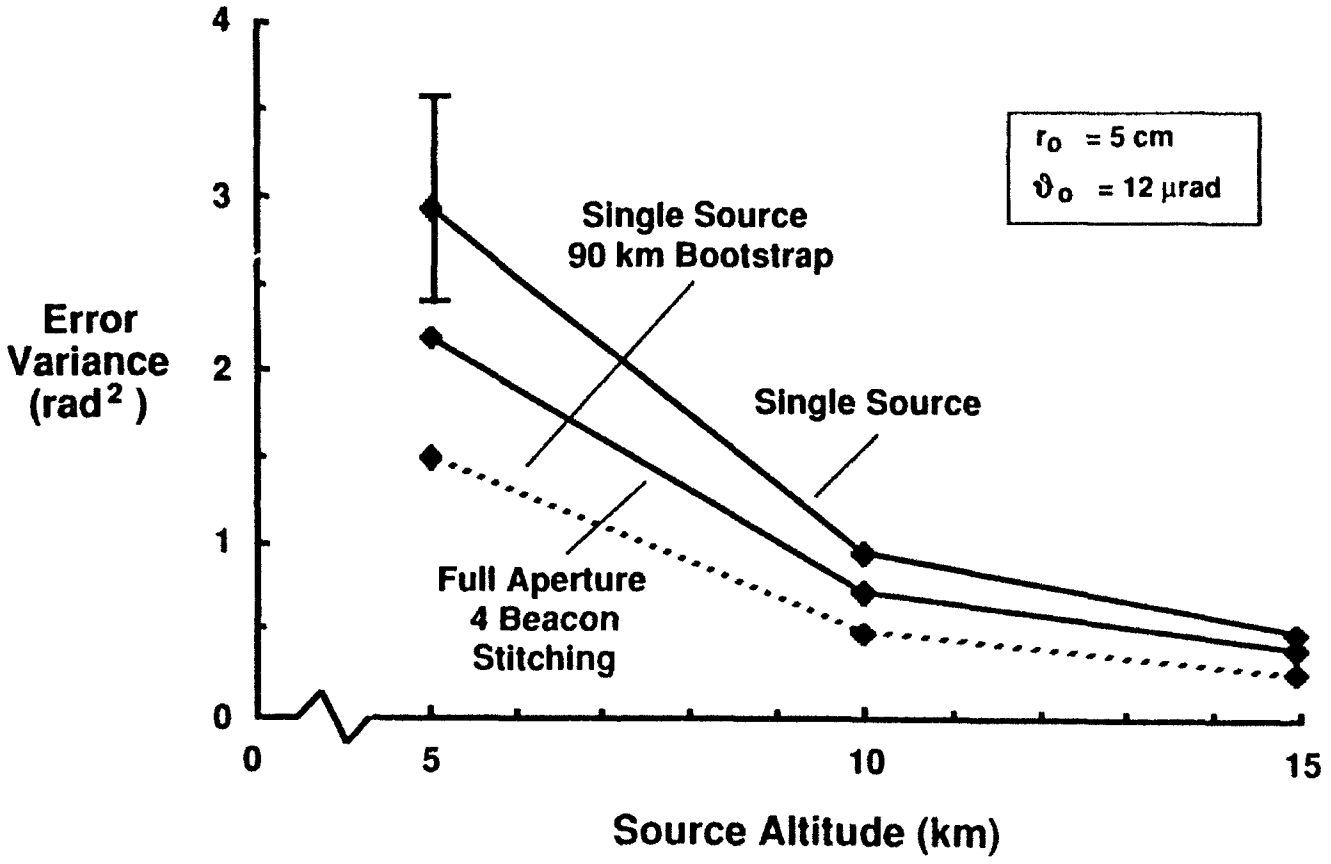

Fig. 5-10. Predicted compensation system performance.

methods should be conducted at the lowest altitude permitted by the timing constraints of the SWAT II hardware (or under more stressing turbulence conditions).

The dotted curve presented in Figure 5-10 is the predicted performance of the so-called 'bootstrapping' approach, in which a high spatial-frequency correction is first applied to the deformable mirror with the aid of a single low-altitude beacon, followed by the measurement and removal of residual section tilts using a second source positioned, in this example, at 90 km. As indicated, the performance of single-beacon bootstrapping and 4-beacon stitching procedures are roughly comparable, which provides a strong motivation for incorporating both horizontal and vertical beacon distribution strategies into the SWAT II test series.

This numerical simulation output is presented primarily as an illustration of existing analysis capabilities, which can be modified and expanded to address virtually any A-method experimental configuration. Work is also in progress to derive closed-form analytical expressions for the more interesting beacon geometries, thus providing both a more efficient computational path and an independent confirmation of the validity of the theoretical results.

6. SWAT II LASER PROPAGATION MEASUREMENTS

Table 1–1, found in the first section of this report, lists three sets of experiments in which scoring lasers and instrumented targets will be employed to measure the performance of selected synthetic-beacon phase-compensation concepts. These tests are intended to supplement and verify the star imaging data that will be collected on a more routine basis. This section presents a brief description of the two target platforms to be used in these active measurements; additional information will be provided in subsequent test plans.

6.1 LACE SATELLITE EXPERIMENTS

The first instrumented exoatmospheric target available for SWAT experimentation will be the LACE (Laser Communications Experiment) satellite, which is scheduled to be launched by the Naval Research Laboratory in late FY88. This platform is gravity-gradient stabilized and will be placed in a 500-km circular orbit inclined at 43° to the equator. With this geometry, several ground-based laser sites, including Maui, White Sands, and Westford, Massachusetts, will be afforded frequent access; a pass exceeding a minute in duration at elevation angles greater than 60° will occur at Maui approximately once every second day. It is anticipated that the useable lifetime of this system will be at least 3 years.

Lincoln Laboratory has had a close involvement with the specification of the LACE detectors, data telemetry, and point-ahead source, so as to ensure its utility for a wide range of cooperative and uncooperative adaptive-optics experiments. In order to minimize tilt anisoplanatic effects during cooperative propagation experiments, the satellite will carry a boom-mounted retro-reflector that can be adjusted between passes to achieve the correct lead-ahead angle for any illumination engagement between zenith and 45°. The reflector is actually an array containing 252 1-inch corner-cubes, which are pseudo-randomly oriented to affect a wide acceptance angle. The array has an effective cross-section of roughly 10^7 m^2/sr at 500–nm. LACE will carry several sensor arrays suitable for calibrated measurements of low-power sources ranging in wavelength from 300 nm to 4 μm. The arrangement of the detector elements for visible wavelength sources is shown in Figure 6-1. The detector arrangement is rectangularly symmetric, covering an area of approximately 16 m^2. A total of 81 sensor positions are included, arranged so as to provide a higher sampling density near the center of the target. In

this manner, both corrected and uncorrected beam profiles can be accurately characterized.

6.2 SOUNDING ROCKET TESTS

To augment the LACE tests and provide a means of conducting specialized propagation experiments, the Laboratory is preparing a set of 5 Terrier-Malemute sounding rockets capable of carrying a 2.5–m long payload. The payload is essentially the same as that used during the third phase of the Atmospheric-Compensation Experiment program,[3] and Sandia National Laboratory will again take responsibility for launching the rockets from Kauai and collecting the high-bandwidth telemetry. The platform provides a reasonably good representation of an orbiting satellite, achieving a range in excess of 600-km during a 10-minute flight. The instrumentation package contains a linear array of 20 detectors, and an 8-inch retro-reflector provides the tracking source.

In order to obtain a two-dimensional beam image from the linear detector array mounted on the rocket body, a scanning device capable of operating at 10-kHz rates while simultaneously chopping the beam at frequencies in the 50 to 100-kHz range will be part of the scoring-laser system. The illumination and data recording schemes are illustrated Figure 6-2.

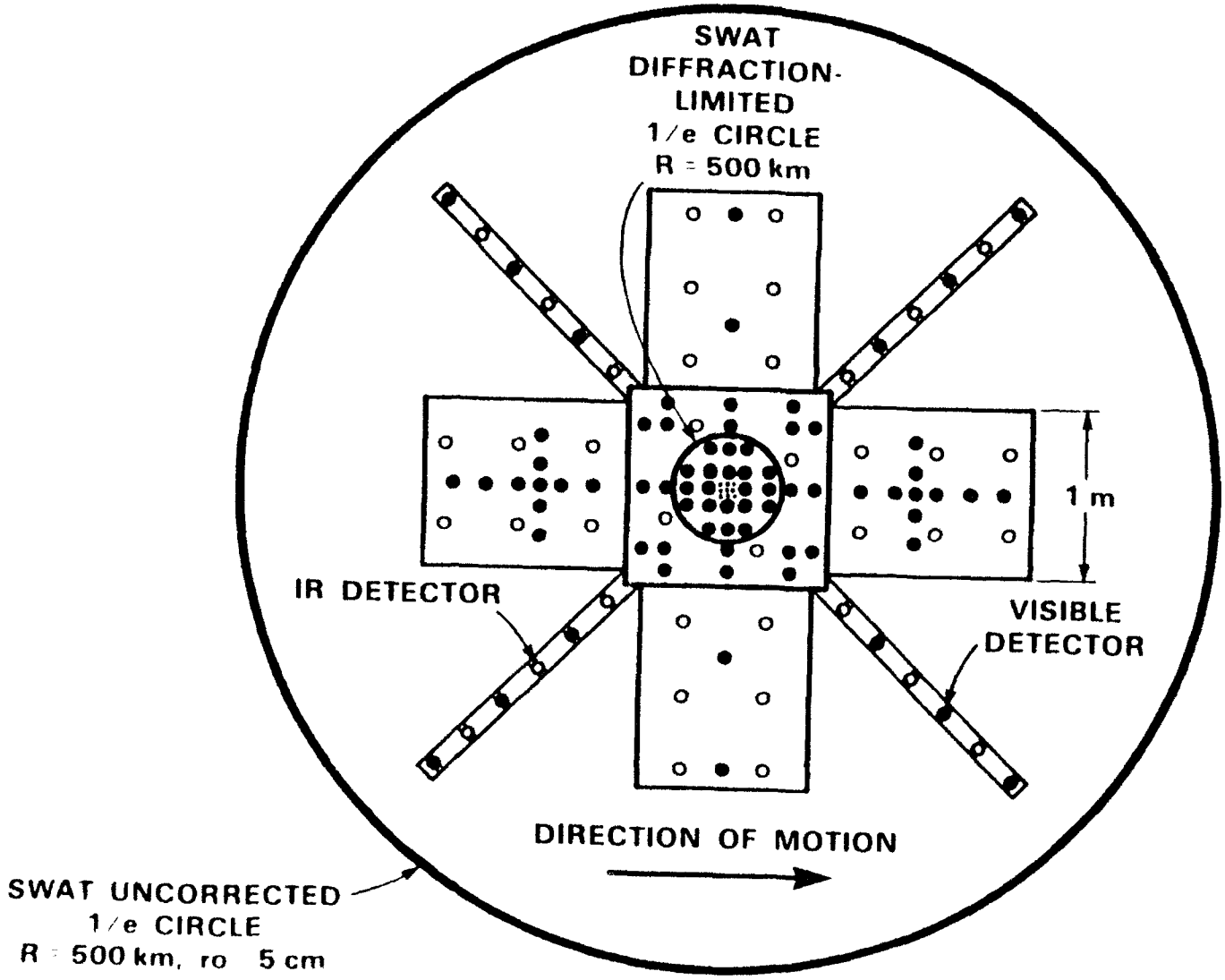

Fig. 6-1. LACE satellite detector configuration.

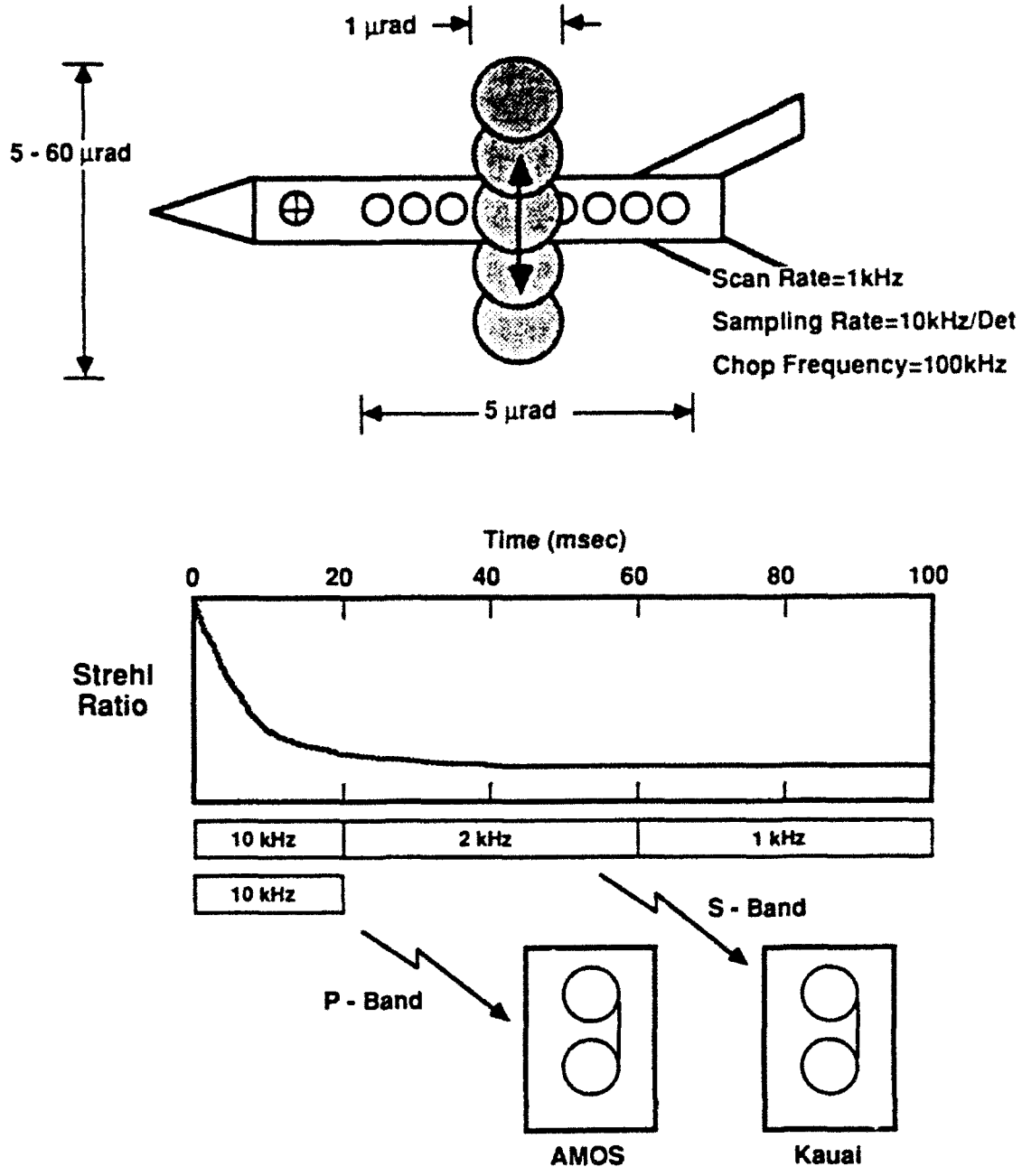

Fig. 6-2. Sounding rocket illumination and data recording

7. FUTURE REPORTING

This report is intended to serve as a general introduction and working roadmap for a comprehensive field effort that is expected to be active into the early 90's. Subsequent documentation will provide a higher level of detail and concentrate on specific program areas, such as S-method verification, tracking experiments, and laser-propagation measurements. Interim data-analysis documents will also be regularly issued following the completion of each set of experiments.

REPORT DOCUMENTATION PAGE

Form Approved
OMB No. 0704-0188

Public reporting burden for this collection of information is estimated to average 1 hour per response, including the time for reviewing instructions, searching existing data sources, gathering and maintaining the data needed, and completing and reviewing the collection of information. Send comments regarding this burden estimate or any other aspect of this collection of information, including suggestions for reducing this burden, to Washington Headquarters Services, Directorate for Information Operations and Reports, 1215 Jefferson Davis Highway, Suite 1204, Arlington, VA 22202-4302, and to the Office of Management and Budget, Paperwork Reduction Project (0704-0188), Washington, DC 20503.

1. AGENCY USE ONLY (*Leave blank*)	2. REPORT DATE	3. REPORT TYPE AND DATES COVERED
	10 March 1993	Project Report

4. TITLE AND SUBTITLE

SWAT II Overview

5. FUNDING NUMBERS

C — F19628-90-C-0002
PE — 63217C, 63221C
PR — 33

6. AUTHOR(S)

Ronald R. Parenti, Patrick N. Everett, Robert Kramer, and Daniel A. Page

7. PERFORMING ORGANIZATION NAME(S) AND ADDRESS(ES)

Lincoln Laboratory, MIT
P.O. Box 73
Lexington, MA 02173-9108

8. PERFORMING ORGANIZATION REPORT NUMBER

PR-SWP-3, Revision 1

9. SPONSORING/MONITORING AGENCY NAME(S) AND ADDRESS(ES)

AF Phillips Laboratory
Kirtland Air Force Base
Albuquerque, NM 87177-6008

10. SPONSORING/MONITORING AGENCY REPORT NUMBER

ESC-TR-92-145

11. SUPPLEMENTARY NOTES

None

12a. DISTRIBUTION/AVAILABILITY STATEMENT

Approved for public release; distribution is unlimited.

12b. DISTRIBUTION CODE

13. ABSTRACT (*Maximum 200 words*)

All adaptive optics systems incorporate devices designed to measure and compensate phase distortions that accumulate over the propagation path of an optical beam. Measurement of the wavefront is accomplished with the aid of a bright source, or beacon, which must be accurately positioned along the beampath. In some scenarios of interest no physical beacon exists; for instance, the propagation of a laser beam to an exoatmospheric object moving at velocity v requires that the beacon lead the target by an angle $2v/c$. In the early 1980's it was proposed that laser backscatter in the atmosphere might provide a suitable alternative source in such cases. Although a synthetic beacon generated in this manner can be placed arbitrarily in angle, any range discrepancy between the target and the beacon can lead to a form of measurement error known as focal anisoplanatism.

Lincoln Laboratory's SWAT (Short-Wavelength Adaptive Techniques) program was initiated in 1983 to provide experimental verification of the most promising synthetic beacon concepts and to quantify the magnitude of the associated focal anisoplanatic errors. The test plan for this program includes passive imaging experiments using single and binary stars, as well as active experiments in which a scoring beam will be projected to rocket and satellite targets.

14. SUBJECT TERMS

adaptive optics
atmospheric turbulence
laser guide star
phase conjugation
synthetic beacon

15. NUMBER OF PAGES
106

16. PRICE CODE

17. SECURITY CLASSIFICATION OF REPORT	18. SECURITY CLASSIFICATION OF THIS PAGE	19. SECURITY CLASSIFICATION OF ABSTRACT	20. LIMITATION OF ABSTRACT
Unclassified	Unclassified	Unclassified	Same As Report